COMPARATIVE PERFORMANCE TESTS ON THERMOSYPHONS AND APPLICATION AS HEAT PIPE HEAT EXCHANGER COOLER OPERATING BETWEEN 30-100°C.

by

CHRISTOPHER LIM YI-JIN

A Master's thesis submitted to the Department of Industrial Engineering,
Faculty of Engineering & Green Technology,
Universiti Tunku Abdul Rahman,
in partial fulfilment of the requirements of the degree of
Master of Engineering Science
September 2015.

ABSTRACT

COMPARATIVE PERFORMANCE TESTS ON THERMOSYPHONS AND APPLICATION AS HEAT PIPE HEAT EXCHANGER COOLER OPERATING BETWEEN 30-100°C

CHRISTOPHER LIM YI-JIN

The overall objective of the research was to develop a modular heat pipe heat exchanger cooling system for molds and dies in the foundry industry. The study was carried out in three phases - A, B and C. Phase A was conducted to determine the evaporating and condensing heat transfer coefficients in water-filled wickless heat pipes (two-phase closed thermosyphons) in order to simulate their performances. Three thermosyphons were fabricated with different length/diameter aspect ratios of from 5.0 – 10.0. Each thermosyphon was heated with electrical resistance wires wound around the evaporator section and cooled with a concentric pipe cooling water jacket around the condenser section. Experiments were carried out with evaporator heat input rates from 5-405 W, coolant water flow rates from 0.003-0.050 kg/s, fill ratios from 0.25-1.00 and pipe inclination angles from 23-90 degrees to the horizontal. The evaporator axial wall temperature distribution was found to be quite uniform at the low power inputs below about 18 W but found to be non-uniform at the higher powers. Evaporator wall temperature could be calculated

from the average bulk temperature or from an arithmetic mean along the evaporator section of the pipe. As a result of the non-uniformity temperature distribution, differences were observed between these two values by as much as 14^{o}C especially at the high power inputs. All three water-filled thermosyphons showed that best performance was obtained with a fill ratio of 1.00 and in a vertical position. A large aspect ratio of 10 was also preferred.

In phase B, a method was proposed to obtain comparative performance test data of various heat pipes rapidly and economically. The method involved measuring and comparing the transient temperature of a pre-heated container of hot water obtained with and without the heat pipe immersed inside the container. The method was demonstrated using a number of different water and air-cooled thermosyphons. The results showed that force air convection cooling was better than natural convection cooling and that high coolant water flow rates was better than low water flow rates.

In phase C, a modular thermosyphon heat pipe heat exchanger (THPHE) cooling system capable of removing up to 2 kW of heat was fabricated and tested. It was filled alternatively with water and R410a and with fill ratios from 0.25-1.00. It was observed that the R410a-filled unit performed better than the water-filled one at high fill ratio but water was preferred at low fill ratio.

PUBLICATIONS

Based on the work of this thesis, one Journal paper has been published while another has been submitted. A conference paper was also presented. Details are shown below:

No	Category	Title	Publisher	Status
1.	Journal.	An experimental procedure to compare thermal performance of thermosyphons rapidly. DOI: http://dx.doi.org/10.5098/fhp.6.2 ISSN: 2155-658X	Frontiers of Heat Pipes.	Published.
2.	Journal.	Performance of water filled thermosyphons between 30-150^{o}C. DOI: http://dx.doi.org/10.5098/fhp.6.3 ISSN: 2155-658X	Frontiers of Heat Pipes.	Published.
3.	Conference.	Comparative performance of thermosyphons.	International Symposium of Green and Sustainable Technology 2014, Malaysia.	Presented.

ACKNOWLEDGEMENTS

I would like to thank my supervisor Prof. Ir. Dr. Ong Kok Seng and my co-supervisor Mr. Yang Chuan Choong for their direction, assistance, and guidance. In particular, Prof. Ir. Dr. Ong Kok Seng's numerous recommendations and suggestions have been invaluable for the project. I would also like to extend a word of thanks to Dr. Chin Wai Meng, Y.N. Solar and PESDC for their contributions to the success of this research.

I would also like to thank my parents and close friends who have encouraged me and supported me through this research. I also wish to thank Mr. Hafiz and Mr. Syahrul, for their assistance in the laboratory. Special thanks to my colleagues Alvin, Jarrod and Lau Wee Teck for assisting in this research.

Last but not least, I offer my deepest regards and blessings to all of those who supported me in any respect throughout the project.

APPROVAL SHEET

This dissertation/thesis entitled "COMPARATIVE PERFORMANCE TESTS ON THERMOSYPHONS AND APPLICATION AS HEAT PIPE HEAT EXCHANGER COOLER OPERATING BETWEEN 30-100°C" was prepared by CHRISTOPHER LIM YI-JIN and submitted as partial fulfillment of the requirements for the degree of Master of Engineering Science at Universiti Tunku Abdul Rahman.

Approved by:

_____

(PROF. IR. DR. ONG KOK SENG) Date:……..
Professor/Supervisor
Department of Industrial Engineering
Faculty of Engineering & Green Technology
Universiti Tunku Abdul Rahman

_____

(MR. YANG CHUAN CHOONG) Date:……..
Co-supervisor
Department of Industrial Engineering
Faculty of Engineering & Green Technology
Universiti Tunku Abdul Rahman

FACULTY OF ENGINEERING AND SCIENCE

UNIVERSITI TUNKU ABDUL RAHMAN

Date: _____

SUBMISSION OF THESIS

It is hereby certified that **CHRISTOPHER LIM YI-JIN** (ID No: **13AGM06818**) has completed this thesis entitled "COMPARATIVE PERFORMANCE TESTS ON THERMOSYPHONS AND APPLICATION AS HEAT PIPE HEAT EXCHANGER COOLER OPERATING BETWEEN 30-100^{o}C" under the supervision of Prof. Dr. Ir. ONG KOK SENG (Supervisor) from the Department of Industrial Engineering, Faculty of Engineering & Green Technology, and Mr. YANG CHUAN CHOONG (Co-Supervisor) from the Department of Industrial Engineering, Faculty of Engineering & Green Technology.

I understand that the University will upload a softcopy of my thesis in pdf format into the UTAR Institutional Repository, which may be made accessible to the UTAR community and the public.

Yours truly,

_____

(CHRISTOPHER LIM YI-JIN)

DECLARATION

I Christopher Lim Yi-Jin hereby declare that the dissertation/thesis is based on my original work except for quotations and citations which have been duly acknowledged. I also declare that it has not been previously or concurrently submitted for any other degree at UTAR or any other institution.

_____

(CHRISTOPHER LIM YI-JIN)

Date_____

TABLE OF CONTENTS

LIST OF TABLES

Table **Page**

LIST OF FIGURES

Table **Page**

LIST OF SYMBOLS / ABBREVIATIONS

A	Cross-sectional area (m^2)
A_e	surface area of evaporator section (m^2)
A_{ins}	surface area of container (= 0.714 m^2)
AR	aspect ratio of evaporator length to pipe diameter (L_e/D_i)
C_{pw}	specific heat of water (kJ/kg K)
D_e	external diameter of evaporator section (m)
D_i	pipe inner diameter (m)
D_o	pipe outer diameter (m)
FR	fill ratio of fill liquid length to evaporator length
h_a	natural convection heat loss (= 2 W/m^2 K)
L_{ad}	adiabatic length (m)
L_c	condenser length (m)
L_e	evaporator length (m)

$\dot{m}_w$	mass flow rate of water (kg/s)
P	power input (W)
P_{sat}	saturation pressure (bar)
Q	volumetric flowrate (m^3/s)
$\dot{q}_b$	heat removed from container (kJ/s)
$\dot{q}_c$	condenser heat transfer rate (kJ/s)
$\dot{q}_e$	evaporator heat transfer rate (kJ/s)
$\dot{q}_{ins}$	heat loss from container (kJ/s)
$\dot{q}_w$	heat transfer to coolant water (kJ/s)
Re	Reynolds number
R_{HP}	overall thermal resistance of heat pipe (K/W)
T_a	ambient temperature/ air temperatures (^oC)
$T_{air,mean}$	Mean temperature of inlet and outlet air temperatures (^oC)
T_{ad1}, T_{ad2}	adiabatic temperatures (^oC)

T_b	container water temperature (^oC)
T_{bu}, T_{bl}, T_w	water temperatures (^oC)
ΔT_b	bulk temperature difference (^oC)
T_c	condenser temperature (^oC)
$T_{e,b}$	evaporator wall bulk temperature (^oC)
$T_{e,m}$	evaporator mean temperature (^oC)
T_{fin1}, T_{fin2}	fin temperatures (^oC)
T_{ins}	insulation surface temperatures (^oC)
ΔT_m	mean temperature difference (^oC)
T_p	temperature at top of condenser (^oC)
T_{sat}	saturation temperature (^oC)
T_w	mean coolant water temperature (^oC)
T_{wi}, T_{wo}	coolant water inlet and outlet temperatures (^oC)
ΔT_w, ΔT_m	mean difference between bath (evaporator) and coolant water temperature (condenser) (^oC)

W_b	mass of water in the container (kg)
θ	pipe inclination angle measured from the horizontal (degrees)
ρ	density of fluid (kg/m^3)
μ	dynamic viscosity of the fluid (kg/m s)
υ	kinematic viscosity (m^2/s)
γ	ratio of heat transfer to the coolant/total heat removed from the container

CHAPTER 1

INTRODUCTION AND OVERALL OBJECTIVE

1.1 Heat pipe

A heat pipe (HP) consists essentially of a vacuumed cylindrical metal container or pipe with a wick insert and a small quantity of working fluid sealed inside. The pipe is segmented into three parts: the evaporator, adiabatic, and condenser sections. Heat applied on the surface of the pipe in the evaporator section by an external heat source causes the working fluid to boil and vaporize, picking up latent heat of vaporization. The vapor travels inside the pipe to the colder condenser section of the pipe where it condenses. At the condenser section, the vapor gives up its latent heat of condensation. The condensate is then transported back to the evaporator section by capillary action or by gravity. Heat is thus transferred from the evaporator section to the condenser section of the heat pipe. This process will continue as long as condensate returns to the evaporator. A wickless heat pipe is shown in Figure 1.1. It is also known as a two-phase closed thermosyphon (TPCT). For a TPCT to work, the condenser section must be located above the evaporator section. The thermal performance of a TPCT is dependent on the heat input, fill ratio, geometrical dimensions and inclination of the pipe from the vertical. The heat extraction capability is also very much dependent upon the design of the condenser. In the case of an air cooled TPCT, either natural or forced convection could be employed. For water cooled pipes, a water coolant jacket

could be attached at the top of the TPCT and forced circulation of water could be employed. Some of the common measurement for aspect ratio (AR) and fill ratio (FR) can be seen in Fig 1.2.

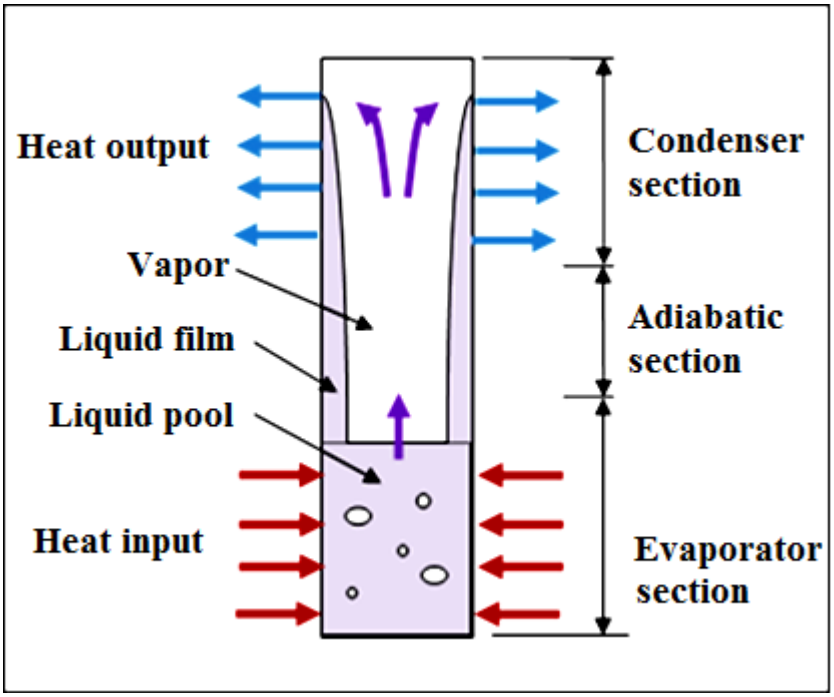

Figure 1.1 Cross sectional view of a thermosyphon

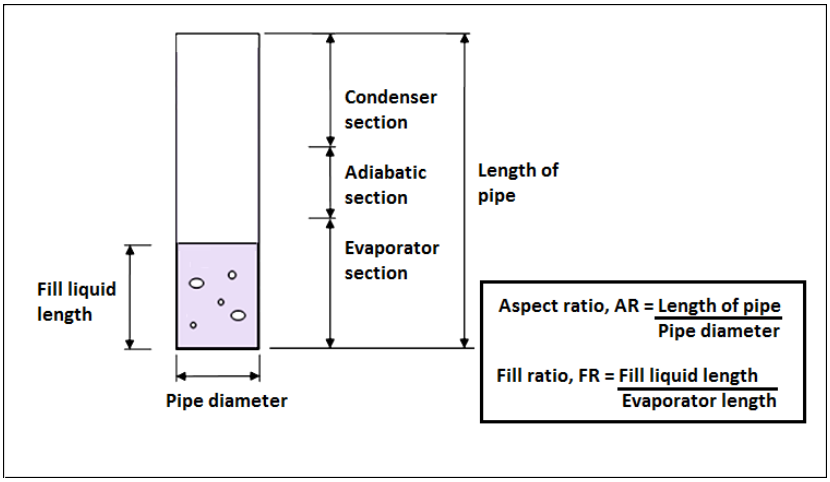

Figure 1.2 Evaluation of AR and FR of a thermosyphon

In most manufacturing and industrial processes, a percentage of energy used will be lost as heat. The waste heat could be recovered via thermosyphon heat pipe heat exchangers (THPHEs). Heat can be recovered from industrial ovens, furnaces, boilers, generators and incinerators. Heat recovery from exhaust gasses can provide large amount of energy savings and reduction in CO_2 emission. A HPHE basically consist of an array of HPs (Dobson and Loubscher 2013). A typical THPHE system is shown in Figure 1.3.

HPs are about 35% more efficient than a conventional heat exchanger and 1000 times better than by pure conduction in a copper pipe. Another advantage of using HPs is that they are enclosed and isolated from the environment, enabling it to recover heat energy from dirty or corrosive environment. Due to the high thermal conductivity the heat transfer is almost instant. The THPHE acts as a passive heat transfer device, where it will continue to function as long as there is a temperature difference between the condenser and evaporator end as low as $5^{o}C$.

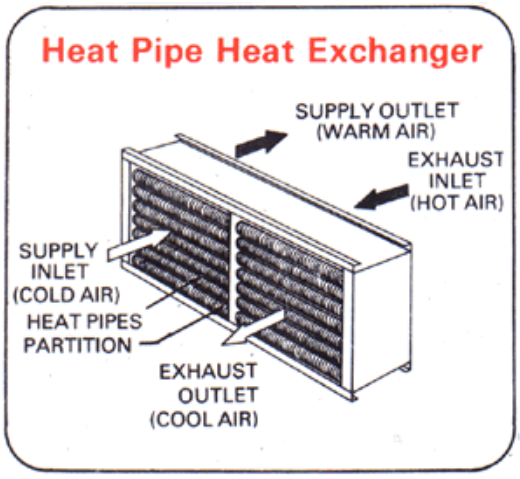

Figure 1.3 Isometric view of an air to air heat pipe heat exchanger (Source: china-heatpipe. Image by: banye)

1.2 Cooling of molds and dies in the foundry industry

Molds and dies in the foundry industry are mainly used to mass produce metal parts with complex design. The molds and dies contain the pattern of the intended product. Hot molten metal is injected into the molds and dies through cavities by means of high pressure injection. Once the molten metal is in place, cold water is cycled through the cooling channels within the molds and dies. The cold water removes heat from the system enabling the molten metal to cool and solidify. At the end of the cycle, the metal product is released from the molds and dies set. Traditionally, plastic injection molds and dies are cooled by water flowing inside cavities, usually supplied from a central cooling tower. There are two types of water circulation, a conventional cooling cycle where water runs throughout the cycle time and a pulse cooling cycle where water flows through the cavity upon sensing the molds surface temperature and applies a pulse of coolant. The advantage of using pulse cooling is direct control over mold surface temperature, quick warm up time, elimination of thermal drift and minimum water consumption. However both the conventional and pulse cooling cycle introduces thermal stress on the molds and dies. Thermal stress causes the molds and dies set to crack after many process cycles due to the rapid expansion and contraction of the metal at the molds and dies. An existing solution to this problem is to use a higher grade of steel for the molds and dies set, marrying (marrying: a process of joining) steel to the molds and dies set or apply chemical lubricant within the molds and dies set to enhance its life span. A newer solution would be to insert heat pipes within molds and dies set, where the heat pipe is able to extract the heat from the

molds and dies set without introducing thermal stress to the system as the heating and cooling occurs at two different locations.

Based on some industrial survey, some molds and dies manufacturer maintain the temperature of a mold and die set to a fix temperature. They do not cool the mold and die set as this will affect the quality of the finished product. Industrialists mentioned that the temperatures of molds and dies are regulated in accordance with the type of plastic used or metal used for the product.

1.3 Cooling towers.

A cooling tower is a heat rejection device. Cooling towers are typically employed in heating, ventilation and air conditioning (HVAC) systems. Cooling towers can be classified into three categories based on heat transfer methods: dry cooling towers, wet cooling towers (open circuit cooling towers), and fluid coolers (closed circuit cooling towers). Dry cooling towers utilize convective heat transfer, such as in a tube-to-air heat exchanger. Wet cooling towers are more commonly used for their higher efficiency due to evaporative cooling. Fluid coolers are similar to dry cooling towers except clean water is sprayed and a fan-induced draft is applied to the external surface of the heat exchanger. Fluid coolers are preferred if the application is sensitive to contamination or environmental exposure.

Figure 1.4 illustrates the operation of a dry cooling tower. Heated water from a heat source is pumped through the heat exchanger typically with fins. Heat is removed by mechanical draft. The working fluid is cooled at the end of the heat exchanger and recycled to the heat source. The advantage of this method is that the working fluid is isolated from environmental exposure; this eliminates the risk of contamination from environment.

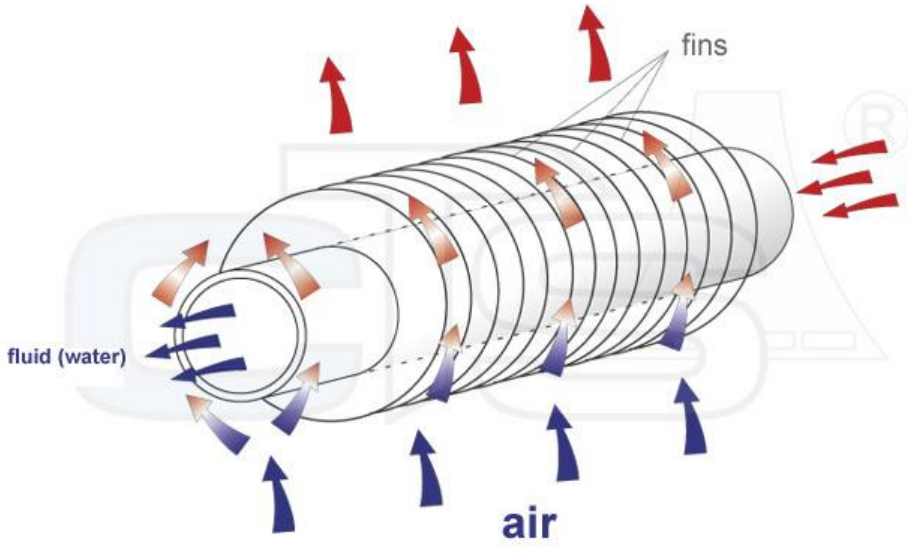

Figure 1.4 Dry cooling tower operation (Source: cts-cooling. Image by Unknown)

An open air type cooling tower is shown schematically in Figure 1.5. Heated water from a heat source (1) is pumped to the top of a cooling tower. The heated water is evenly dispersed over the tower fill (2). The water flows down the fill, which spreads the water over a larger surface area to increase the rate of evaporation and remove heat. A large fan draws air across the fill (3) which accelerates evaporation and the water continues to flow down the tower

cell and back to the system (4). As system water evaporates, only pure water is lost. To make up for the water that is lost through evaporation, fresh water is introduced to the system through a make-up line (5). The more water that is lost through evaporation the greater the need for make-up water and the faster the concentration of elements are built up. To reduce the concentration of elements in the water, a bleed out valve is opened and dumps a portion of the water as waste water (6). This waste water discharge must also be replenished by adding more make-up water into the system. The make-up water contains fewer elements than system water it will slowly reduce element concentration. During normal operation evaporation, bleed off and make-up are balanced to maintain a proper water volume while creating a continuous open loop.

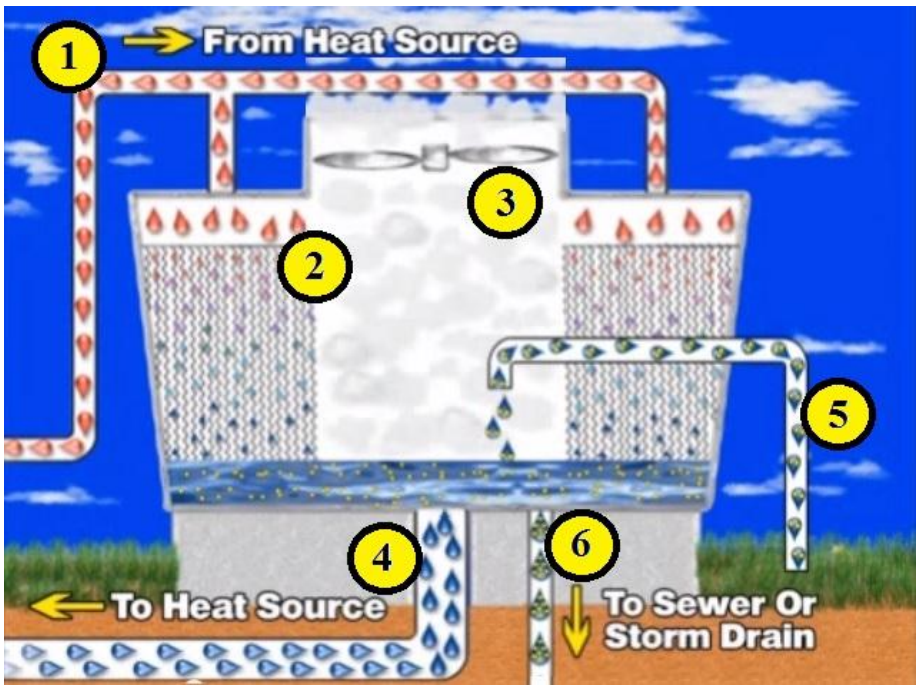

Figure 1.5 Open air type cooling tower (Source: terlyntech. Image by Unknown)

Figure 1.6 and Figure 1.7 illustrates a fluid cooling tower. Heated working fluid from a heat source is pumped from the bottom of the cooling tower to the top. Cooling liquid is evenly dispersed over the tower fill and the water flows down the fill, which spreads the water over a larger surface area to increase the rate of evaporation and remove heat. Air is drafted horizontally and vertically across the fill which accelerates evaporation and the cooling liquid continues to flow down the tower cell and is recycled as the process repeats. The fluid cooling tower is a hybrid combination of the dry cooling tower and wet cooling tower, where the advantages of having a separate system to eliminate contamination is present as well as applying enhanced evaporative cooling to further cool down the working fluid.

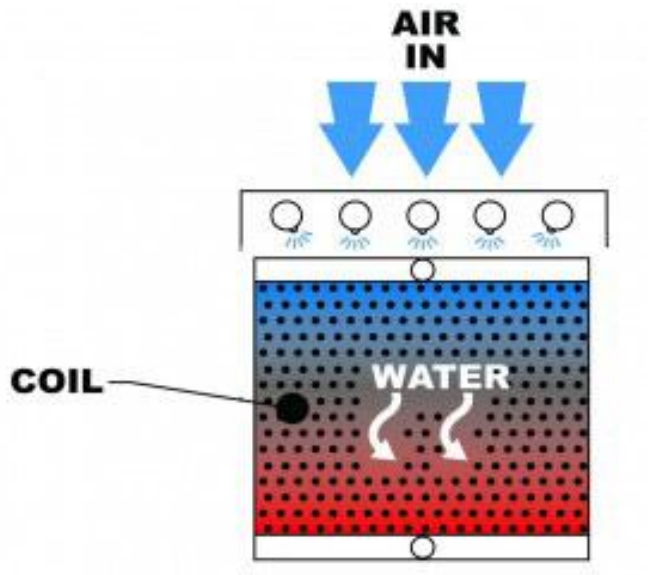

Figure 1.6 Fluid cooling tower operation (Source: baltimoreaircoil. Image by Unknown)

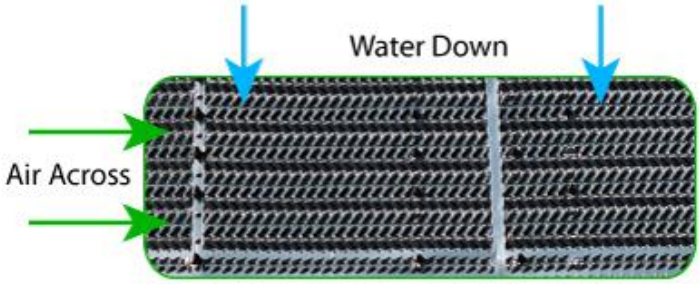

Figure 1.7 Fluid cooling tower cut away section (Source: baltimorecoil. Image by Unknown)

1.4 Problem statement

The need for energy grows as technology advances. Some of the areas to address this issue would be energy efficiency and sustainable energy especially for cooling. In the mold and die injection industry, a large amount of energy is required to cool the mold and dies during the injection process. This usually entails a small number of large cooling towers to service the cooling needs of numerous injection machines connected together. In certain instances, only a small number of machines could be operating simultaneously. Hence there is a need to find alternative cooling methods where only a small number of machines are running to reduce the temperatures of a device. For this reason small energy efficient modular cooler central cooling towers should be made to replace larger less efficient systems.

1.5 Overall objective of this thesis

The objective of the research is to develop a thermosyphon heat pipe heat exchanger (THPHE) cooling system for cooling of molds and dies in the foundry industry. In particular, the THPHE would replace the conventional cooling tower to remove heat from the molds and dies set during operation. The investigation would be carried out in three phases:-

1. Phase A: To determine the evaporating and condensing heat transfer coefficients in various water-filled thermosyphons. This will enable a theoretical model to be prepared in order to simulate their thermal performance.
2. Phase B: To propose a method to obtain comparative performance test data of various HPs rapidly and economically. Existing test methods require expensive set ups and long testing times.
3. Phase C: To fabricate and test a modular THPHE cooler to replace a conventional cooling tower for the cooling of molds and dies in the foundry industry.

1.6 Outline of Thesis

The layout of this thesis is presented in the following chapters.

In chapter 2, a brief review on thermosyphons operations and thermosyphon performance are introduced. The procedure for phase A are described aptly in this chapter. A theoretical model is proposed and presented in chapter 2 also. The results of the performance of various thermosyphons at different coolant flowrates, fill ratios, thermosyphon inclination angle and aspect ratio are presented and discussed. The performance is determined by a power versus temperature difference plot and an overall thermal resistance versus power plot. Beside the performance of various thermosyphons under various settings, the heat transfer coefficient for both evaporator, h_e, and condenser, h_c, were obtained experimentally. The values of h_e and h_c are presented and discussed.

In chapter 3, a brief review on thermosyphons types and thermosyphon performance testing methods are introduced. The procedure for phase B are described aptly in this chapter. A novel method to determine the performance of a heat pipe is proposed and presented. The results of the novel method and along with the comparison with a traditional method and simulated results are presented and discussed. The novel method is compared to the results obtained in phase A and simulated results from the theoretical model proposed in phase A.

In chapter 4, a brief review on heat exchangers designs, thermosyphon heat pipe heat exchangers and work done on heat exchanger systems are introduced. The procedure and fabrication of the THPHE cooler details are described in chapter 4. The performance of the thermosyphon heat pipe heat

exchanger, THPHE, cooler using water and R410a are presented and discussed. The results obtained from phase C experimentally are compared against the results from the theoretical model are presented and discussed as well.

In chapter 5, suggestions for future work for phase A, B and C are proposed. Improvement on experimental setups and procedures are proposed. In addition to that, improvement to the current THPHE designs are suggested.

The last chapter contains the conclusion of this thesis.

CHAPTER 2

PHASE A: PERFORMANCE OF WATER FILLED THERMOSYPHONS BETWEEN 30-150^{O}C

In chapter 2, a brief review on thermosyphons operations and thermosyphon performance are introduced. The procedure for phase A are described aptly in this chapter. A theoretical model is proposed and presented also. The results of the performance of various thermosyphons at different coolant flowrates, fill ratios, thermosyphon inclination angle and aspect ratio are presented and discussed. The performance is determined by a power versus temperature difference plot and an overall thermal resistance versus power plot. Aside from the performance of various thermosyphons under various settings, the heat transfer coefficient for both evaporator, h_e, and condenser, h_c, were obtained experimentally. The values of h_e and h_c are presented and discussed.

The objective of this chapter is:-

i) To determine the evaporating and condensing heat transfer coefficients in various water-filled thermosyphons. This will enable a theoretical model to be prepared in order to simulate their thermal performance.

ii) To determine the effect of coolant flowrates ($\dot{m}_w$), fill ratio (FR), thermosyphon inclination angles (θ) and aspect ratio (AR) on the performance of the thermosyphon.

2.1 Literature survey

2.1.1 Heat pipe

The performance of a thermosyphon is dependent on the fill ratio (FR), type of fill liquid, power input at the evaporator (P), pipe inclination (θ), and length/diameter aspect ratio (AR). An optimal FR is important as too much fill liquid can cause flooding and too little will cause dry out. Both of these phenomena are undesirable as they can reduce the performance of the heat pipe. Flooding occurs when liquid collecting in the condenser and adiabatic regions are unable to return to the evaporator section. Dry out occurs when the rate of return of the condensate from the condenser section is insufficient to meet the evaporation rate due to high heat flux in the evaporator section. The operating heat flux applied to the evaporator section is important as well. A high heat flux can induce violent boiling in the evaporator section causing blockage of returning condensate. Prolong exposure to high heat flux can also induce dry outs. There is an optimum pipe diameter related to a vapour flow such that any increase in the pipe diameter may contribute to the flooding phenomenon. An increased pipe diameter is desirable to avoid flooding. Axial heat conduction occurs along the pipe wall. The magnitude of this heat transfer compared to the heat transfer by evaporation and condensation in a thermosyphon would be comparable if the heat input is small. Generally, a small temperature difference between evaporator and condenser section of about $5^{o}C$ is required to initiate operation of the thermosyphon. This would depend on the type of fill liquid and the physical dimensions of the pipe.

2.1.2 Previous investigations on thermal performance of heat pipes and thermosyphons

Nguyen-Chi and Groll (1981) investigated the entrainment or flooding limit in a closed two-phase thermosyphon with a water-filled 20 mm OD x 17 mm ID x 2.5 m long copper thermosyphon with inner circumferential grooves. Evaporator and condenser sections were each 1.0 m long. The evaporator section was heated with electrical resistance wires and the condenser cooled via a water cooling jacket. FR was between 0.38-0.88, inclination angle from 1-80^{o}, evaporator wall temperature from 20-80 ^{o}C and power input between 100-420 W. They derived an empirical correlation to predict the maximum performance for the inclined thermosyphon and recommended further work to be performed to determine the influence of parameters like FR, aspect ratio, internal surface roughness of pipe, and type of working fluid.

Gurses and Cannistraro (1991) studied the inclination effect on water filled heat pipes for solar energy applications with an 18 mm OD x 15 mm ID x 1.93 m long copper pipe. The air-cooled condenser was 420 mm long fitted with external 400 mm diameter fins. Power input of up to 1200 W resulted in an evaporator wall temperature as high as 70 ^{o}C. They concluded that the best inclination angles are between 45-90^{o} due to entrainment limit and capillary limit, and is dependent on the power input range.

Terdtoon et al. (1996) investigated the effect of aspect ratio on the heat transfer characteristics of a two-phased closed loop thermosyphon. They used

copper pipes with 7.5, 11.1, and 25.9 mm diameter with corresponding AR values of 5, 10, 20, 30, and 40. Evaporator temperatures were kept about 10 ^{o}C and FR at 0.8. Fill liquids were R22, ethanol, and distilled water. They concluded that the best inclination angles were between 40-70^{o} depending on aspect ratio. The author determined the best inclination angles by comparing the output power at a particular angle to the output power at a vertical orientation (γ = power output at an angle/ power output at vertical). He found that refrigerant R-22 filled heat pipe peaked at γ = 1.3 at 20^{o}, ethanol filled heat pipe peaked at γ = 1.2 at 50^{o} and water filled heat pipe peaked at γ = 1.1 at 70^{o}. The authors mentioned that the aspect ratio had more effect on the performance of a thermosyphon compared to type of fill liquid or inclination.

Payaruk et al. (2000) correlated the heat transfer characteristics of an inclined, closed two-phase thermosyphon at normal operating conditions. They used pipes of 7.5, 11.1, and 25.4 mm ID with R22, R123, R134a, ethanol, and water. They also used FRs at 0.50, 0.80 and 1.00, and ARs of 5, 10, 20, 30 and 40. Inclination angles were between 10-90^{o} with incremental steps of 10^{o}. The controlled adiabatic wall temperature ranged from 0-30 ^{o}C. From their work they concluded that FR has no effect at 90^{o} but instead the type of fill liquid affected the heat transfer characteristics.

Khandekar et al. (2003) investigated the operational regimes of a heat pipe using a 2 mm ID copper heat pipe with R123, water and ethanol, and inclination angles set between 0-90^{o}. The evaporator temperature range

achieved was 100 ^{o}C at 47 W with water and 22 W with ethanol. The optimal FR was found to be between 0.25-0.65 depending on fill liquid type.

Noie (2005) investigated the heat transfer characteristics of water filled two-phase closed thermosyphons with 25 ID x 32 mm OD copper pipes. Each thermosyphon was 980 mm long with a 51 mm OD x 380 mm long water cooled jacket. Electrical resistance heating was applied with input power varying from 100-900 W. Evaporator wall temperature ranged from 100-180 ^{o}C. ARs of 7.45, 9.80, and 11.80 were obtained by varying the evaporator and adiabatic lengths. Only the evaporator section was insulated with 55 mm thick rock wool. FRs were kept at 0.30, 0.60, and 0.90. The results showed that evaporator wall temperature distribution was almost isothermal especially at the low power input. Also, for each thermosyphon, the maximum evaporator wall temperature attained is dependent on a combination of FR and AR; viz. AR = 7.45 with FR = 0.90 and AR = 11.8 with FR = 0.60. The author compared his heat transfer coefficients for AR = 9.8 at the various FRs and concluded that they were in reasonable agreement with the empirical correlations by Rohsenow (1962) and Imura et al. (1977).

Ong et al. (2014) investigated the axial temperature distribution and performance of R410a and water filled thermosyphons with various fill ratios (0.25, 0.40, 0.66, and 0.93) and inclinations (30, 50, 70, and 90^{o}) using a 38 mm OD x 807 mm long copper heat pipe. They varied the heat input from 100-830 W which generated evaporator wall temperatures of up to 65 ^{o}C. They found that the performance increased as FR and inclination was reduced. They

also concluded that the R410a filled thermosyphon performed better at all inclinations and fill ratios between 30-65 ^{o}C.

Guo and Nutter (2009) separated the evaporator section of a thermosyphon from the condenser section with a non-conducting adiabatic piece to examine the effect of axial conduction along a heat pipe wall. They noted that axial conduction along a continuous thermosyphon wall causes non-uniform wall temperatures along the evaporator section up to ±5 ^{o}C. The evaporator section exhibited a more uniform temperature distribution, within ±2 ^{o}C, once separated by a non-conductive wall material from the condenser sections.

Previous investigations by Ong and Haider (2003) on low temperature R134a filled thermosyphons showed that a minimum of 3 ^{o}C was required for the thermosyphon to operate.

2.1.3 Theoretical simulation of thermosyphon

Wrobel, Fadhl and Jourhara (2013) modelled the temperature distribution in a two-phase closed thermosyphon using experimental and simulated data. In their experimental phase they used a 22 mm OD x 500 mm long copper heat pipe with power inputs between 50-500 W, a fill ratio of 0.5 and a cooling jacket for cooling. The evaporator wall temperature was around 70-97 ^{o}C while the condenser cooling water was kept between 39-57 ^{o}C. In the simulation phase the authors used a two-dimensional model with ANSYS

FLUENT to simulate the two-phase flow and heat transfer phenomena in a thermosyphon. The author used different mesh sizes to test grid independence. The authors found that mesh sizes from 19,603-87,800 showed little to no difference between temperature readings in the condenser and evaporator section respectively. They managed to simulate the boiling pool and condensing film as seen in Figure 2.1. The CFD simulation of the overall thermal resistance was 50-60 % similar to the experimental results. The experimental results showed a decrease from 0.3 to 0.1 K/W (K/W: Kelvin/Watt) and CFD showed a decrease from 0.5 to 0.2 K/W.

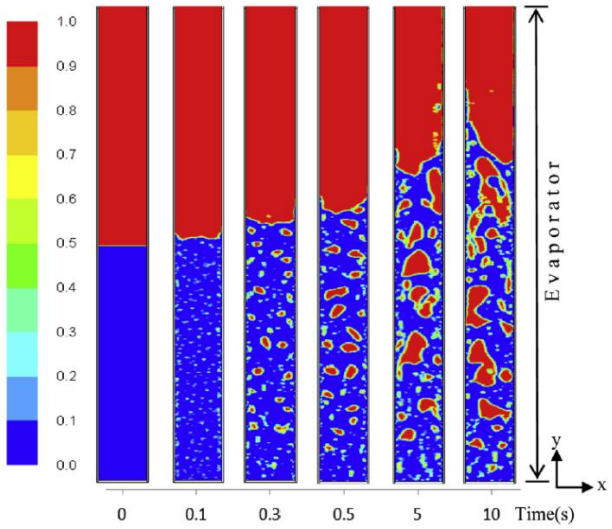

Figure 2.1 Contours of volume fraction of pool boiling in the evaporator section at different times (Wrobel, Fadhl and Jouhara 2013)

Liu et al. (2009) numerically simulated and experimented on a flat two-phase thermosyphon made of quartz glass and brass pieces measuring 85 mm OD x 6 mm long (quartz glass). The top and bottom of the thermosyphon was made of brass,3 mm thick, and the heat source was 30 mm OD with water as a working fluid. The evaporator section was made up of four heating rods

providing heat flux between $0.25x10^5$ and $0.99x10^5$ W/m^2 which resulted in a maximum temperature of 60 ^oC. The condenser section was a fan blowing vertically onto the cooling surface. A two-dimensional heat and mass transfer model was used to simulate the vapour velocity and temperature distribution as seen in Figure 2.2. The authors found that boiling of the nucleate and maximal vapour velocity happens at the heating area and seldom spread to the side walls of the thermosyphon. There was an uneven spreading of heat at the evaporator, creating heat spots, which reduced the efficiency of the heat pipe.

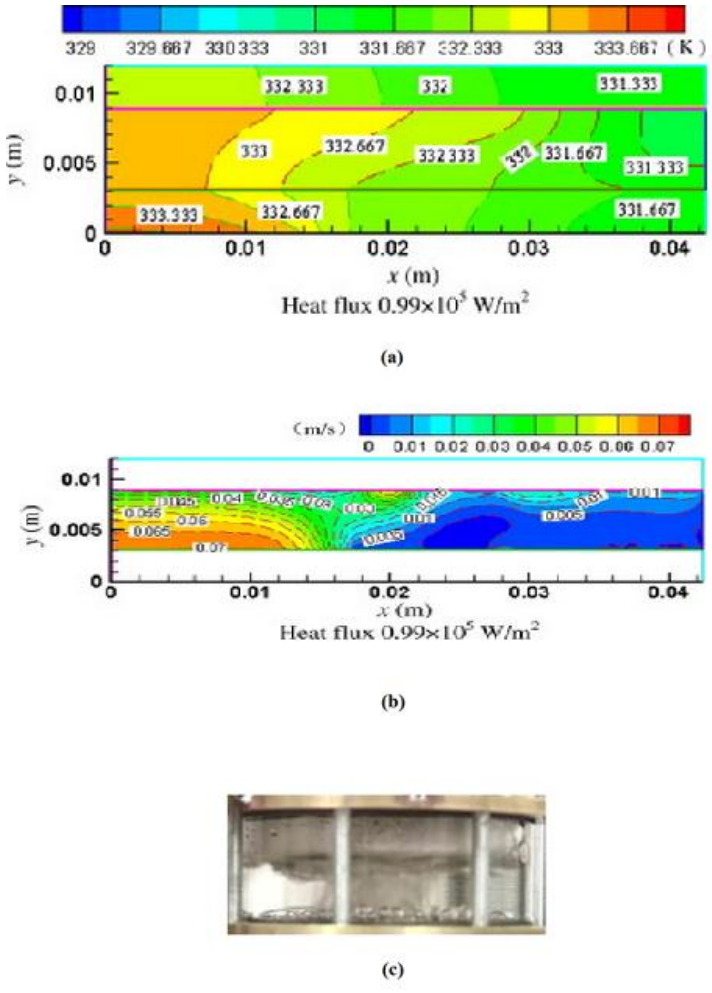

Figure 2.2 (a) Temperature distribution of a two-phase thermosyphon (b) The distribution of vapor y-velocity (c) Photograph of boiling phenomenon

Wrobel, Fadhl and Jouhara (2015) modelled a two-phase thermosyphon charged with R134a and R404a with slight modifications to their earlier work (Wrobel et al., 2013). A different fill liquid, and improved boundary condition assumptions were now used. Comparing Figure 2.1 and Figure 2.3, the difference observed was the nucleating bubble sizes. Water exhibits a larger bubble size as opposed to refrigerants which exhibit smaller bubble sizes. This was attributed to the physical properties of the fill liquid itself. Using FLUENT the authors successfully simulate the complex boiling and condensing process occuring within a thermosyphon.

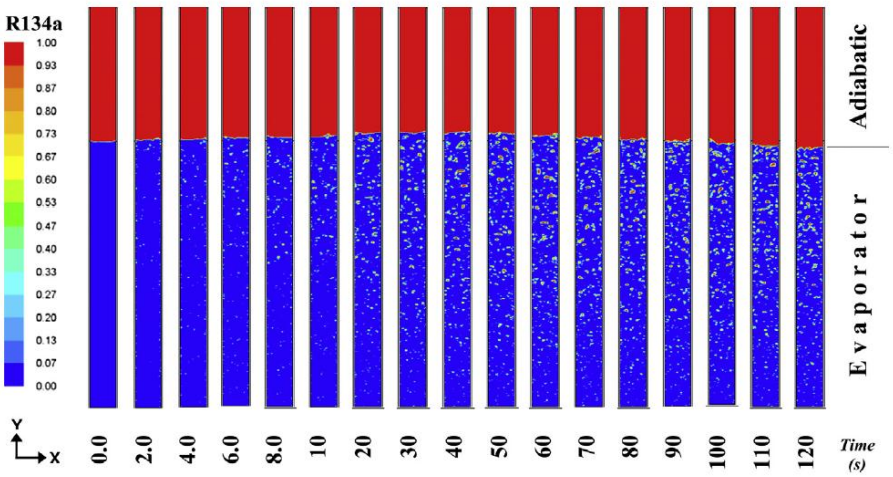

Figure 2.3 Pool boiling process in the evaporator section for an R134a-filled thermosyphon (Wrobel, Fadhl and Jouhara 2015)

Rahimi, Alizadehdakhel and Alsairafi (2010) modelled the flow and heat transfer in a thermosyphon. The authors used a 19 mm OD x 1000 mm long copper heat pipe to verify their CFD findings. The power input was between 350-700 W and FR was between 0.3 and 0.8. The best performing FR was in the order of 0.5, 0.8 and 0.3 based on the experimental results. The

authors used FLUENT to model their CFD and the volume of fluid (VOF) technique was used to simulate the boiling and condensing phases inside a thremosyphon. The results obtained from the CFD model and the experimental results conformed within ± 10 %.

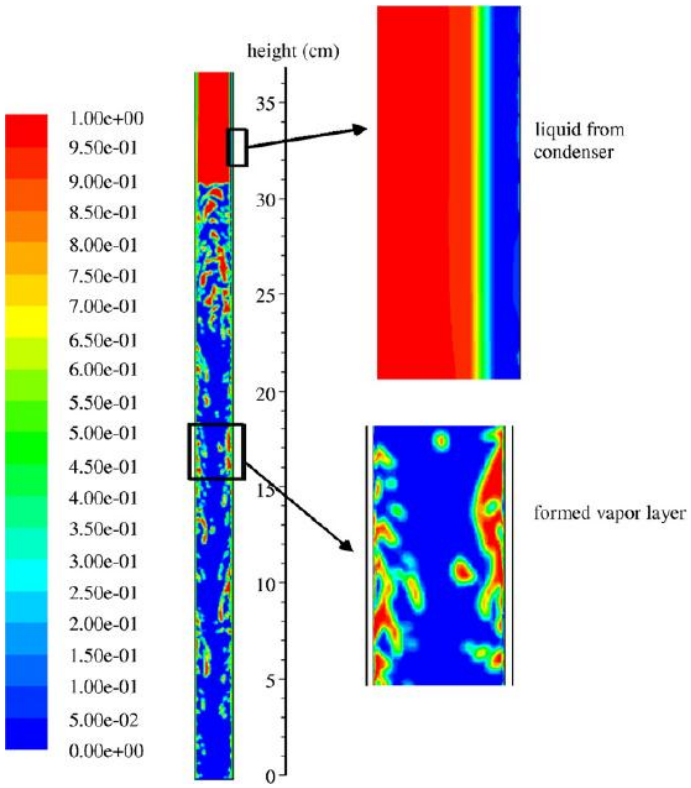

Figure 2.4 Contour plots of vapor volume fraction in the evaporation section (FR=0.8) (Rahimi, Alizadehdakhel and Alsairafi 2010)

Kafeel and Turan (2014) simulated the response of a thermosyphon under pulse heat input conditions. Kafeel and Turan (2014) reached similar consensus with the work of Wrobel (2013) and Wrobel (2015) in which mesh size was tested grid independent. Kafeel and Turan (2014) used the Eularian two-fluid methodology to simulate the response of the thermosyphon. Figure

2.5 shows that the experimental and simulation results are very similar with a ± 10 % difference.

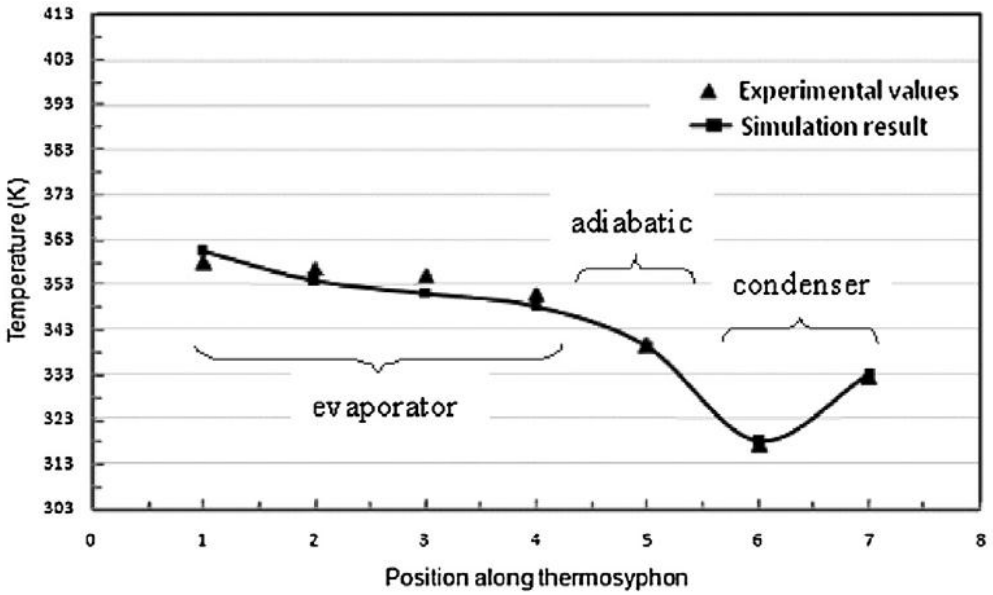

Figure 2.5 Temperature profile along the outer walls of thermosyphon (Kafeel and Turan 2014)

2.2 Theoretical model

2.2.1 Model description

A simple theoretical model for the thermosyphon is proposed in Figure 2.6 (a) is proposed. The model used to predict the performance of the thermosyphon heat pipe heat exchanger (THPHE) system is based on the thermal resistance network. The thermal resistance network for the model is shown in Figure 2.6 (b). The model assumed no heat loss to the surroundings.

Hence power input at the evaporator section is equaled to the heat removed at the condenser section. It is further assumed that there are no heat transfer along the pipe wall, $R_{wall} = 0$.

2.2.2 Resistance network

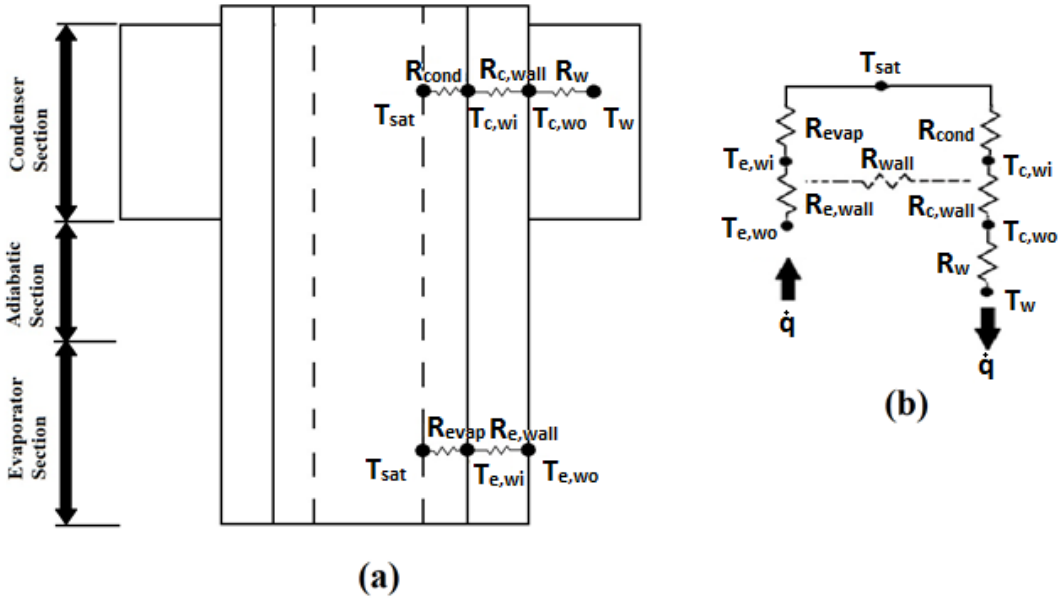

Figure 2.6 (a) Theoretical model (b) Thermal resistance network

The total resistance to the heat transfer, ΣR, is found by adding up the individual resistance to heat flow. The individual resistances are defined and calculated as follows:

Evaporator wall: $$R_{e,wall} = \frac{\ln\left(\frac{D_O}{D_i}\right)}{2\pi k_{wall} L_e} \quad [K/W]$$ **Equation 1**

where k_{wall} = 401 W/mK

Boiling at evaporator: $R_{evap} = \frac{1}{(\pi D_i L_e h_{evap})}$ [K/W] **Equation 2**

where h_{evap} is obtained from the experiment in phase A

Condensation at condenser: $R_{cond} = \left(\frac{1}{\pi D_i L_c h_{cond}} \right)$ [K/W] **Equation 3**

where h_{cond} is obtained from the experiment in phase A

Condenser wall: $R_{c,wall} = \frac{\ln\left(\frac{D_o}{D_i}\right)}{2\pi k_{wall} L_c}$ [K/W] **Equation 4**

Ext film at condenser: $R_w = \frac{1}{(\pi D_o L_c h_w)}$ [K/W] **Equation 5**

where h_w = 13.1 W/m^2 K

The temperatures at the respective interfaces in Figure 2.6 can be calculated from the following equations; where ΔT_m is the mean difference between the evaporator and condenser section.

$$T_{e,wi} = T_{e,wo} - \frac{R_{e,wall}}{\sum R}\Delta T_m \qquad [^{\circ}\mathrm{C}] \qquad \textbf{Equation 6}$$

$$T_{sat} = T_{e,wo} - \frac{R_{e,wall} + R_{evap}}{\sum R}\Delta T_m \qquad [^{\circ}\mathrm{C}] \qquad \textbf{Equation 7}$$

$$T_{c,wi} = T_{e,wo} - \frac{R_{e,wall} + R_{evap} + R_{cond}}{\sum R}\Delta T_m \qquad [^{\circ}\mathrm{C}] \qquad \textbf{Equation 8}$$

$$T_{c,wo} = T_{e,wo} - \frac{R_{e,wall} + R_{evap} + R_{cond} + R_{c,wall}}{\sum R}\Delta T_m \qquad [^{\circ}\mathrm{C}] \qquad \textbf{Equation 9}$$

$$T_{w} = T_{e,wo} - \frac{R_{e,wall} + R_{evap} + R_{cond} + R_{c,wall} + R_{w}}{\sum R}\Delta T_m \qquad [^{\circ}\mathrm{C}] \qquad \textbf{Equation 10}$$

The simulation is started by inserting known variables such as the evaporator temperature (T_e), the pipe outer diameter (D_o), pipe inner diameter (D_i), mass flow rate of water, water inlet temperature (T_{wi}), fill ratio (FR), evaporator length (L_e), condenser length (L_c), adiabatic length (L_{ad}), power input (P), heat transfer coefficient of water (h_w) and thermal conductivity of copper (k_{wall}). The evaporator and condenser heat transfer coefficient are obtained from the experiment in phase A and tabulated in Appendix A. Different values of heat transfer coefficient are used depending on the temperature range and power input range which varies from 50-600 W/m^{2}K for h_e and 1000-6000 W/m^{2}K for h_c.

Once the variables are inserted into the simulation model using the thermal resistance network, the individual resistances and interface temperature can then be predicted. With these results a simulated run can be produced with the given inputs. The simulation is simply mathematical models which are presented in Equation 1 through 10.

2.3 Experimental investigation

2.3.1 Experimental apparatus

The experimental set up is shown in Figure 2.8. Three thermosyphons were constructed from 305 mm long copper tubes with different diameters as shown in Table 1. Aspect ratios (ARs), defined as the ratio of evaporator length (L_e)/evaporator inner diameter (D_i) equal to 10.0, 6.7 and 5.0 were obtained for the three units. The thermosyphons were filled with distilled water and the non-condensable gasses were removed using a vacuum pump. The thermosyphons were then covered with 100 mm thick rockwool insulation. Fill ratio (FR) was defined as the ratio of liquid/evaporator internal volume. Fill ratios were kept at 0.25, 0.50, 0.75, and 1.00. Cooling was effected by a 50 mm OD x 34 mm ID x 127 mm long concentric water cooling jacket surrounding the condenser section. Coolant water was circulated by a 20 W submersible water pump. Coolant inlet temperature varied between 24-30 ^{o}C and flow-rate was kept between 0.003 – 0.05 kg/s (± 0.001 kg/s). Heating was provided by nichrome wire wound round the evaporator section. Power (P) was regulated using an AC-transformer and varied from 5-405 W (± 3.5 %). Type T copper-constantan

thermocouples (± 0.5 ^{o}C) were mechanically attached to the thermosyphon to measure the temperature at the evaporator (T_{e1}–T_{e4}) and adiabatic (T_{ad1}, T_{ad2}) wall sections at locations shown in Figure 2.9. Temperature at the end-of-condenser pipe wall (T_p), saturation (T_{sat}), coolant inlet (T_{wi}) and outlet (T_{wo}), ambient (T_a) and external insulation surface (T_{ins1}, T_{ins2}) were logged at 1 min intervals. Saturation pressure (P_{sat}) was noted before and after each experiment. Tests were carried out at various thermosyphon inclinations of 23^{o}, 45^{o}, 68^{o}, and 90^{o} to the horizontal. Each series was repeated 3 times in order to ensure repeatability. The experimental results were found to be reproducible to within ± 3 ^{o}C.

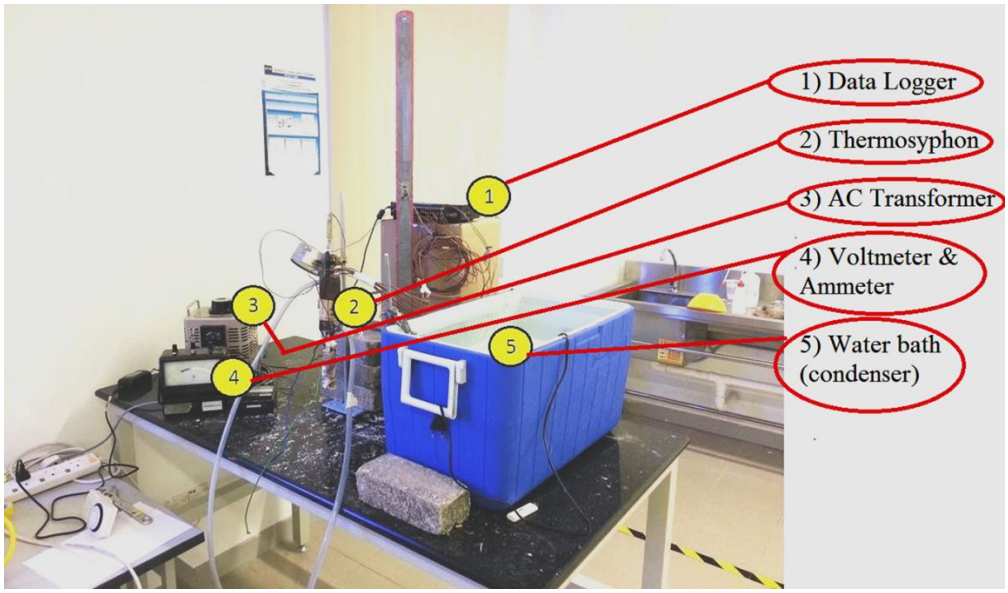

Figure 2.7 Photograph of experimental set-up

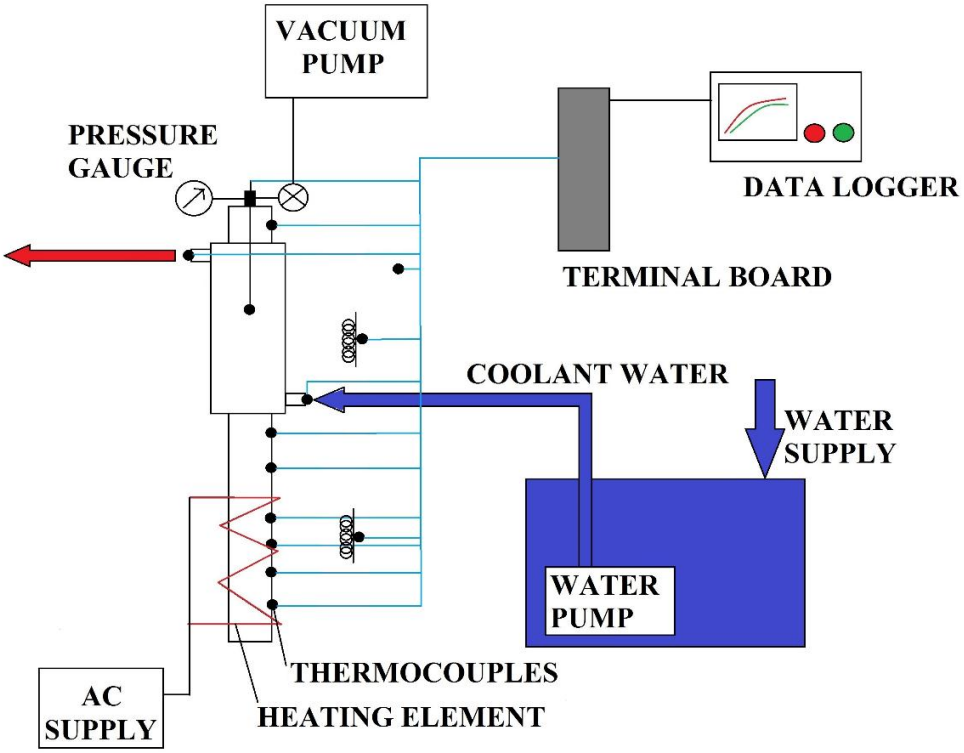

Figure 2.8 Experimental Set-up

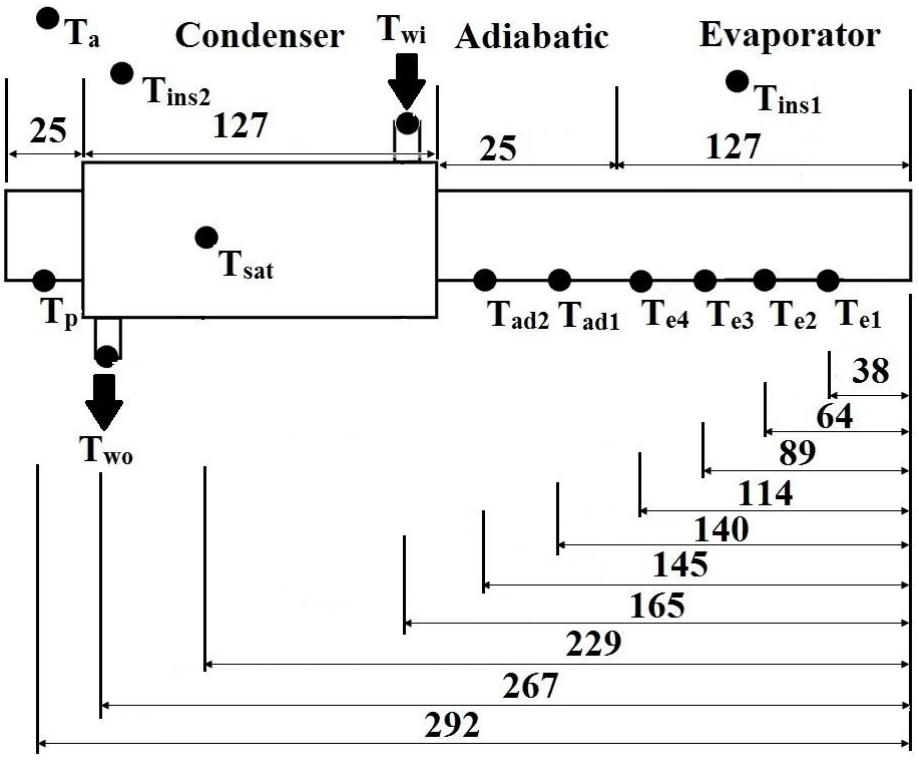

Figure 2.9 Dimensions and location of thermocouples in thermosyphon

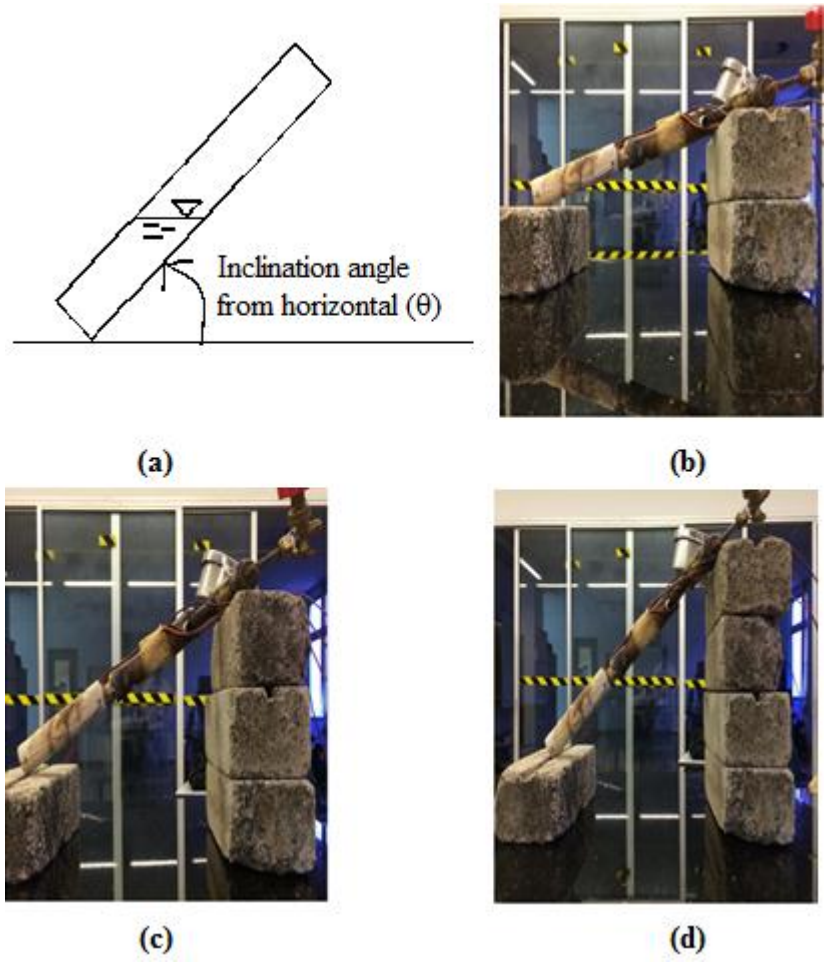

Figure 2.10 Photograph of thermosyphon at different angles. (a) inclination angle measured from horizontal (b) 23^{o} from horizontal (c) 45^{o} from horizontal (d) 68^{o} from horizontal

Table 1 Dimensions of thermosyphons

HP #	D_o (mm)	D_i (mm)	L_e (mm)	L_{ad} (mm)	L_c (mm)	L_e/D_i AR	P/A_e (kW/m^2)
1	15.8	12.7	127	25.4	127	10	10-30
2	22.2	19.1	127	25.4	127	6.7	5-48
3	28.6	25.4	127	25.4	127	5	4-24

2.3.2 Experimental procedure

The effect of coolant flow rates were investigated first by varying the coolant flow rates between 0.003 – 0.05 kg/s (± 0.001 kg/s). The power was varied between 5 - 405 W for each coolant flow rate. The fill ratio was kept at 1.0 and inclination angle of 90^{o}. The only fill liquid type used for phase A was distilled water.

The effect of fill ratio was investigated next. The FR were kept at 0.25, 0.50, 0.75 and 1.0. The coolant flow rate was kept constant at 0.05 kg/s, power was varied between 5 – 405 W, and inclination angle of 90^{o} for each FR.

The effect of thermosyphon inclination angle was investigated next. The thermosyphon inclination angle were tested at 23^{o}, 45^{o}, 68^{o} and 90^{o}. At each inclination angle the FR were kept at 0.25, 0.50, 0.75 and 1.0. Power was varied between 5 – 405 W for each setting. The coolant flow rate was kept constant throughout at 0.05 kg/s.

The effect of aspect ratio were investigated as well. Three different diameter pipes were selected with a fix length of 305mm. The AR used were 10.0, 6.7 and 5.0 respectively. The FR was fixed at 1.0, the coolant mass flowrate at 0.05 kg/s and inclination angle of 90^{o}.

Each run was performed three times for reproducibility and the summary of experimental runs performed is tabulated in Table 2.

Table 2 Summary of experimental runs conducted for performance of heat pipes at high temperature, Phase A

Runs	HP#	Power (W)	$\dot{m}_w$ (kg/s)	θ (^{o})	FR	Heat flux (W/m^2)
A/1	2	5, 18, 38, 70, 113, 210, 360	0.003	90	1.0	660 - 41,400
A/2			0.019			
A/3			0.05			
A/4	2	5, 18, 38, 70, 113, 210, 360	0.05	90	0.75	660 - 41,400
A/5					0.5	
A/6					0.25	
A/7	2	5, 18, 38, 70, 113, 210, 360	0.05	68	1.0	660 - 41,400
A/8					0.75	
A/9					0.5	
A/10					0.25	
A/11	2	5, 18, 38, 70, 113, 210, 360	0.05	45	1.0	660 - 41,400
A/12					0.75	
A/13					0.5	
A/14					0.25	
A/15	2	5, 18, 38, 70, 113, 210, 360	0.05	23	1.0	660 - 41,400
A/16					0.75	
A/17					0.5	
A/18					0.25	
A/19	1	50, 100, 150	0.05	90	1.0	9,500 - 29,600
A/20	3	50, 90, 130, 250	0.05	90	1.0	4,400 - 24,200

2.3.3 Theoretical calculations

The following were the equations used in phase A to evaluate the thermal performance of a heat pipe along with the heat transfer coefficient. In

order to compare the performances of various heat pipes, the heat transfer rates could be plotted against the temperature difference between the evaporator and condenser sections. This would give an indication of the overall heat pipe thermal resistance, R_{HP}. A high R_{HP} would indicate a poor performing HP and vice versa. A lower R_{HP} value indicates a better performing heat pipe as there is lower resistance towards heat transfer. When there is a lower resistance for heat transfer, heat is more readily transported from one end to the other.

Power input (P) or heat supplied at the evaporator section ($\dot{q}_w$) was assumed equal to the heat removed by the cooling water ($\dot{q}_c$), viz.:

$$P = \dot{q}_C = \dot{q}_W = \dot{m}_w C_{pw}(T_{wo} - T_{wi}) \quad [\mathrm{W}] \qquad \textbf{Equation 11}$$

The condenser wall surface temperature was calculated from

$$T_C = \frac{T_p + T_{ad1}}{2} \quad [^{\circ}\mathrm{C}] \qquad \textbf{Equation 12}$$

The evaporator wall surface temperature can be obtained from the bulk temperature, defined as

$$T_{e,b} = \frac{\int_0^{x=L_e} T_e dx}{L_e} \quad [^{\circ}\mathrm{C}] \qquad \textbf{Equation 13}$$

or from a simple arithmetic mean

$$T_{e,m} = \frac{T_{e1} + T_{e2} + T_{e3} + T_{e4}}{4} \quad [^{\circ}\mathrm{C}] \qquad \textbf{Equation 14}$$

The operating temperature differences between evaporator and condenser sections could be defined by either the bulk temperature difference

$$\Delta T_b = T_{e,b} - T_c \quad [^{\circ}\mathrm{C}] \qquad \textbf{Equation 15}$$

or from the mean temperature difference

$$\Delta T_m = T_{e,m} - T_c \quad [^{\circ}\mathrm{C}] \qquad \textbf{Equation 16}$$

The mean coolant water temperature was calculated from the average inlet and outlet water temperatures as

$$T_w = \frac{T_{wo} + T_{wi}}{2} \quad [^{\circ}\mathrm{C}] \qquad \textbf{Equation 17}$$

The evaporator heat transfer coefficient was calculated from

$$h_{evap} = \left(A_e \left[\frac{(T_e - T_{sat})}{P} - \frac{\ln(d_O/d_i)}{2\pi k_{wall} L_e} \right] \right)^{-1} \quad [\mathrm{W/m^2K}] \qquad \textbf{Equation 18}$$

The condenser heat transfer coefficient was calculated from

$$h_{cond} = \left(A_e \left[\frac{(T_{sat} - T_C)}{P} - \frac{\ln(d_O/d_i)}{2\pi k_{wall} L_C} \right] \right)^{-1} \quad [W/m^2K] \qquad \textbf{Equation 19}$$

The Reynolds number was calculated from

$$\mathrm{Re} = \frac{QD}{\upsilon A} \qquad \textbf{Equation 20}$$

Where Q is the volumetric flowrate, D is the inner pipe diameter, υ is the kinematic viscosity and A is the cross-sectional area of the pipe.

The kinematic viscosity is calculated from

$$\upsilon = \frac{\mu}{\rho} \qquad \textbf{Equation 21}$$

Where μ is the dynamic viscosity of the fluid (μ_{water} = 8.94 x10^{-4}kg/m s) and ρ is the density of the fluid (ρ_{water} = 999.97 kg/m^3).

The performance of a thermosyphon could be gauged from the overall resistance (R_{HP}), defined by

$$R_{HP} = \frac{\Delta T}{P} \quad [K/W] \qquad \textbf{Equation 22}$$

2.3.4 Experimental results

The axial wall temperature distribution for runs A/1 to A/20 are shown in Figure 2.11 to Figure 2.30.

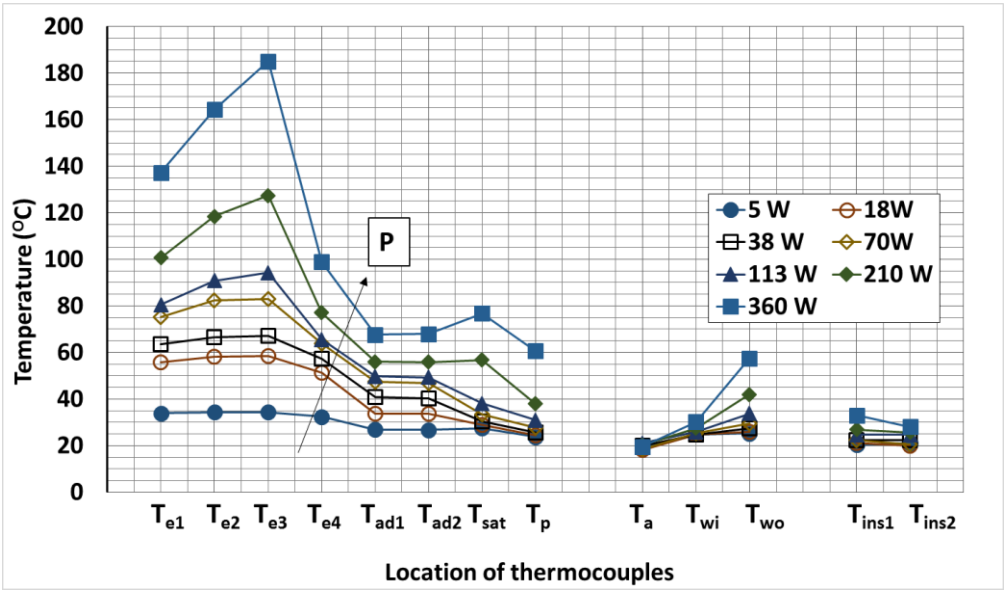

Figure 2.11 Axial wall temperatures (Run A/1)

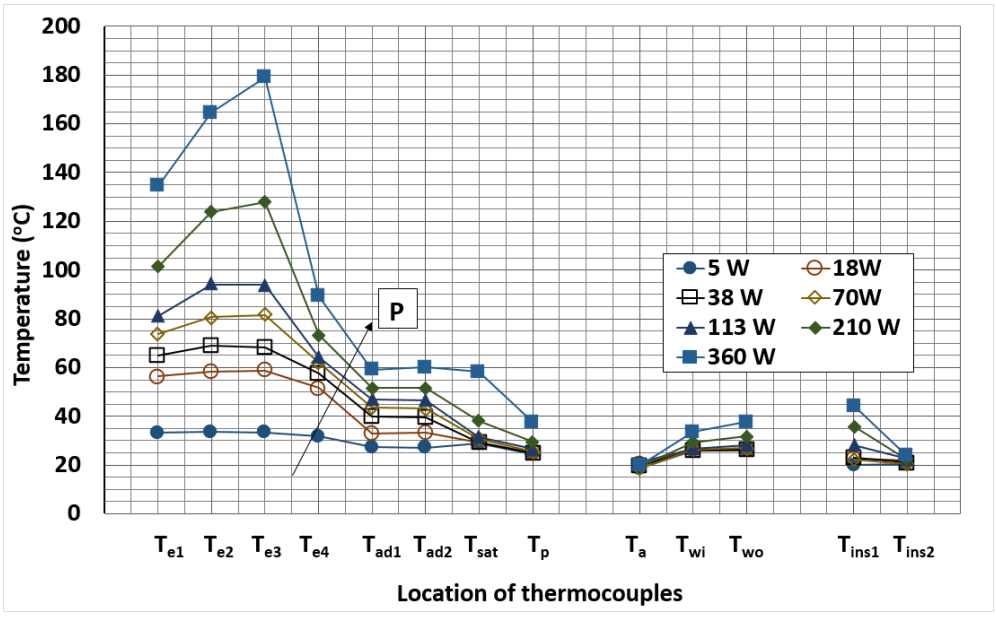

Figure 2.12 Axial wall temperatures (Run A/2)

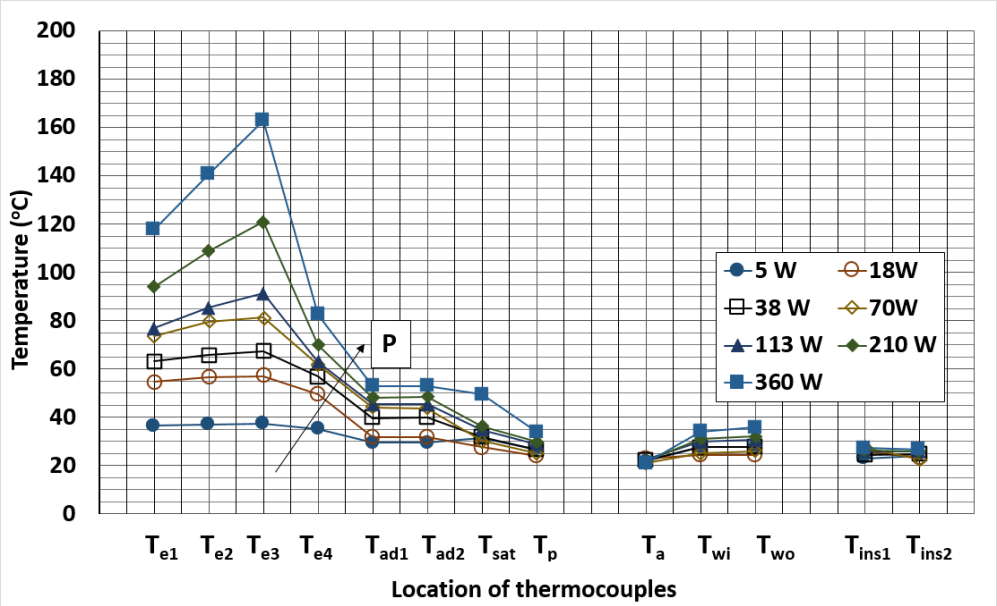

Figure 2.13 Axial wall temperature (Run A/3)

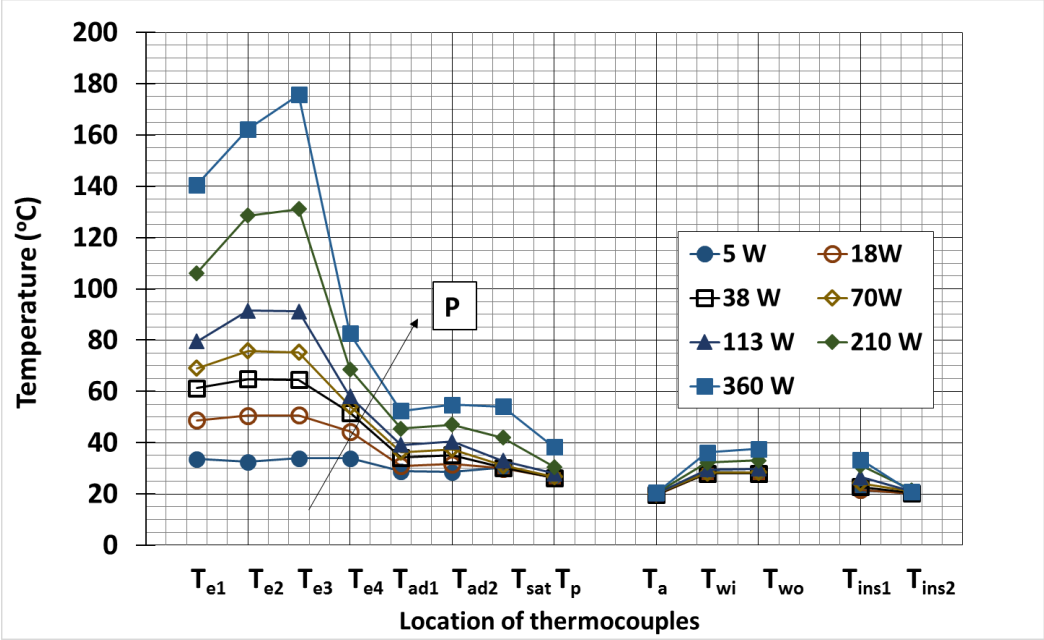

Figure 2.14 Axial wall temperature (Run A/4)

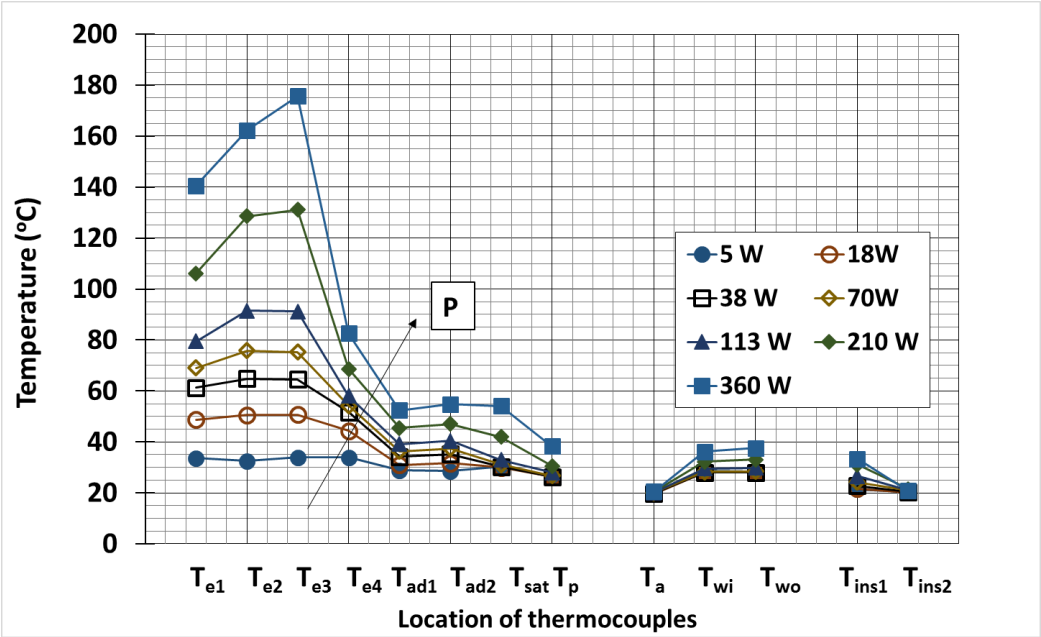

Figure 2.15 Axial wall temperature (Run A/5)

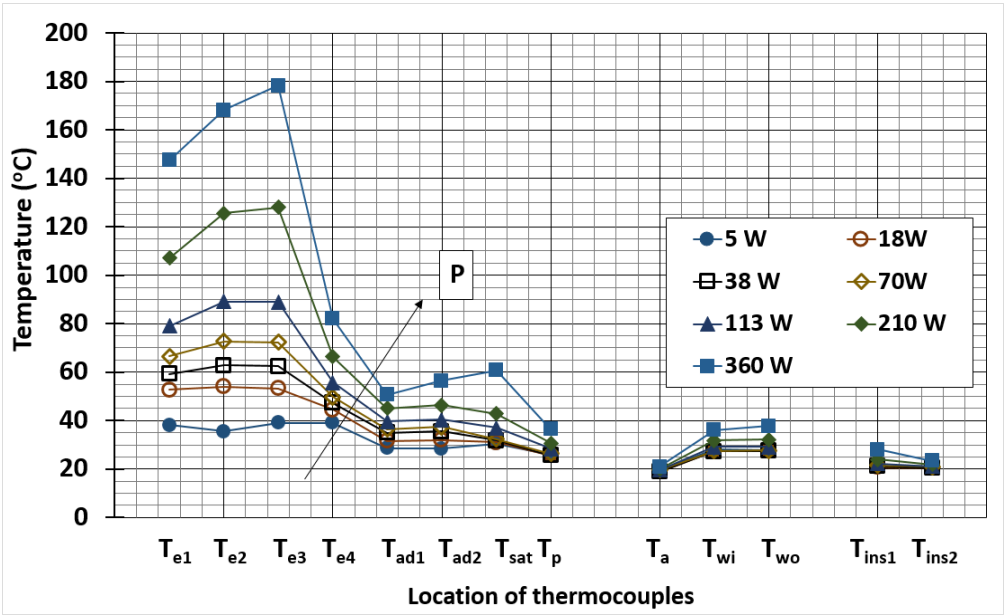

Figure 2.16 Axial wall temperature (Run A/6)

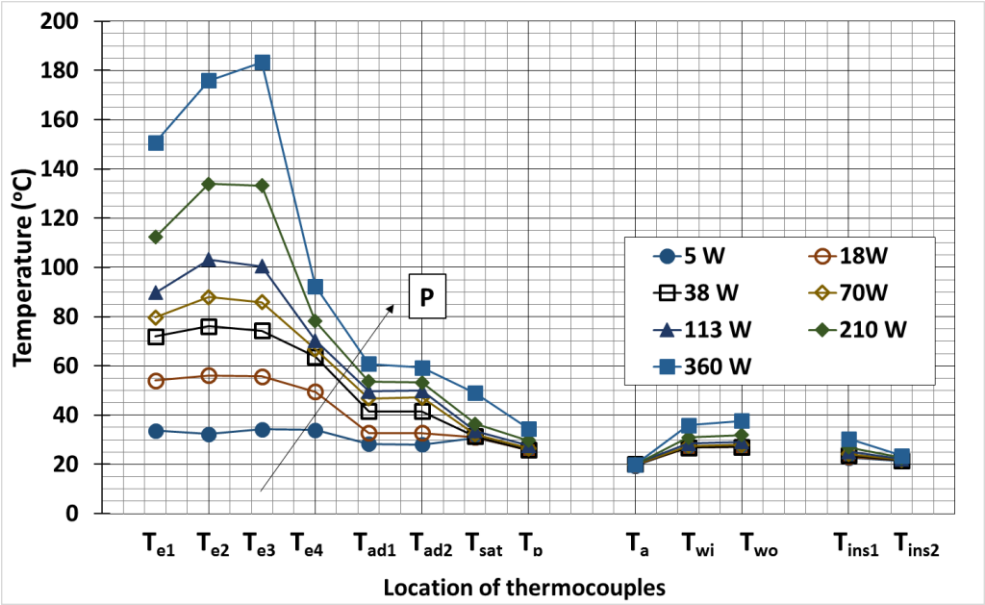

Figure 2.17 Axial wall temperature (Run A/7)

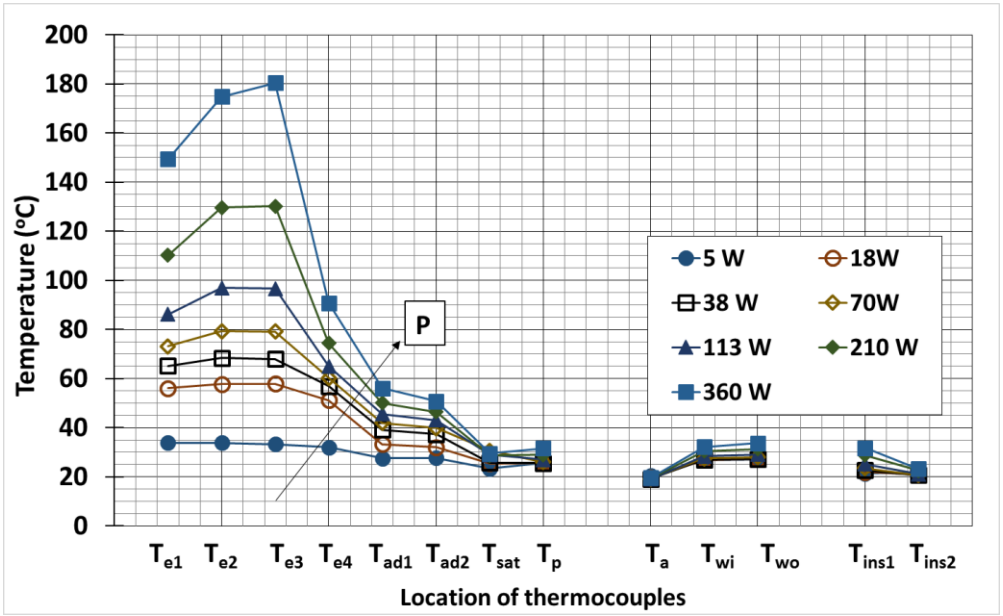

Figure 2.18 Axial wall temperature (Run A/8)

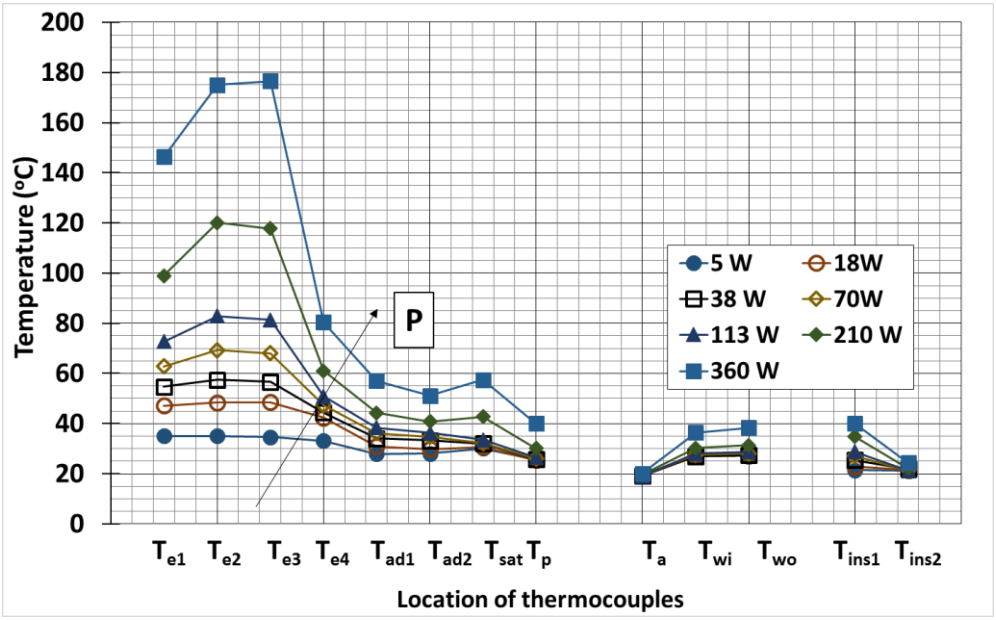

Figure 2.19 Axial wall temperature (Run A/9)

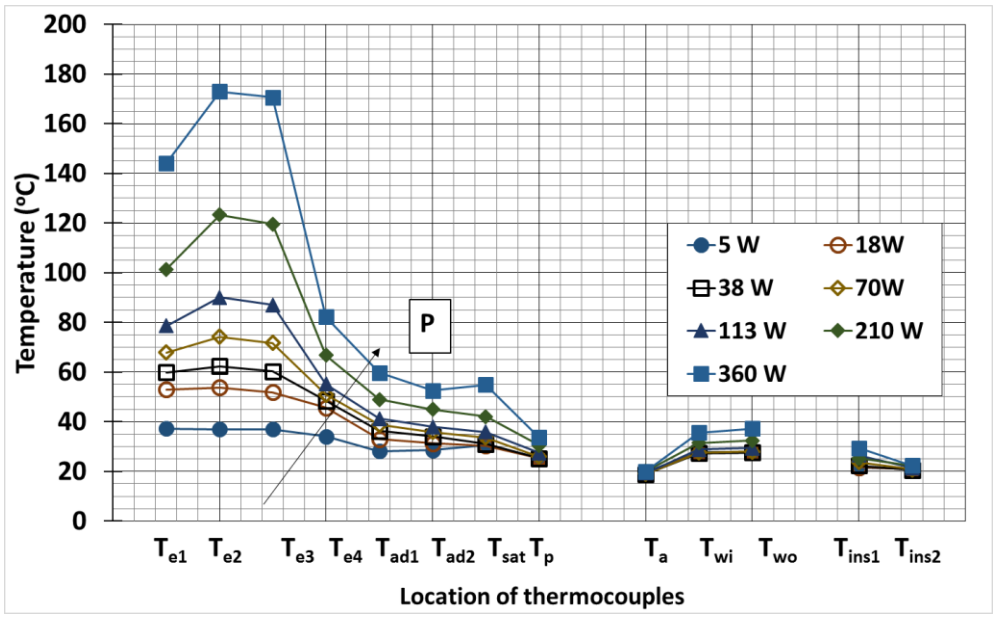

Figure 2.20 Axial wall temperature (Run A/10)

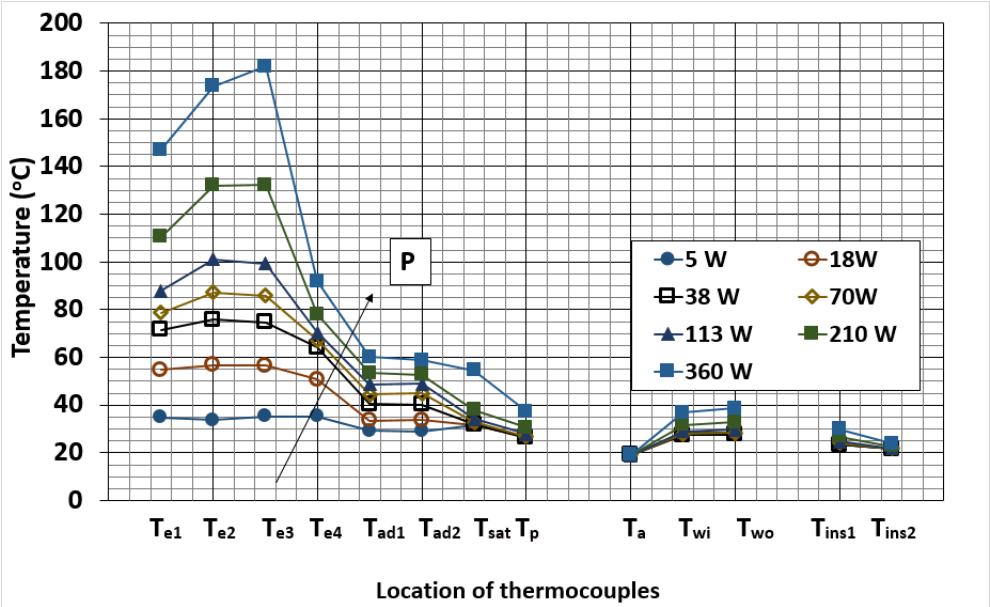

Figure 2.21 Axial wall temperature (Run A/11)

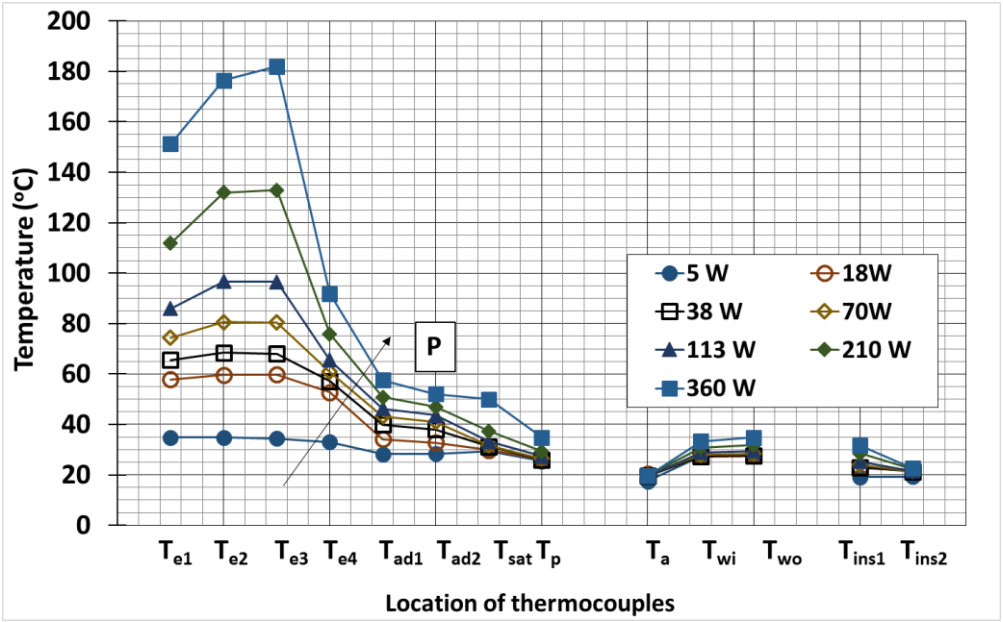

Figure 2.22 Axial wall temperature (Run A/12)

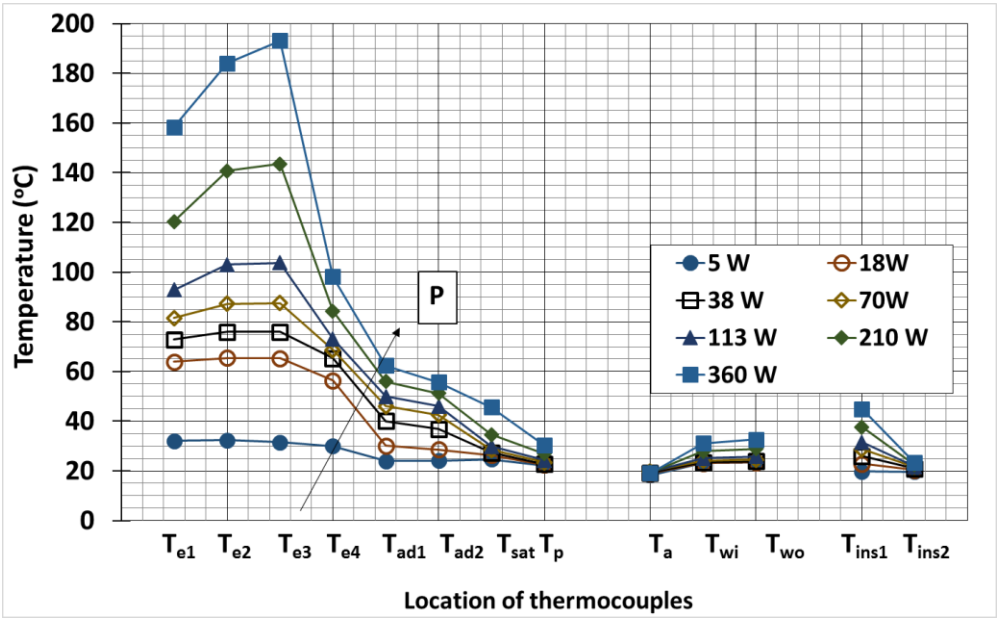

Figure 2.23 Axial wall temperature (Run A/13)

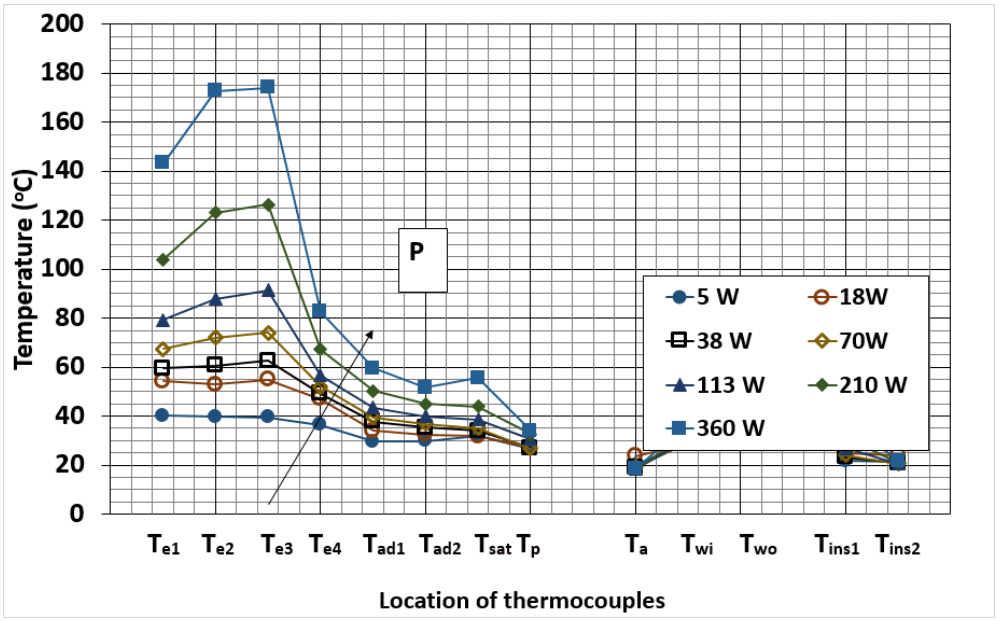

Figure 2.24 Axial wall temperature (Run A/14)

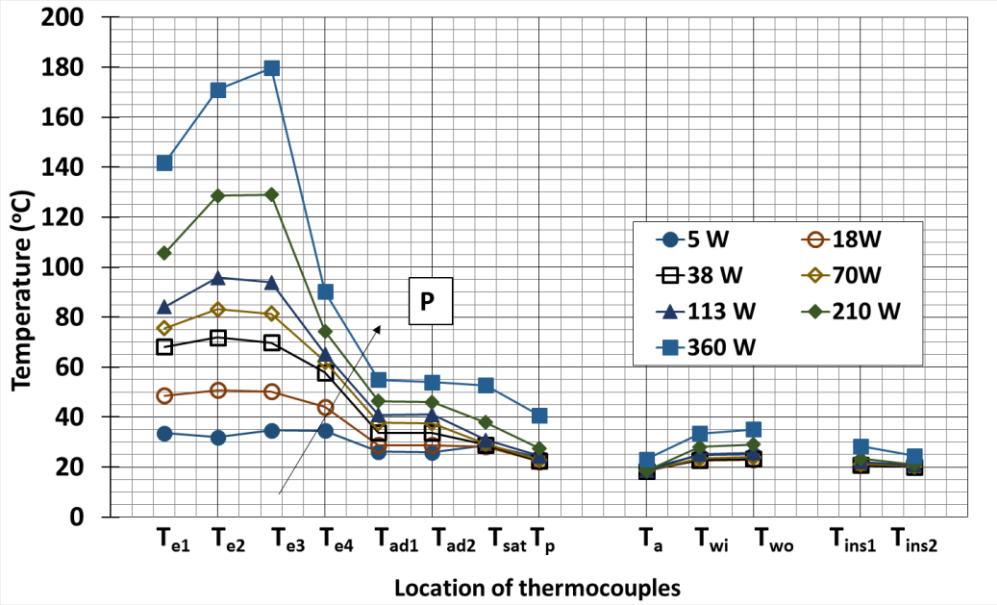

Figure 2.25 Axial wall temperature (Run A/15)

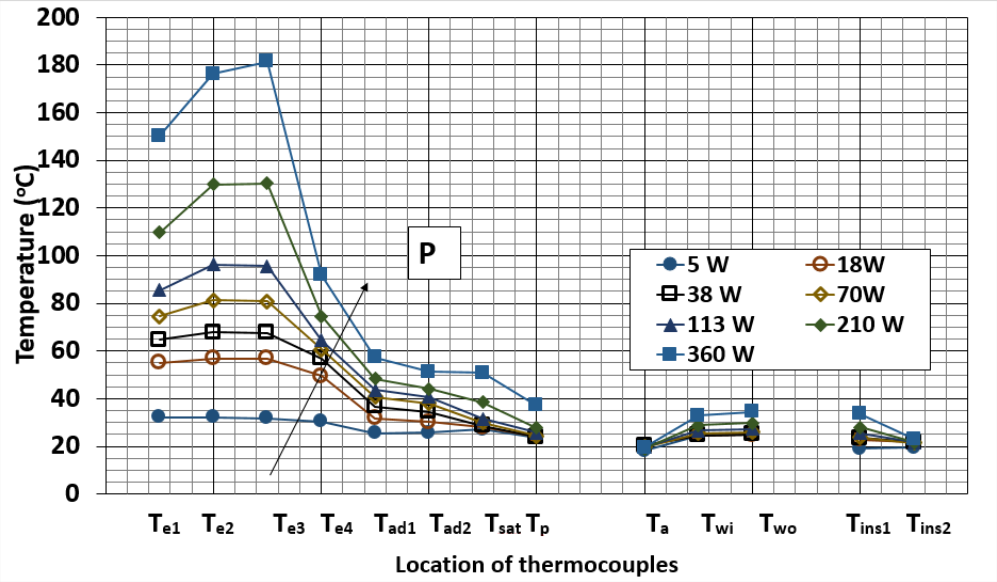

Figure 2.26 Axial wall temperature (Run A/16)

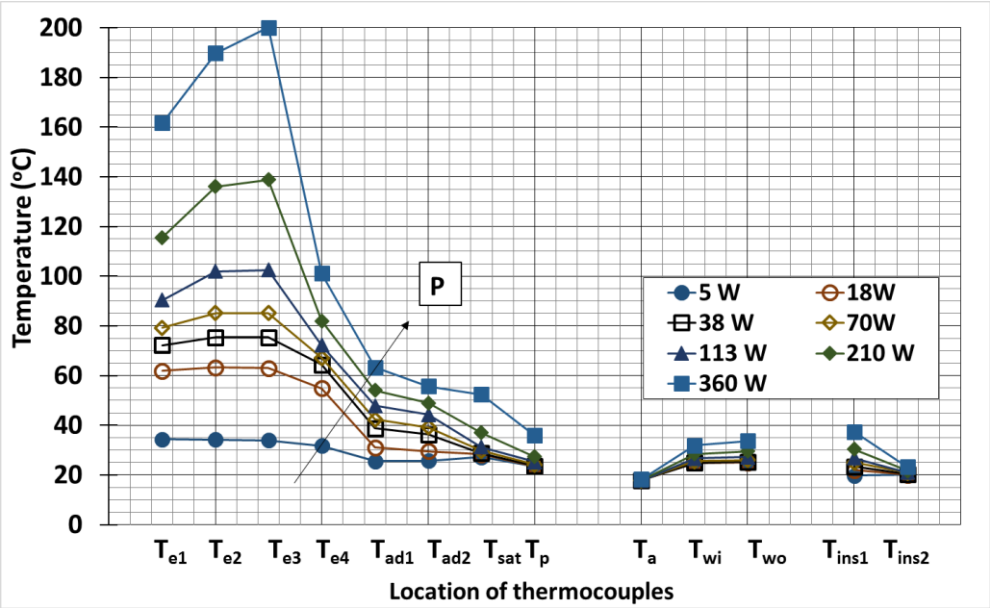

Figure 2.27 Axial wall temperature (Run A/17)

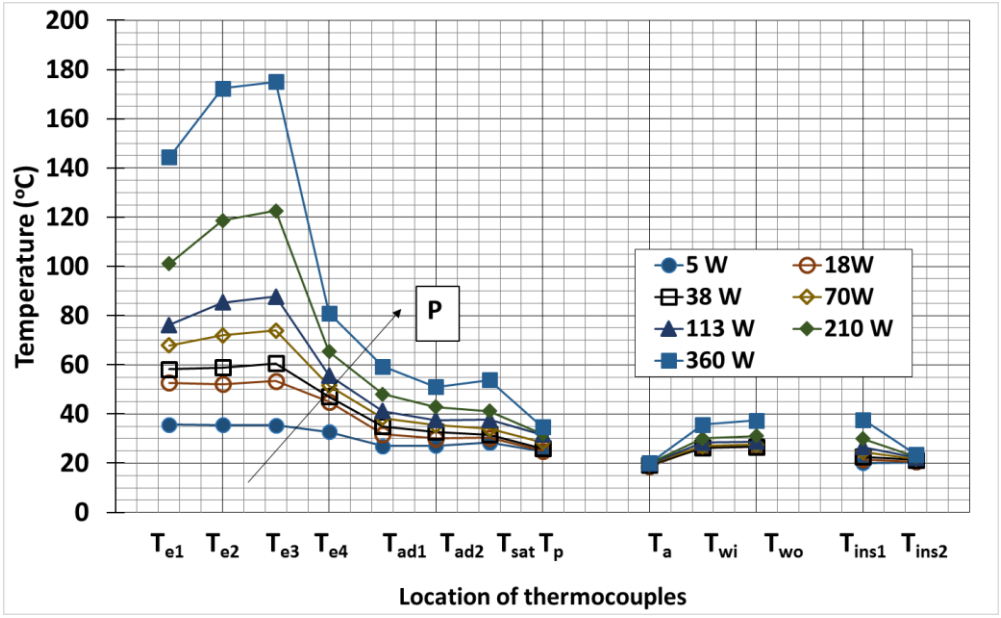

Figure 2.28 Axial wall temperature (Run A/18)

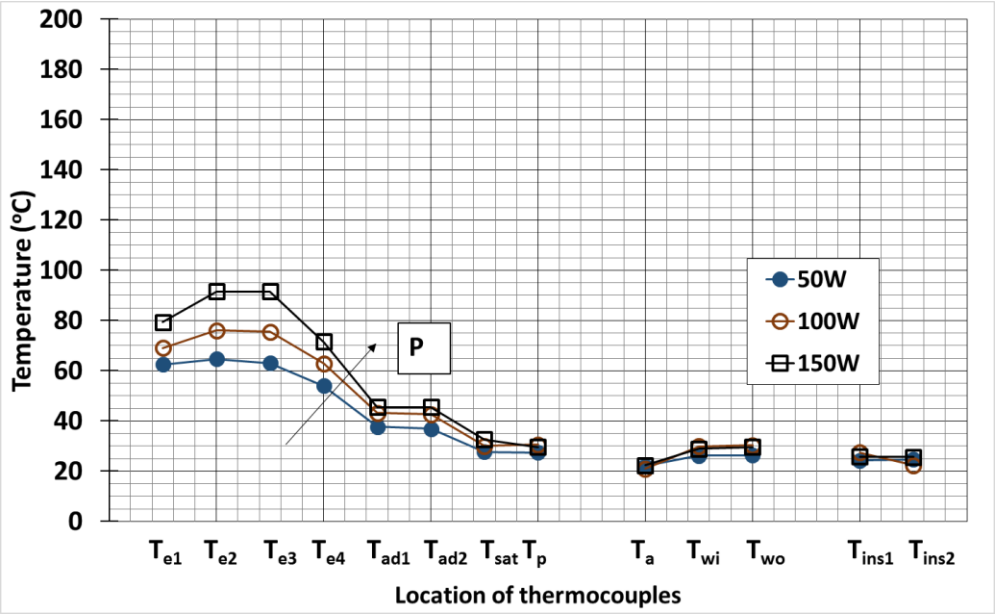

Figure 2.29 Axial wall temperature (Run A/19)

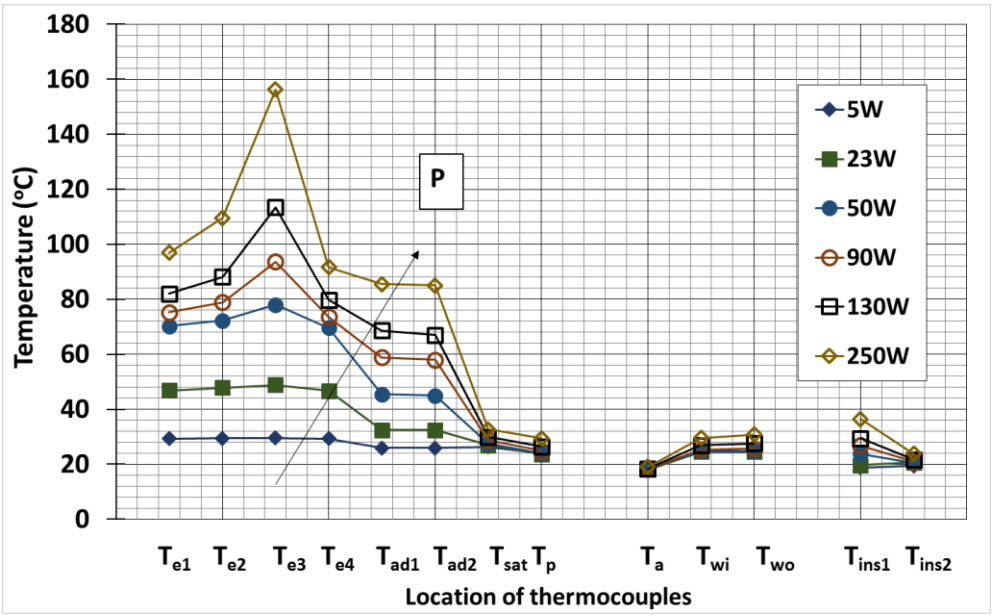

Figure 2.30 Axial wall temperature (Run A/20)

The effect of using bulk temperature difference and mean temperature difference is shown in Figure 2.31. In which power versus temperature difference is plotted.

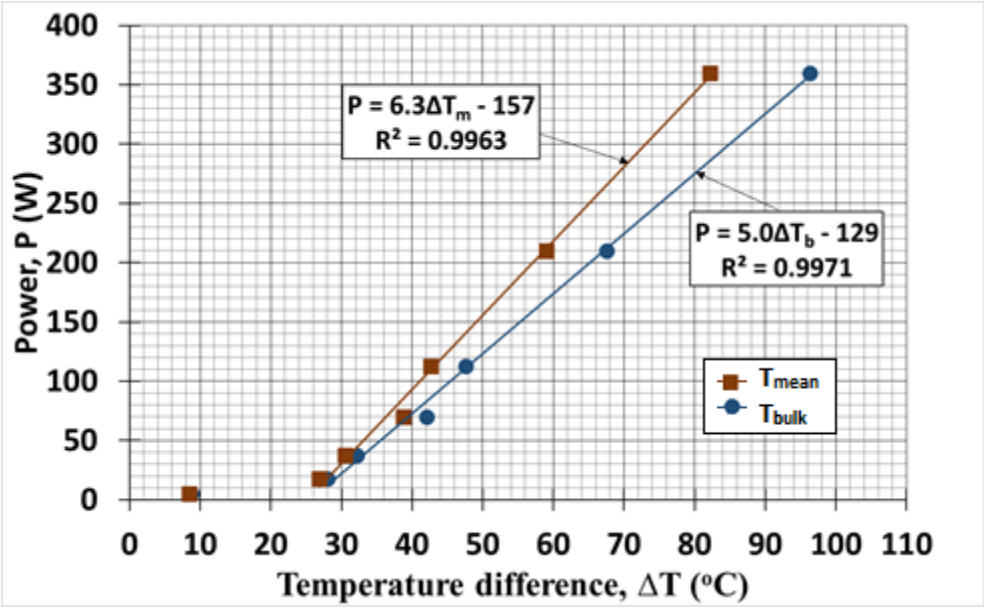

Figure 2.31 Comparison of typical performance based on mean and bulk temperature difference (Run A/3)

The effect of different mass flow rates on temperature distribution, power versus temperature difference, and heat pipe resistance is shown in Figure 2.32 to Figure 2.34 respectively.

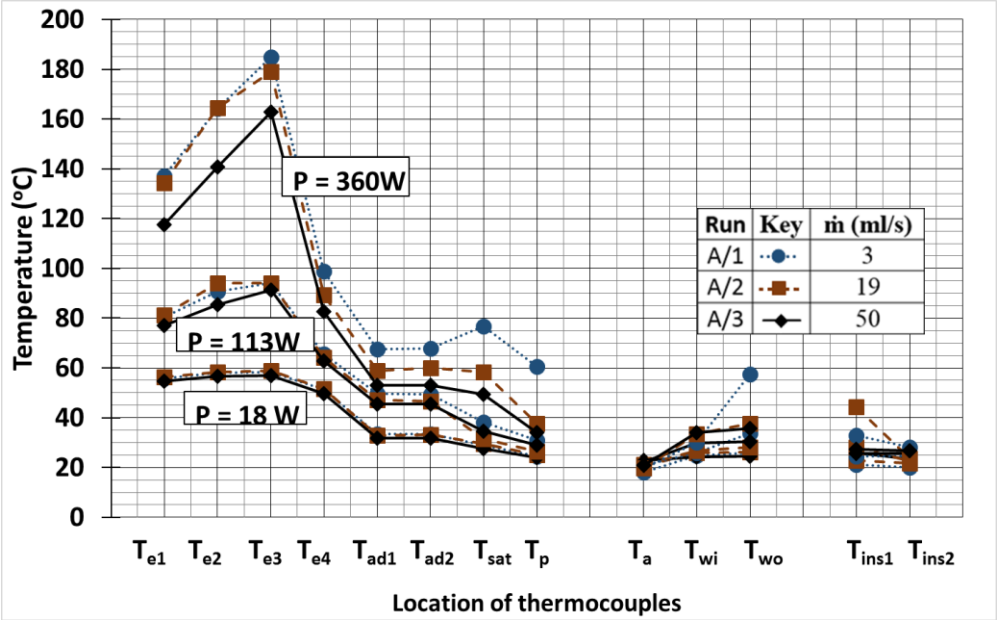

Figure 2.32 Effect of coolant mass flow rate on axial wall temperature distribution (Runs A/1, A/2 and A/3)

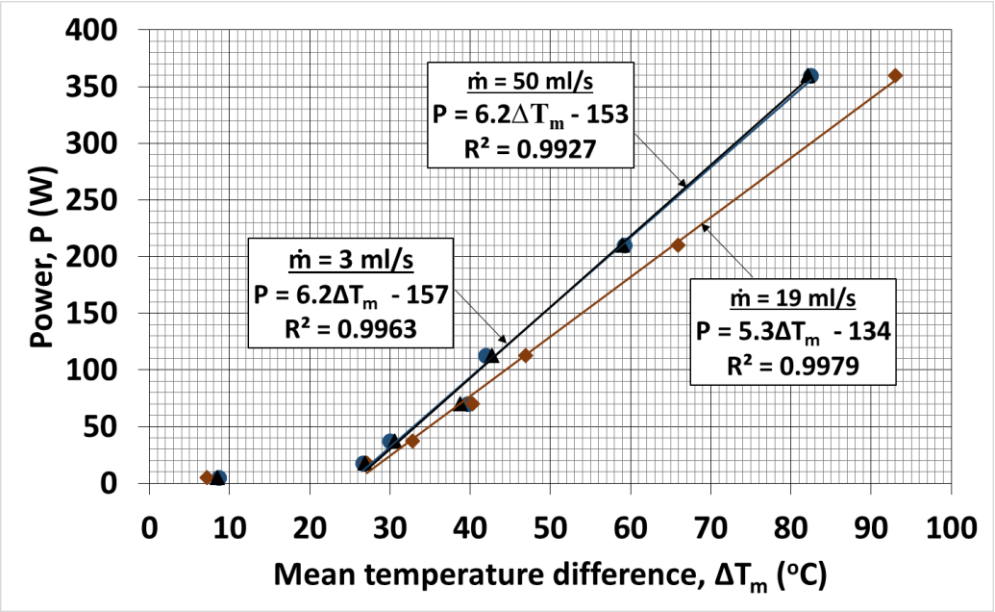

Figure 2.33 Effect of coolant mass flow rate on performance using mean evaporator temperature (Run A/1-A/3)

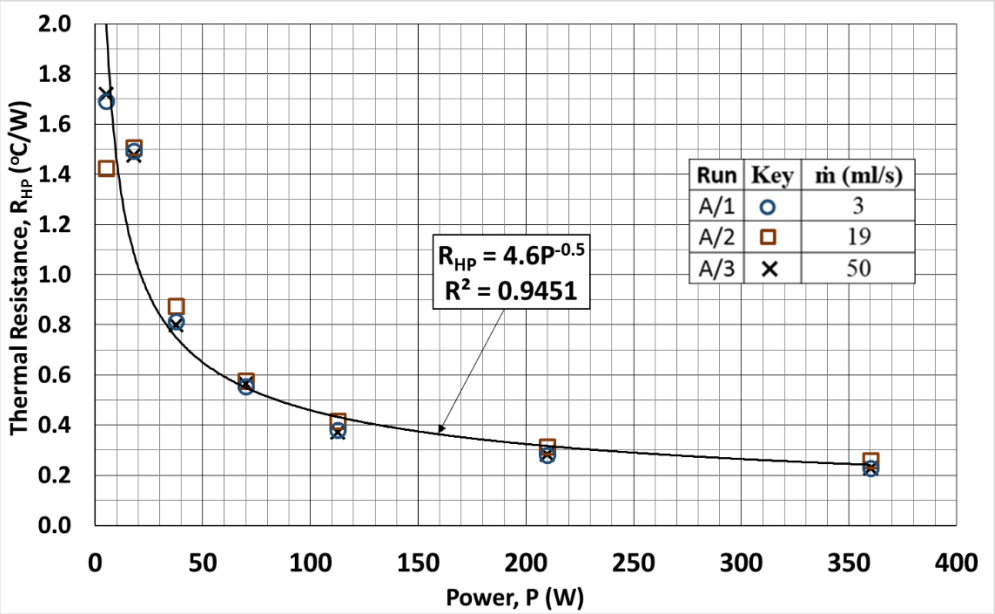

Figure 2.34 Effect of coolant mass flow rate on heat pipe thermal resistance (Run A/1-A/3)

The effect of fill ratio on the performance of a heat pipe using the power versus temperature difference method is shown in Figure 2.35 to Figure 2.38.

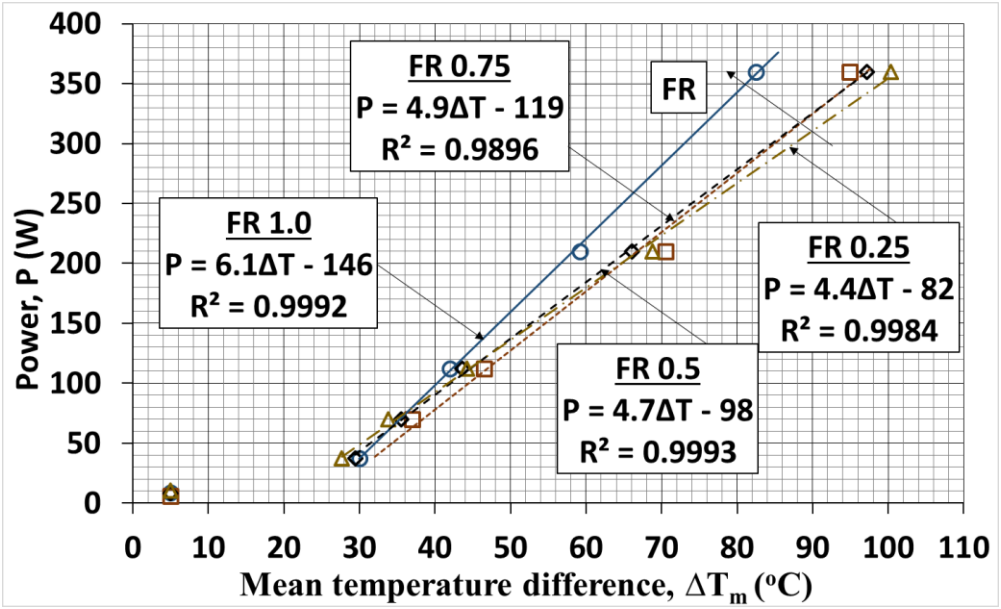

Figure 2.35 Effect of fill ratio on performance at 90° (Runs A/3 to A/6)

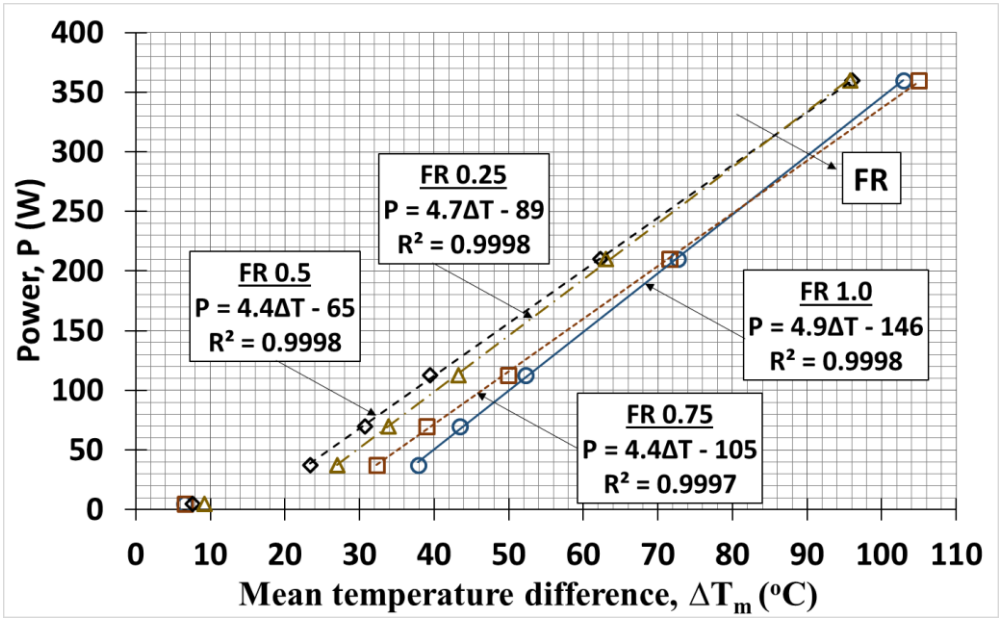

Figure 2.36 Effect of fill ratio on performance at 67° (Runs A/7 to A/10)

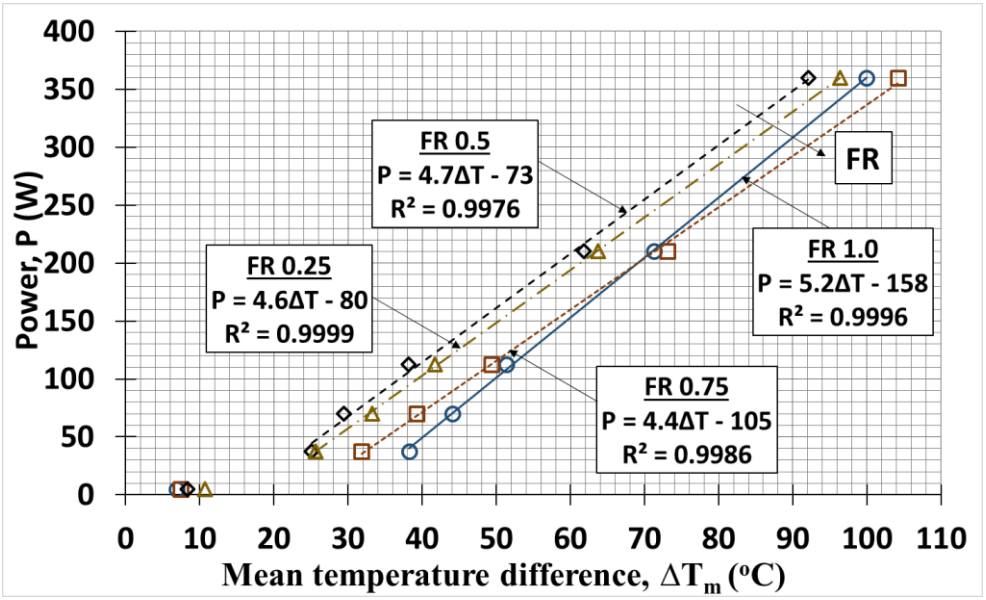

Figure 2.37 Effect of fill ratio on performance at 45° (Runs A/11 to A/14)

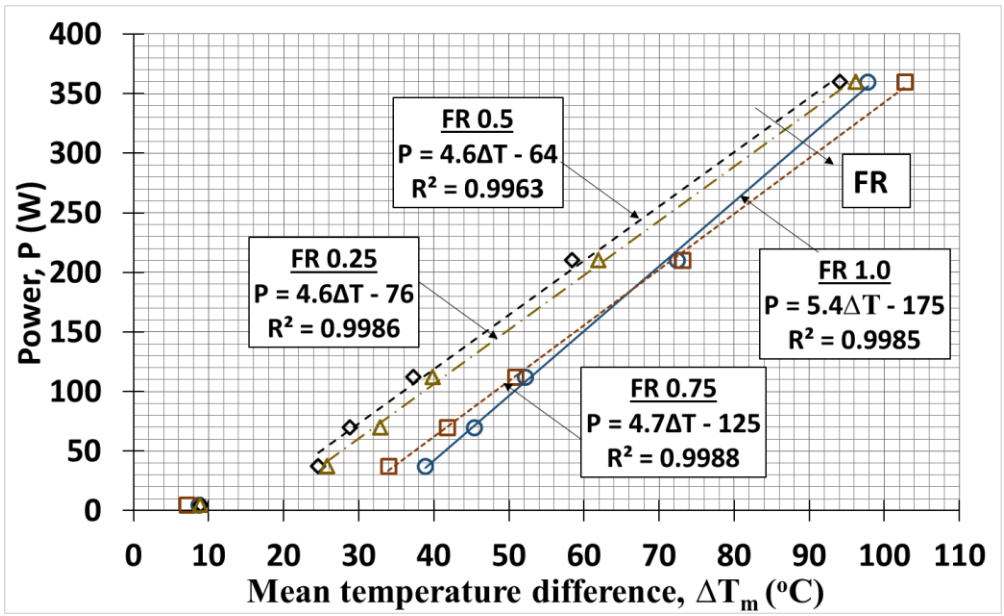

Figure 2.38 Effect of fill ratio on performance at 23° (Runs A/15 to A/ 18)

The effect of thermosyphon inclination angle on thermosyphon performance based on the power versus temperature difference method is shown in Figure 2.39 to Figure 2.42.

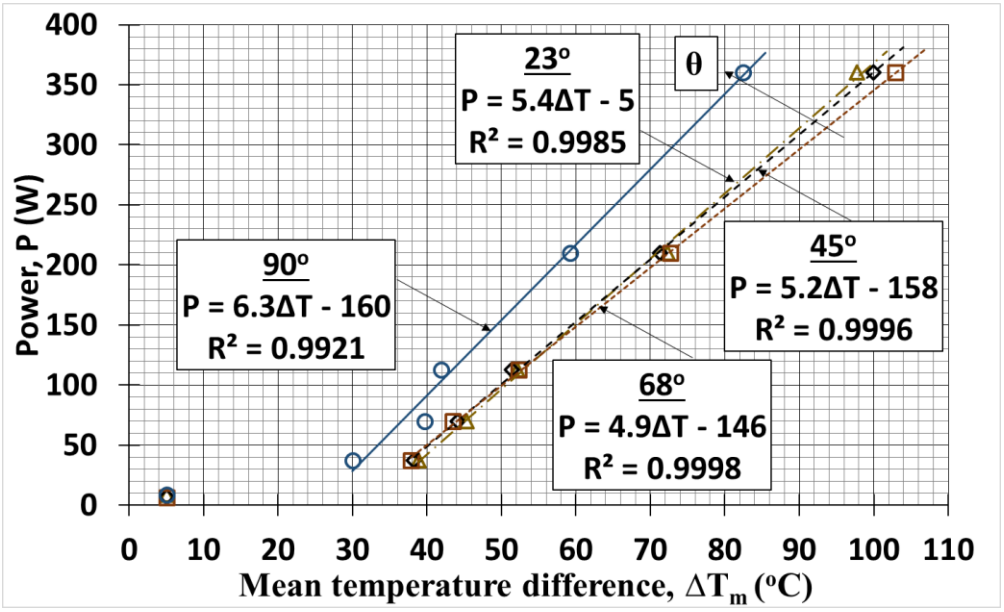

Figure 2.39 Effect of inclination on performance at FR 1.0 (Runs A/3, A/7, A/11 and A/15)

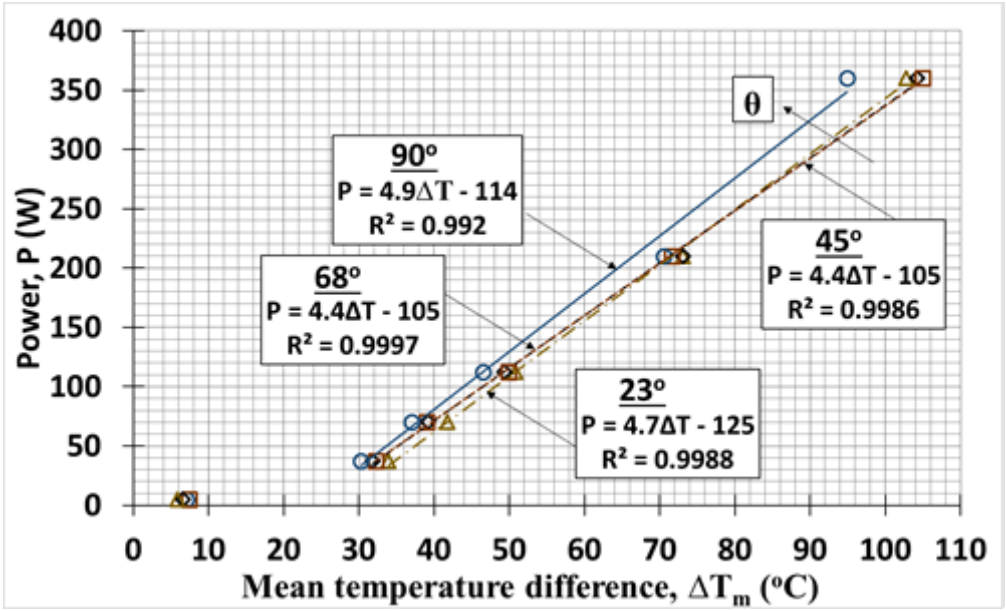

Figure 2.40 Effect of inclination on performance at FR 0.75 (Runs A/4, A/8, A/12 and A/16)

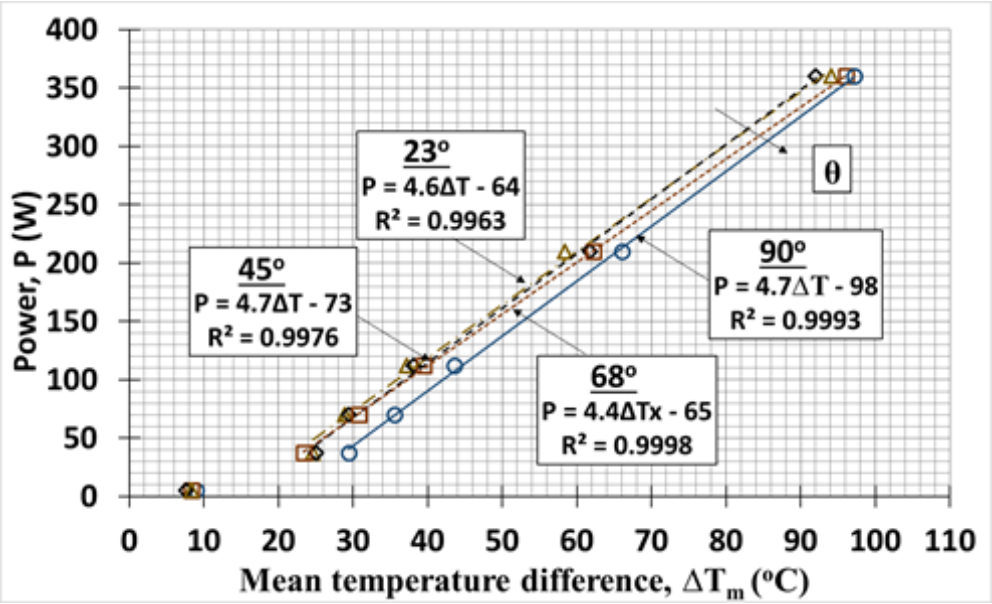

Figure 2.41 Effect of inclination on performance at FR 0.5 (Runs A/5, A/9, A/13 and A/17)

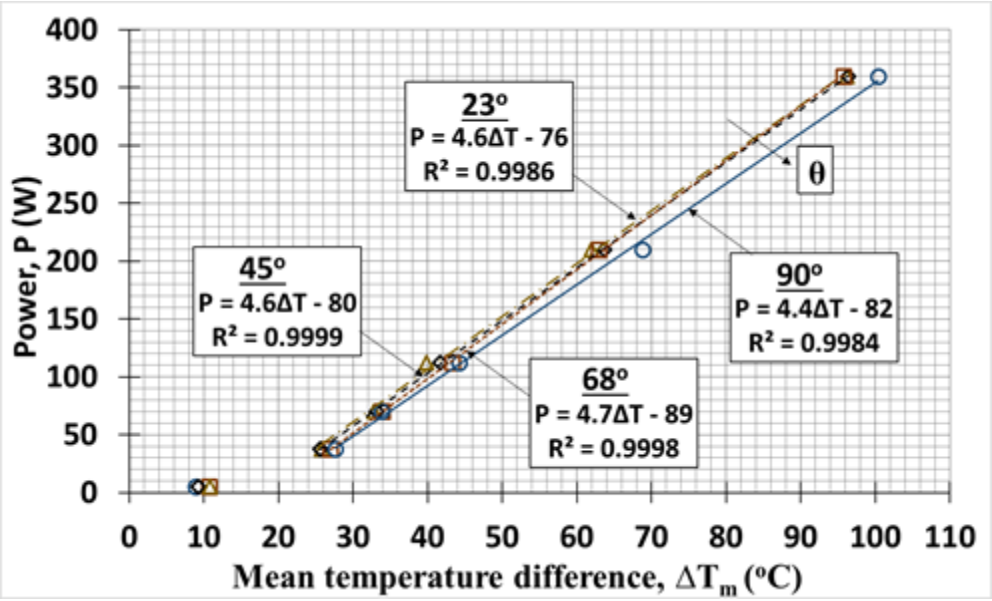

Figure 2.42 Effect of inclination on performance at FR 0.25 (Runs A/6, A/10, A/14 and A/18)

The effect of fill ratio on heat pipe resistance against power input is shown in Figure 2.43 to Figure 2.46.

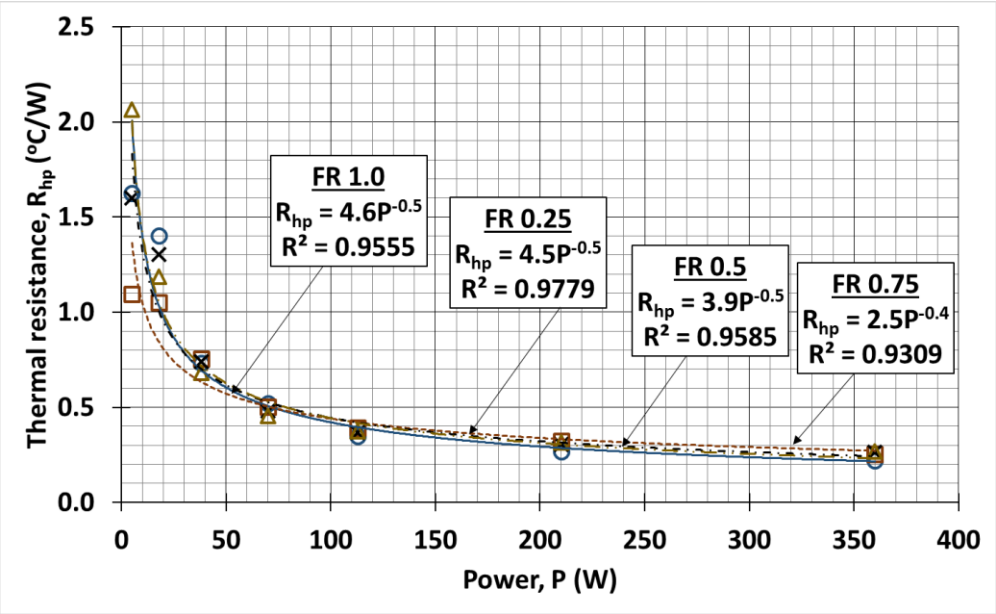

Figure 2.43 Effect of fill ratio on performance at 90° (Runs A/3 to A/6)

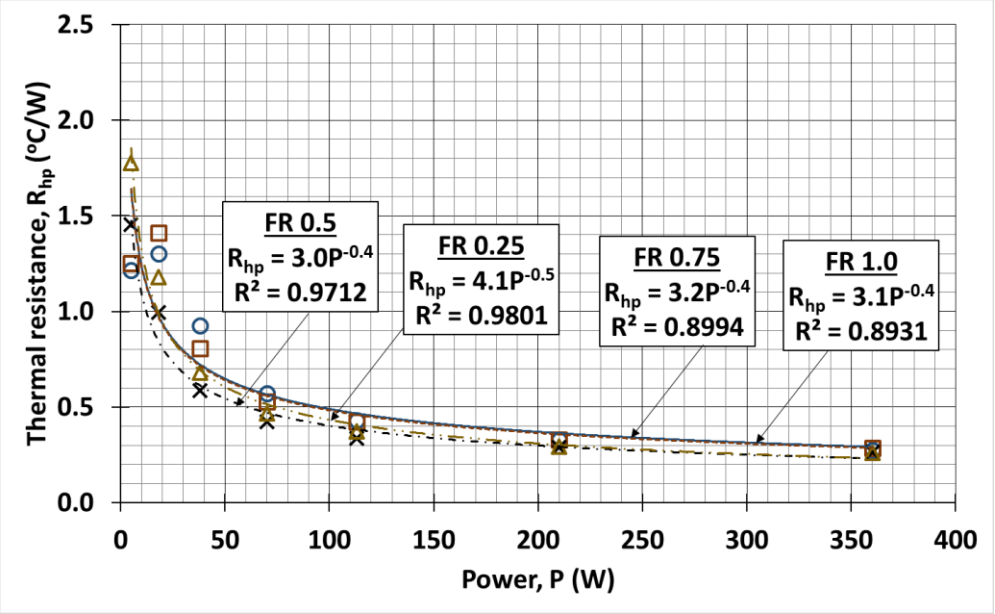

Figure 2.44 Effect of fill ratio on performance at 68° (Run A7 to A/10)

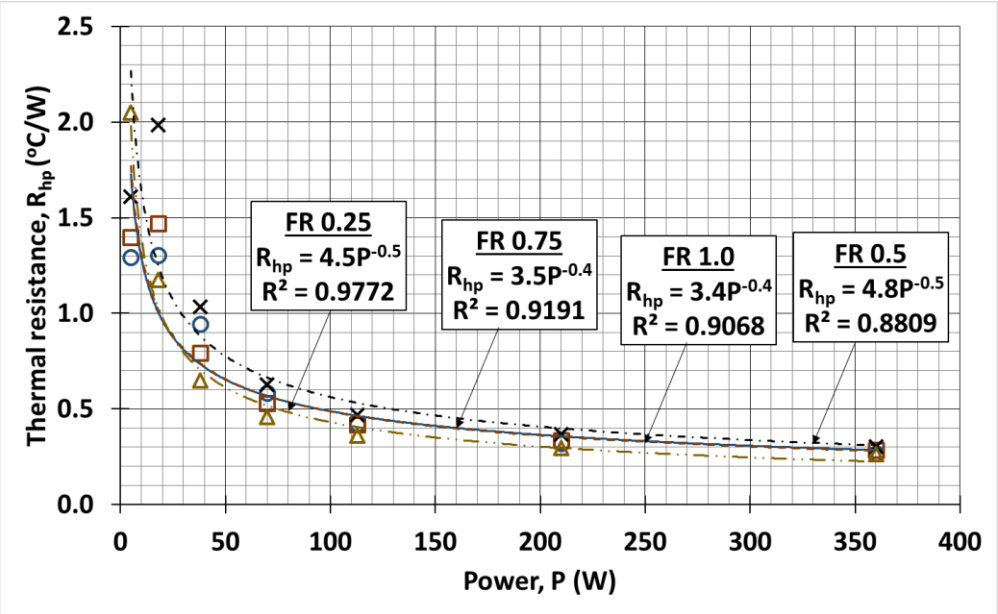

Figure 2.45 Effect of fill ratio on performance at 45^o (Runs A/11 to A/14)

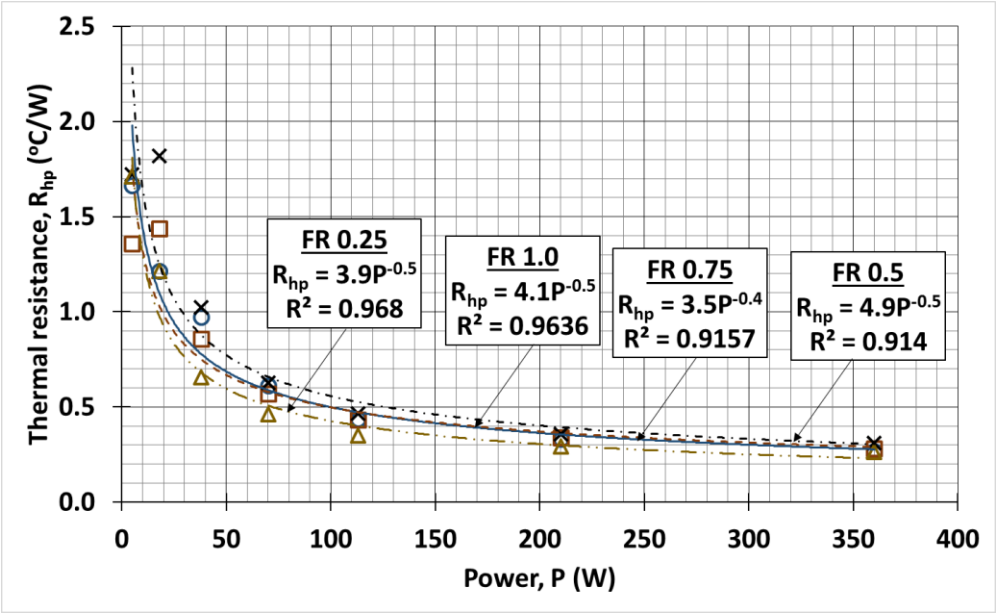

Figure 2.46 Effect of fill ratio on performance at 23^o (Runs A/15 to A/ 18)

The effect of pipe inclination angle on heat pipe resistance against power input is shown in Figure 2.47 to Figure 2.50.

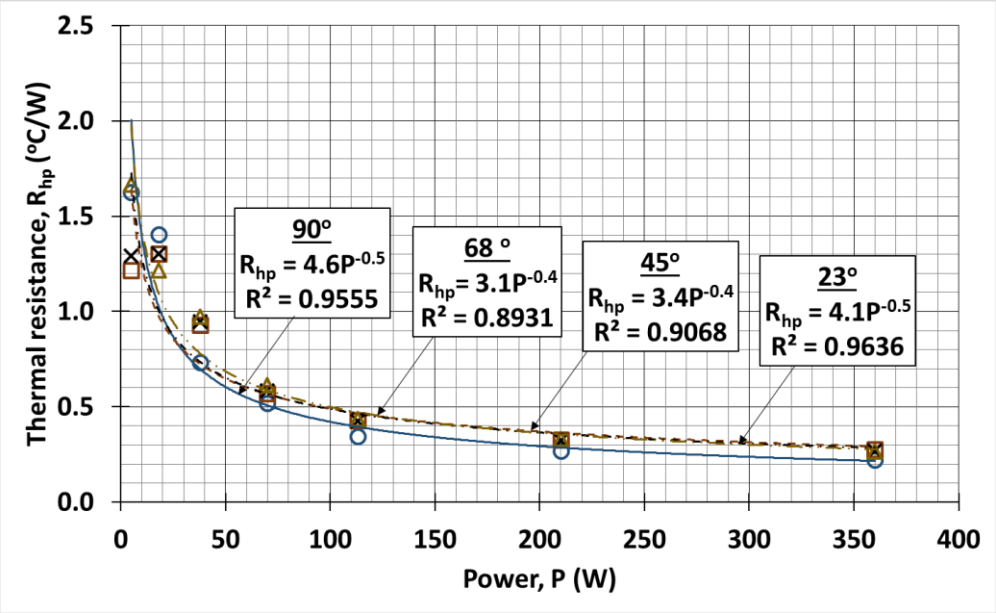

Figure 2.47 Effect of inclination on performance at FR 1.0 (Runs A/3, A/7, A/11 and A/15)

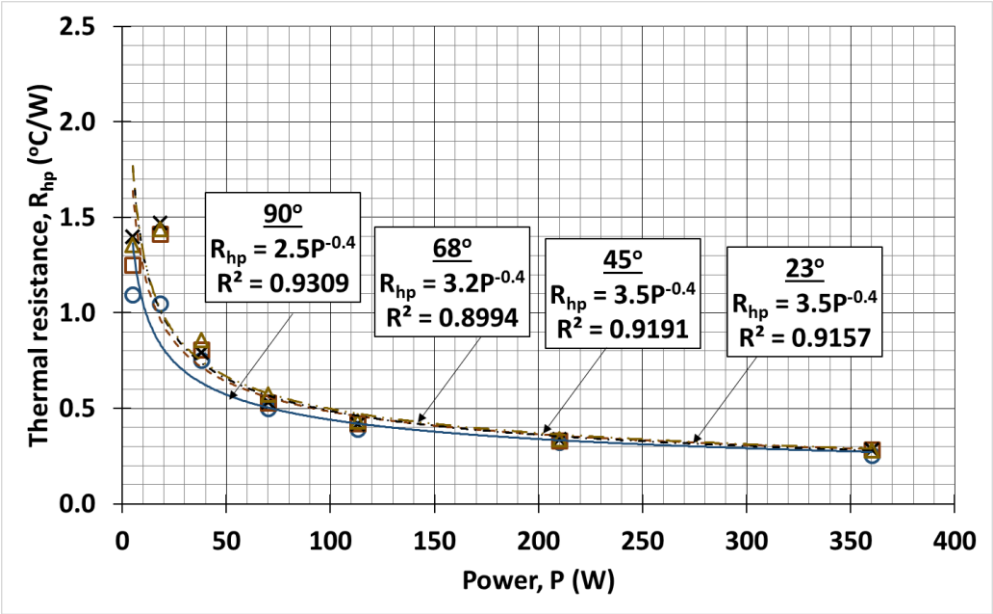

Figure 2.48 Effect of inclination on performance at FR 0.75 (Runs A/4, A/8, A/12 and A/16)

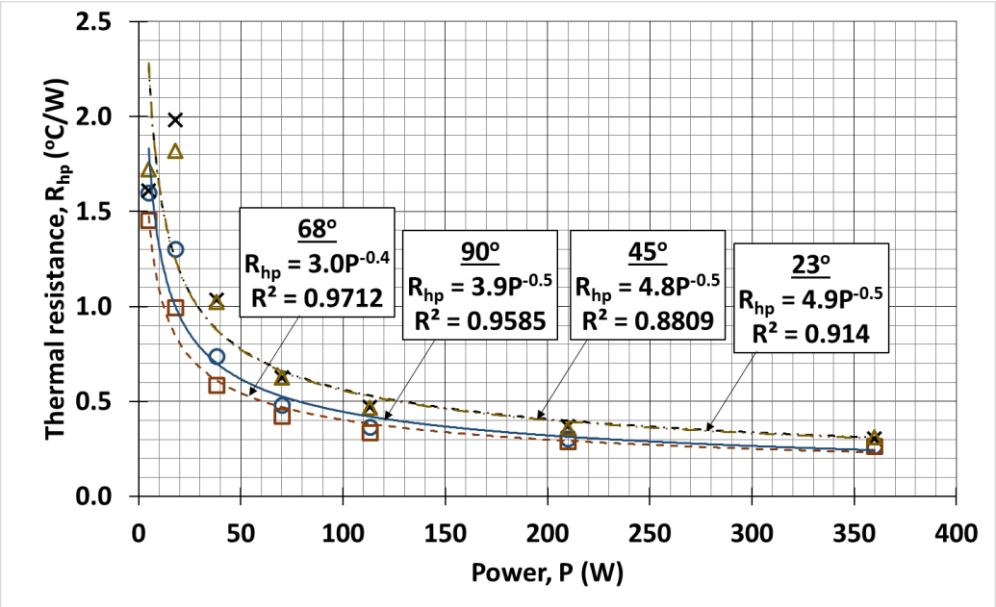

Figure 2.49 Effect of inclination on performance at FR 0.5 (Runs A/5, A/9, A/13 and A/17)

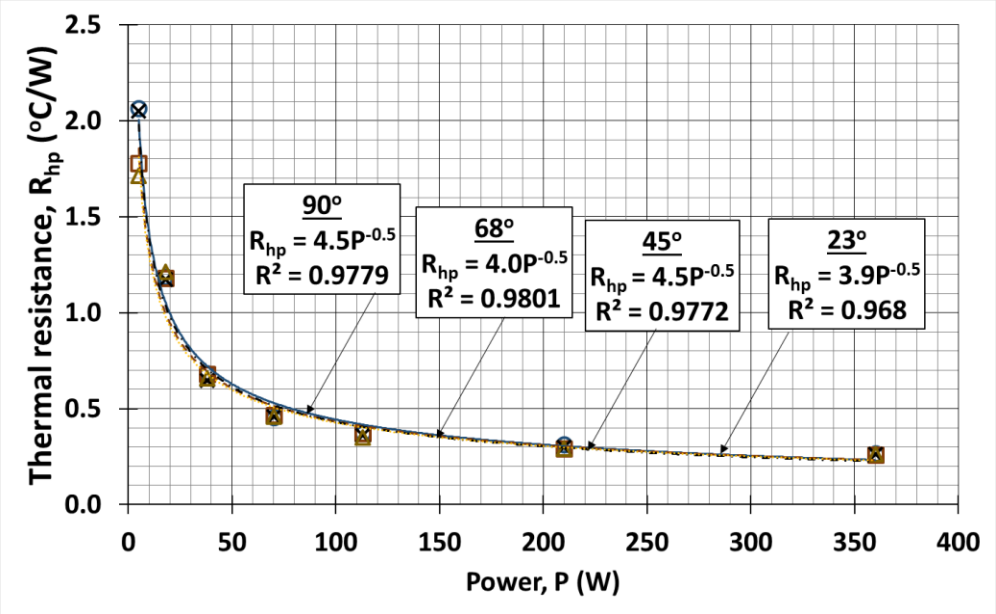

Figure 2.50 Effect of inclination on performance at FR 0.25 (Runs A/6, A/10, A/14 and A/18)

Figure 2.51 shows the effect of various average FR and average pipe inclination angle on heat pipe resistance against power input. An overall heat pipe resistance was also plotted in Figure 2.51.

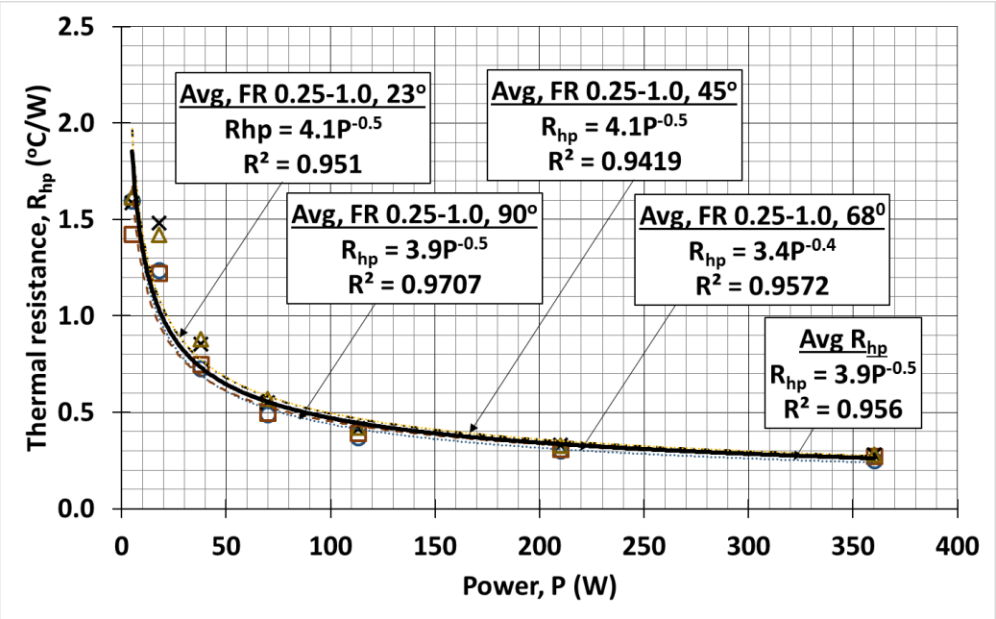

Figure 2.51 Effect of various FRs and inclinations on performance (Run A/3 to Run A/18)

The effect of power input on both evaporator and condenser heat transfer coefficient at various FRs is shown in Figure 2.52 to Figure 2.59.

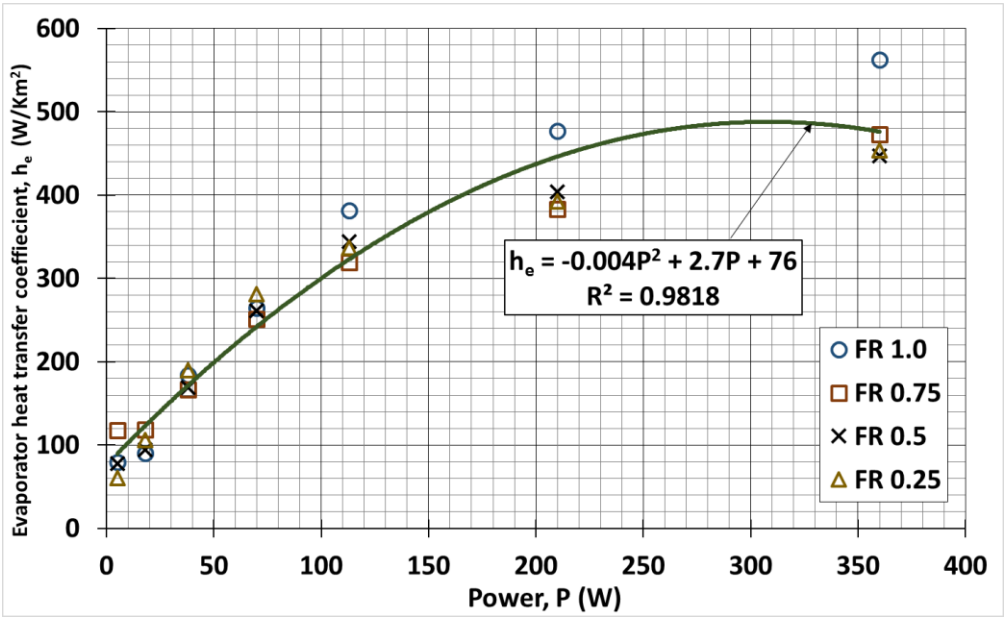

Figure 2.52 Effect of evaporator heat transfer coefficient at 90^o (Runs A/3 to A/6)

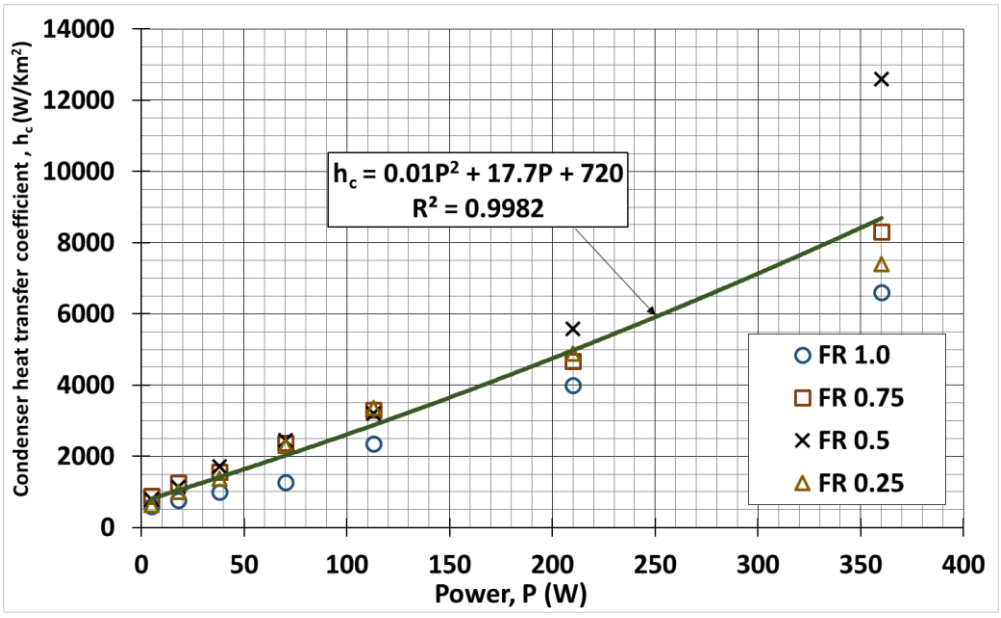

Figure 2.53 Effect of condenser heat transfer coefficient at 90^o (Runs A/3 to A/6)

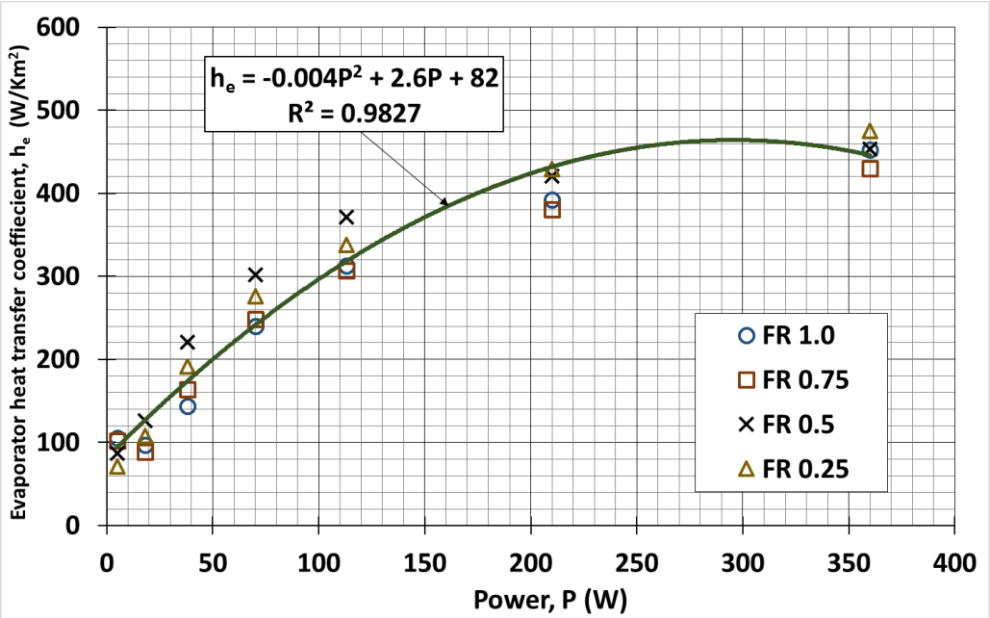

Figure 2.54 Effect of evaporator heat transfer coefficient at 68° (Runs A/7 to A/10)

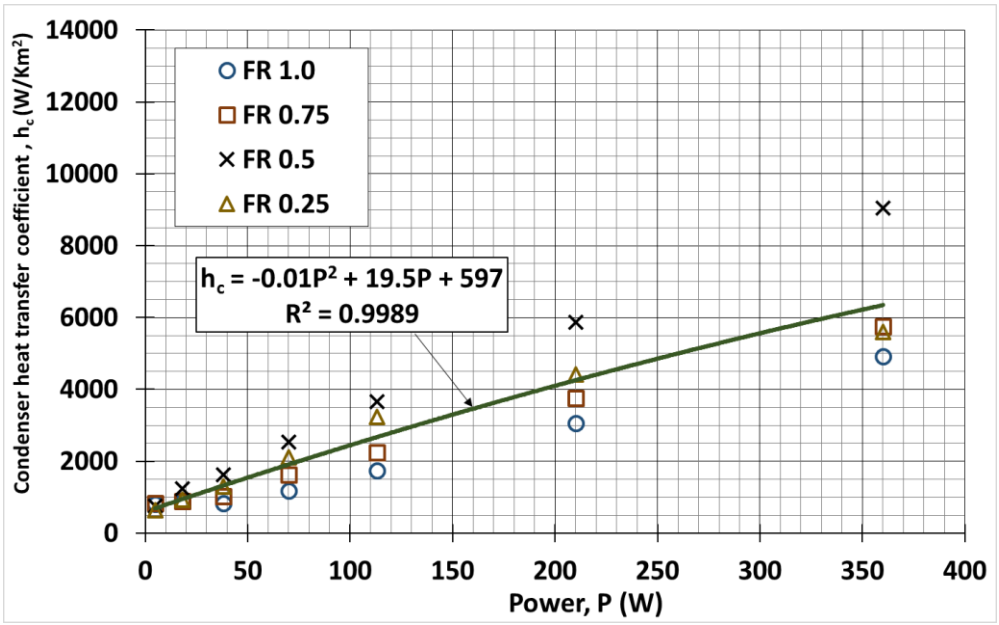

Figure 2.55 Effect of condenser heat transfer coefficient at 68° (Runs A/7 to A/10)

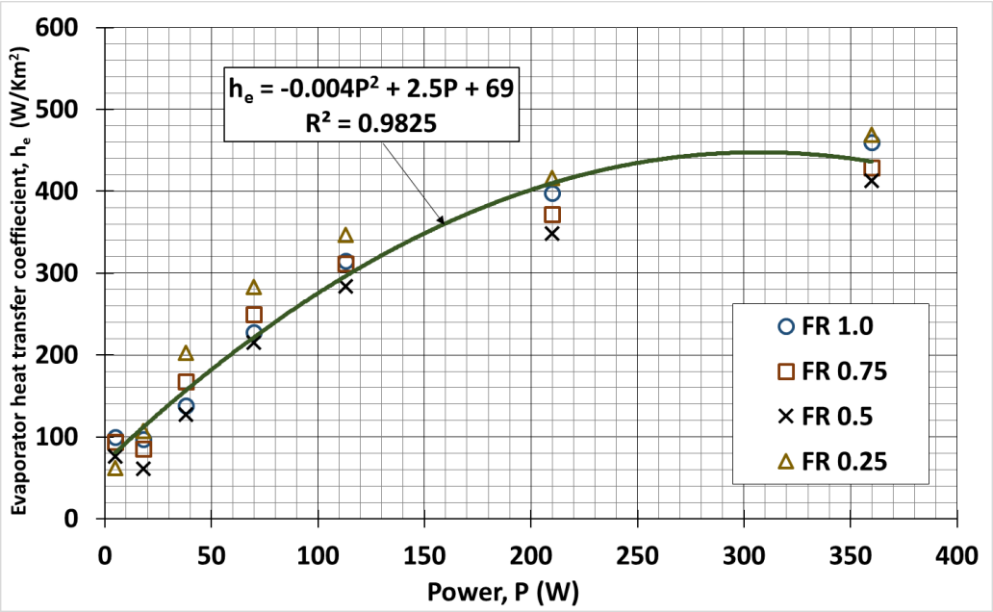

Figure 2.56 Effect of evaporator heat transfer coefficient at 45^o (Runs A/11 to A/14)

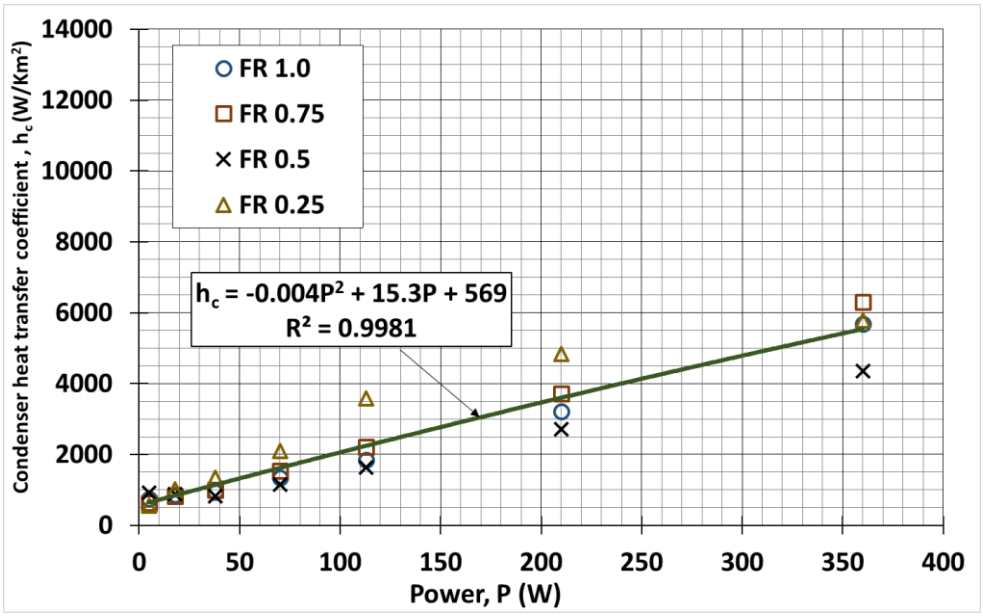

Figure 2.57 Effect of condenser heat transfer coefficient at 45^o (Runs A/11 to A/14)

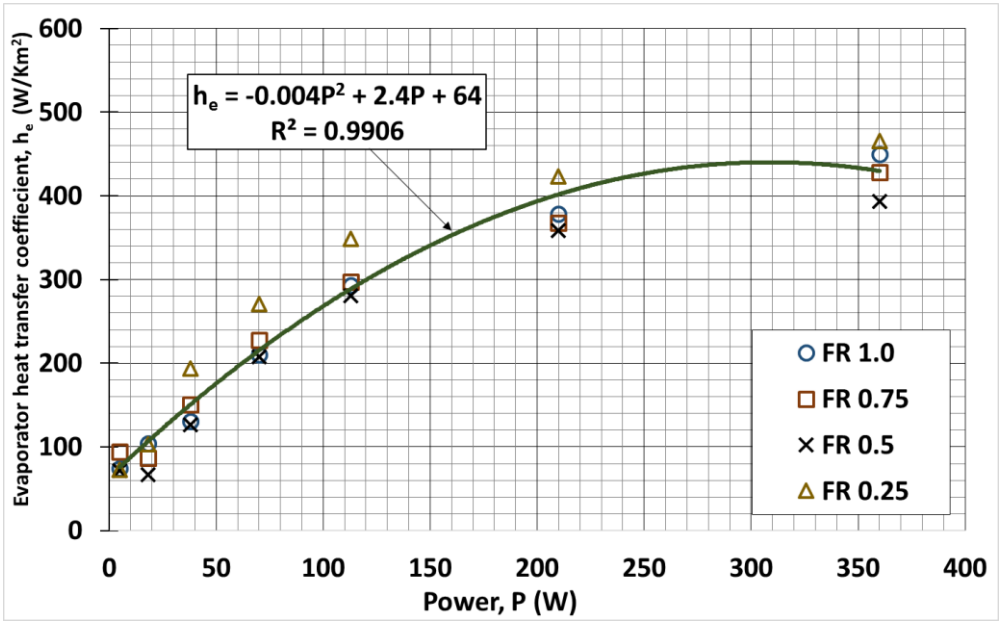

Figure 2.58 Effect of evaporator heat transfer coefficient at 23^o (Runs A/15 to A/18)

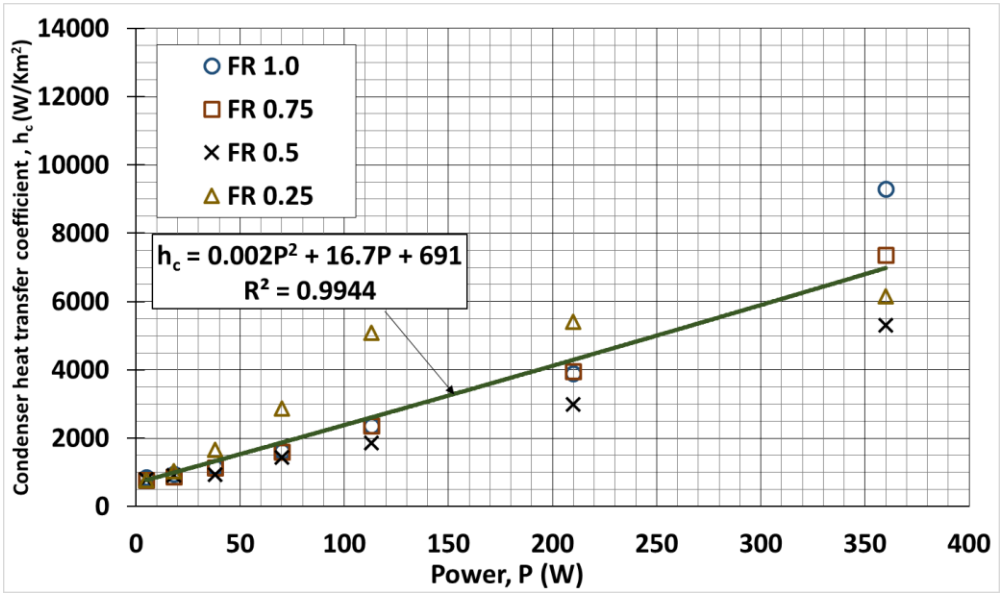

Figure 2.59 Effect of condenser heat transfer coefficient at 23^o (Runs A/15 to A/18)

The effect of power input on both evaporator and condenser heat transfer coefficient at various pipe inclination angle is shown in Figure 2.60 to Figure 2.67.

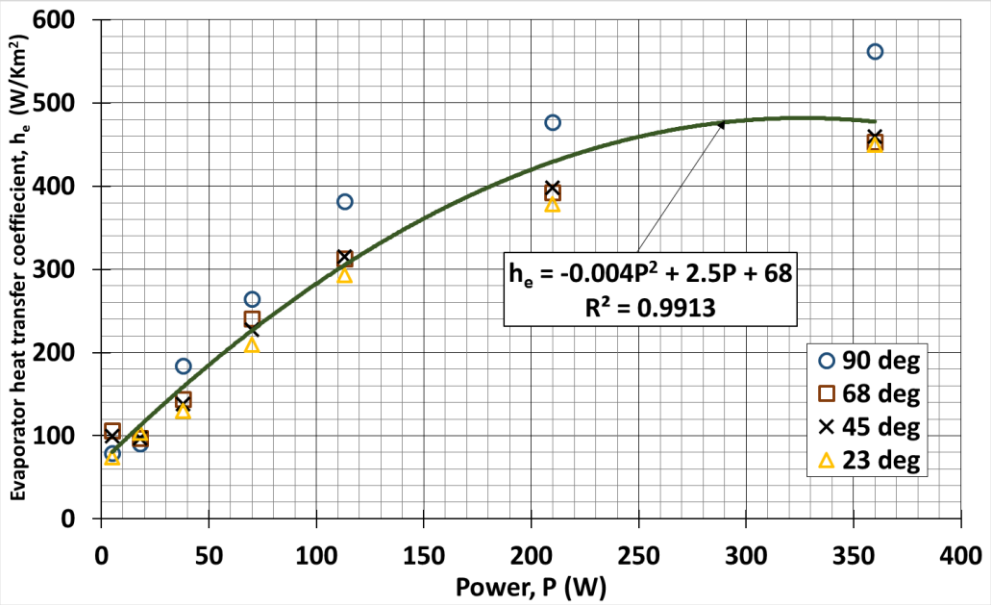

Figure 2.60 Effect of evaporator heat transfer coefficient at FR 1.0 (Runs A/3 to A/6)

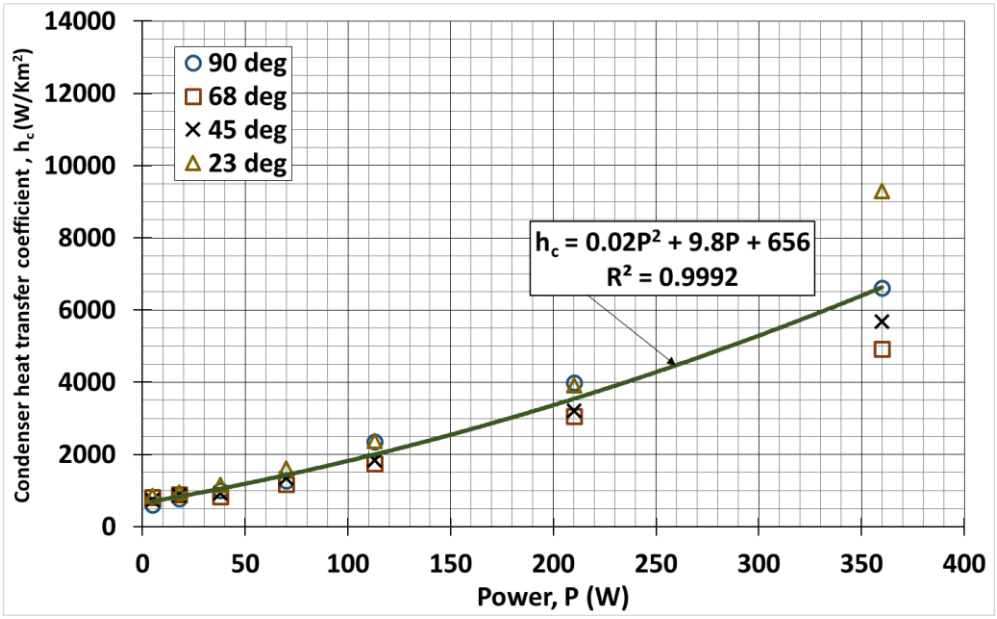

Figure 2.61 Effect of condenser heat transfer coefficient at FR 1.0 (Runs A/3 to A/6)

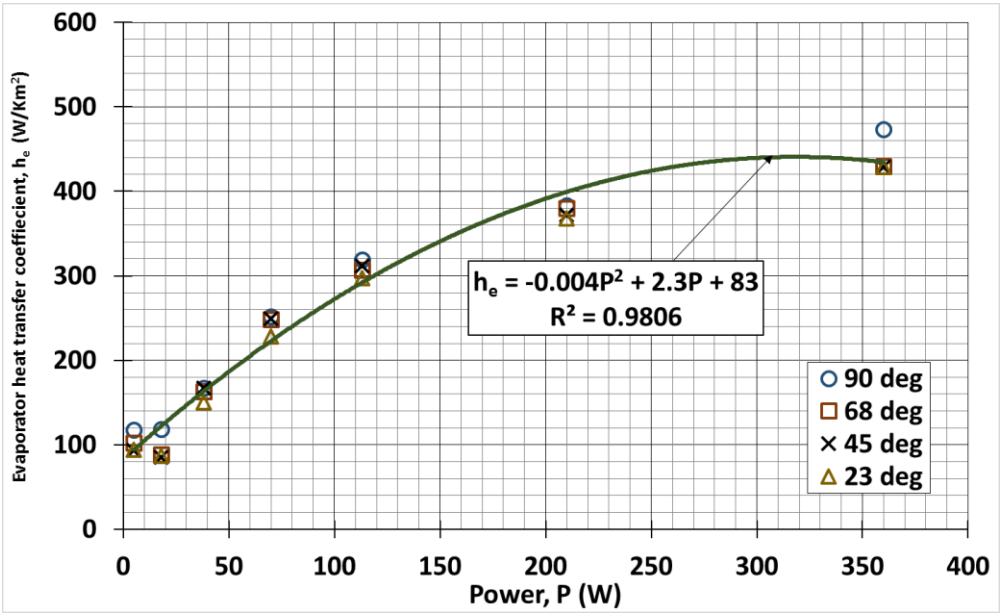

Figure 2.62 Effect of evaporator heat transfer coefficient at FR 0.75 (Runs A/7 to A/10)

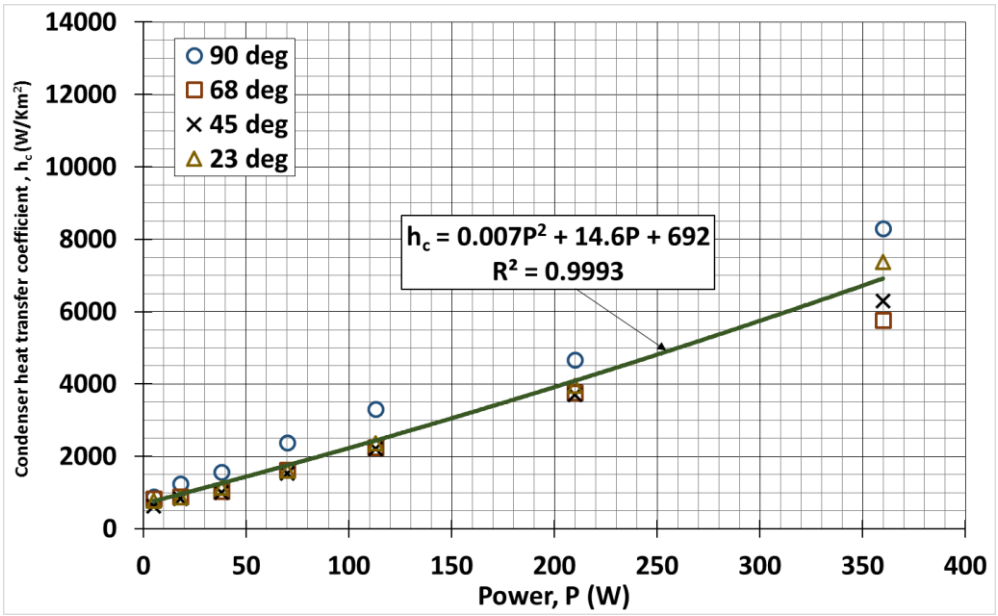

Figure 2.63 Effect of condenser heat transfer coefficient at FR 0.75 (Runs A/7 to A/10)

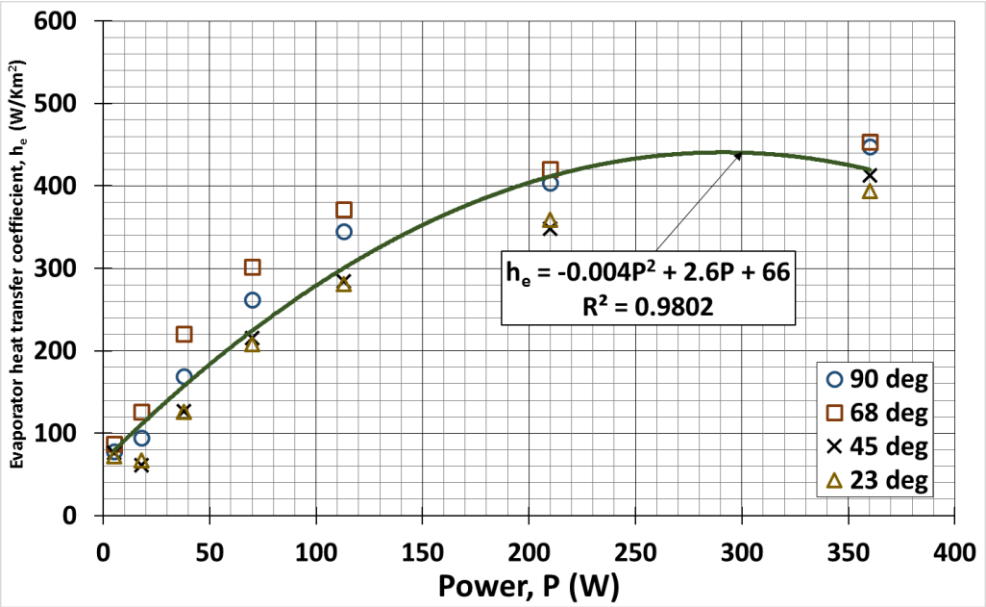

Figure 2.64 Effect of evaporator heat transfer coefficient at FR 0.5 (Runs A/11 to A/14)

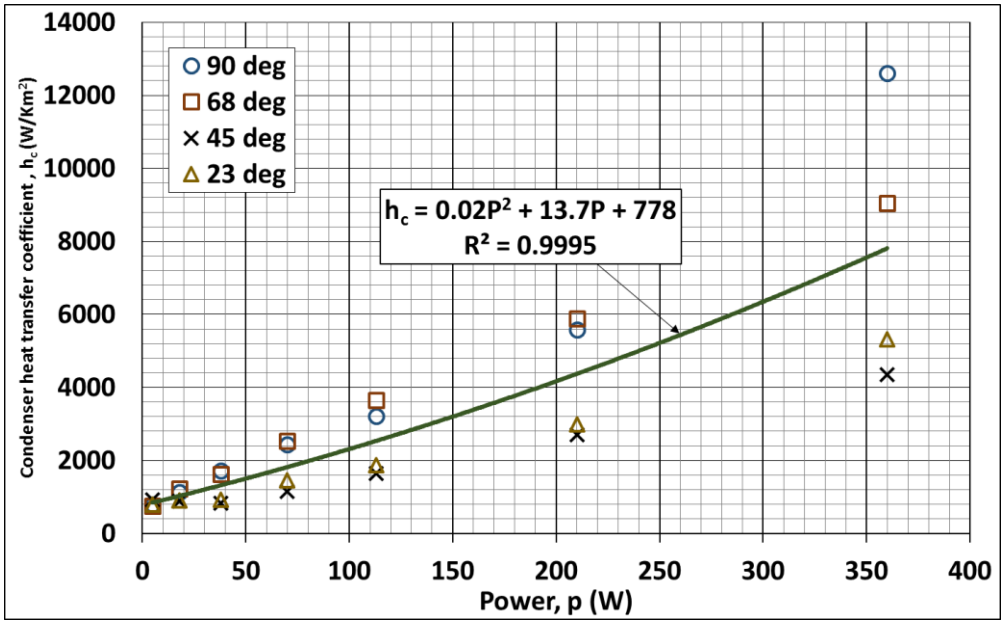

Figure 2.65 Effect of condenser heat transfer coefficient at FR 0.5 (Runs A/11 to A/14)

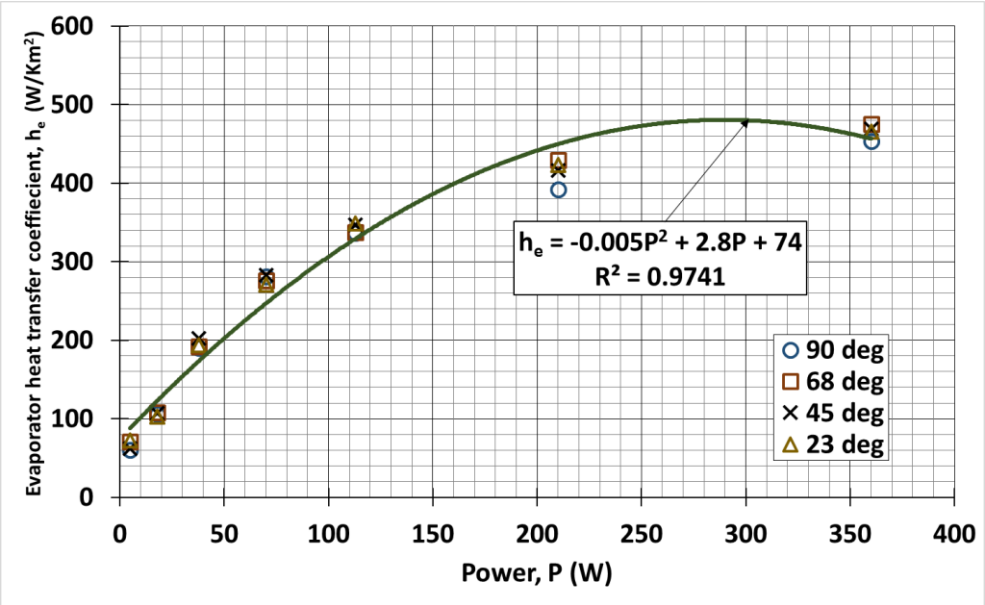

Figure 2.66 Effect of evaporator heat transfer coefficient at FR 0.25 (Runs A/15 to A/18)

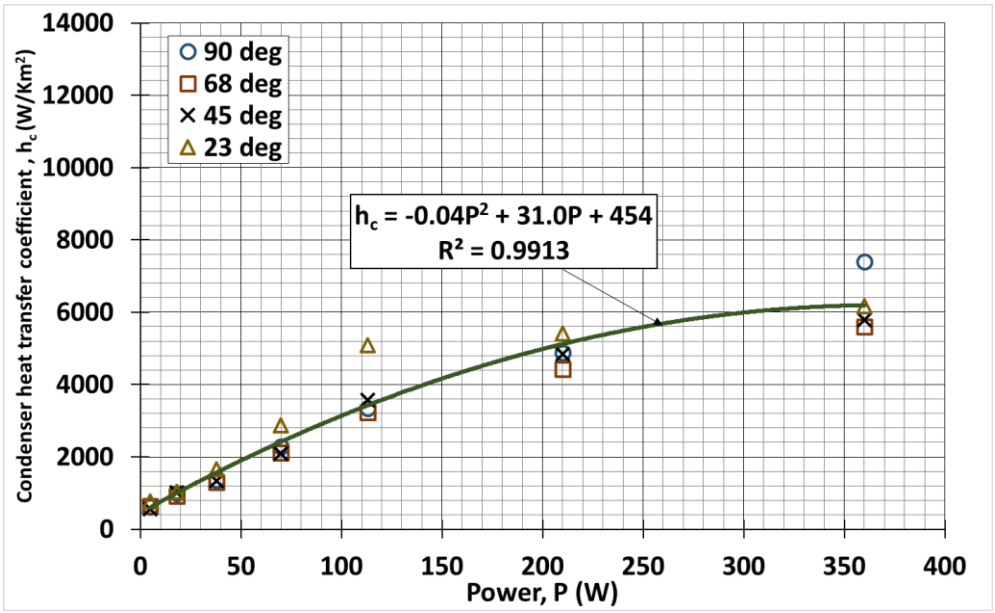

Figure 2.67 Effect of condenser heat transfer coefficient at FR 0.25 (Runs A/15 to A/18)

Figure 2.68 to Figure 2.69 shows the effect of power input on both the evaporator and condenser heat transfer coefficient. The average FR values at a fix pipe inclination angle were presented together with an overall average evaporator and condenser heat transfer coefficient.

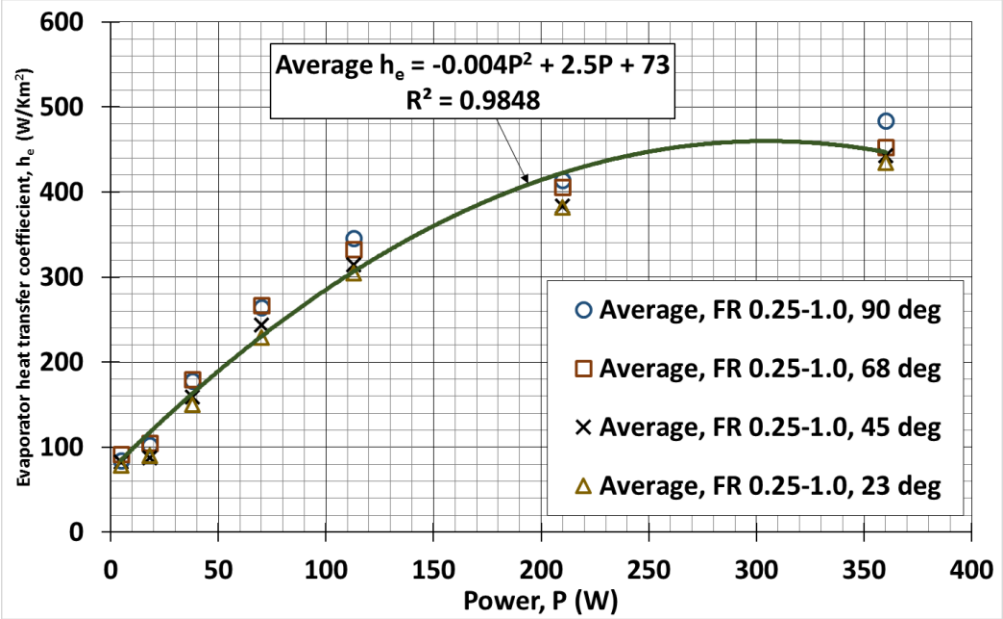

Figure 2.68 Comparison of evaporator heat transfer coefficient at various FRs and inclinations (Runs A/3 to A/18)

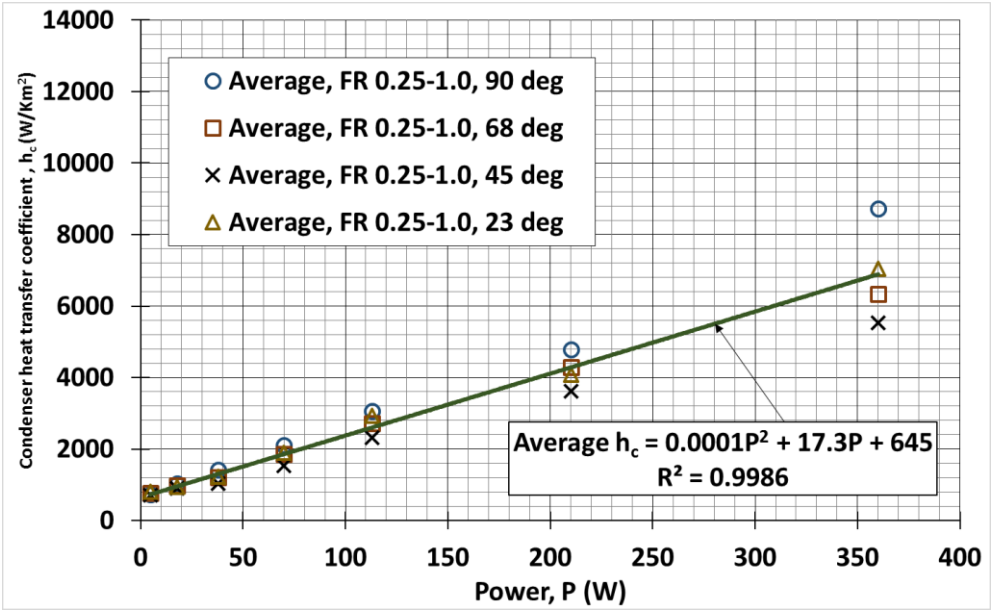

Figure 2.69 Comparison of condenser heat transfer coefficient at various FRs and inclinations (Runs A/3 to A/18)

Figure 2.70 shows the heat pipe thermal resistance values at various AR from phase A as well as results from Nazarul (2014) and Jouhara (2010).

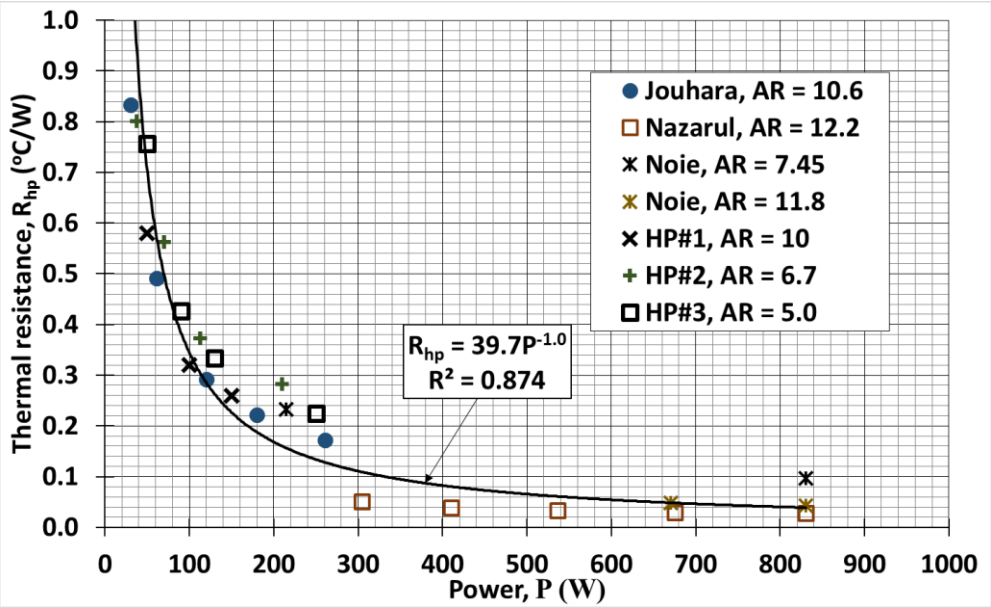

Figure 2.70 Comparison of R values with others

2.4 Discussion of experimental results

2.4.1 Effect of power input on axial temperature distribution

Typical axial temperature distribution for various power inputs at the high water coolant flow rate of 0.05 kg/s (run A/3) are shown in Figure 2.13. The results generally show that the thermosyphon wall temperature distribution increased with power input. This was expected as higher heat input at the evaporator section would result in a higher operating temperature. The increase in evaporator wall temperature was higher than in the adiabatic or condenser sections. The results also show that at low input power, the evaporator wall

temperature was quite uniform. At power inputs beyond 18 W, the distribution tended to be non-uniform. The evaporator wall temperature was observed to reach a maximum of 35 ^{o}C at 5 W and 185 ^{o}C at 360 W. Adiabatic wall temperatures were nearly uniform: about 27 ^{o}C at 5 W and 68 ^{o}C at 360 W. The temperature at the top end of the condenser section exhibited slightly higher temperatures than the adiabatic section, and the coolant water temperature increased by about 0.5 ^{o}C. Mean coolant temperature was lower than adiabatic or condenser top end temperatures.

2.4.2 Bulk and mean wall temperatures

The average evaporator wall temperature could be obtained from the bulk wall temperature (T_b) or from the mean wall temperature ($T_{e,m}$) as calculated from Equation 13 and Equation 14. The results indicate that the calculated bulk wall temperature could reach about 16 ^{o}C higher than the calculated mean value at 360 W (high power) and by 0.3 ^{o}C at 5 W (low power) due to the non-uniformity of axial temperature distribution. Using these calculated average values, the corresponding operating temperature differences based on bulk and mean evaporator wall temperatures calculated from Equation 15 and Equation 16 were utilized in Figure 2.31, which showed a set of typical results for power vs. the two defined operating temperature differences for run A/1. The results show that power varied linearly with either ΔT_m or ΔT_b with regression coefficients greater than 0.99 at the input power above 18 W. Although both sets of results exhibited a linear relationship, the difference between ΔT_b and ΔT_m obtained at 360 W was about 14 ^{o}C but below 18 W (low power), the

difference is negligible and a different set of linear relationships were observed. For simplicity, most investigators used the mean evaporator temperature, T_m.

The performance of a thermosyphon could be gauged from the overall resistance (R_{HP}), defined by

$$R_{HP} = \frac{\Delta T}{P} \quad [\text{K/W}] \qquad \textbf{Equation 22}$$

Here, different values of R_{HP} could be obtained depending on the definition of ΔT. From Figure 2.31, the reciprocal of the gradients of the P vs ΔT_m or ΔT_b curves would give the value of R_{HP}. Here, we obtain values of R_{HP} 0.23 with ΔT_m and 0.27 with ΔT_b. This difference is quite substantial considering that the thermocouple is capable of measuring temperature differences within ± 1 ^oC and the actual temperature difference between evaporator and condenser ranged from 30–90 ^oC. However, the mean temperature relationship is employed henceforth when comparing the performance of the thermosyphons as previously described by other investigators. In order to compare the performances of various heat pipes, the heat transfer rates could be plotted against the temperature difference between the evaporator and condenser sections. This would give an indication of the R_{HP} of the pipe. A high R_{HP} would indicate a poor performing HP and vice versa. A lower R_{HP} value indicates a better performing heat pipe as there is lower resistance towards heat transfer. When there is a lower resistance for heat transfer, heat is more readily transported from one end to the other.

2.4.3 Effect of condenser cooling rate

Condenser cooling water inlet temperature was not controlled. It varied between 27-30 ^{o}C (± 1 ^{o}C). Experiments were performed to determine the effect of condenser cooling rate with various water circulation rates of 0.003, 0.019 and 0.05 kg/s. The axial temperature distribution results for run A/1 to A/3 are plotted in Figure 2.32 for the low power input of 18 W and high power of 360 W. The results show that temperature distribution increases with increasing power and with decreasing mass flow-rates. High power input raises the thermosyphon temperature throughout. Low coolant flow rates result in less cooling due to higher condenser temperatures. The Reynolds number for the coolant water flow ranged from 28-1400 indicating that the flow regime is laminar in the concentric tube water jacket. With the short condenser length, it is also expected to be in the developing flow region. The difference between coolant water inlet and outlet temperature varied from 27 ^{o}C at high power and low flowrate to about 0.5 ^{o}C at low power and high flowrate. For the subsequent series, high flow rate at 0.05 kg/s was employed for a more uniform condenser section temperature. However, at this high flow rate, it was not possible to evaluate the heat transfer at the condenser section accurately. Hence heat transfer at the evaporator section of the thermosyphon was assumed to be equal to the electrical power input.

The effects of mass flow rates for runs A/1-A/3 are shown in Figure 2.33. The results show that generally, input power (P) or heat transfer from the thermosyphon varies linearly with mean operating temperature difference

(ΔT_m). Both low and high flow rates are seen to perform similarly and better compared to medium flow rate. As mentioned above, when different flow rates were applied the evaporator operating temperature and condenser temperature will change accordingly. When high flowrate was applied, the evaporator operating temperature was reduced, together with a reduction in condenser temperature. When low flowrate was applied the evaporator and condenser temperature will increase. It follows that when a medium flow rate is applied, the evaporator and condenser temperature should fall to a region between the low and high flowrate temperature profile. However, the drop in temperature in the condenser section was higher than the drop in temperature in the evaporator section as seen in Figure 2.32. The difference in mean temperature in Figure 2.33 could also be due to the inaccuracy of the thermocouple probe, which experimental repeatability was within ± 3 ^{o}C, coupled with the accuracy of the probe of ±1 ^{o}C, the plots in Figure 2.33 could actually be overlapping each other.

In Figure 2.34 the heat pipe thermal resistance, R_{HP}, was plotted to evaluate the effect of mass flowrate of water. There was little difference between the three flowrates in terms of R_{HP} which decreased from 1.8 to 0.2 ^{o}C/W over power input 5-360 W. A power thermal resistance-power curve was obtained, $R_{HP} = 4.6P^{-0.5}$, with a regression value of $R^2 = 0.9451$. There was some difference initially at 5 W and 18 W, due to the sensitivity of the equation used in Equation 21, in which a small temperature difference over a small value of power input could result in a large thermal resistance value.

2.4.4 Effect of fill ratio

The effects of FR at various inclinations (90^o, 67^o, 45^o, and 22.5^o) for runs A/3-A/18 are shown in Figure 2.35 to Figure 2.38 and Figure 2.43 to Figure 2.46 respectively. The results show that generally, input power (P) or heat transfer from the thermosyphon varies linearly with mean operating temperature difference (ΔT_m). Two distinct operating regions are observed, viz., low power region 0-40 W and high power region above 40 W. The different operating regions were attributed to the effect of pure axial heat conduction directly along the thermosyphon wall from the evaporator to the condenser section. This conduction effect was greater at lower power input. At high power input, the performance was nearly linear with regression coefficients greater than 0.99. The present investigation focuses on high operating power or high evaporator wall temperature. At high power, the results of Figure 2.35 show that at 90^o inclination, the thermosyphon with FR = 1.00 out-performed the others. The results of Figure 2.36 to Figure 2.38 show that at low inclinations, the lesser filled thermosyphons performed better.

When using the thermal resistance method to evaluate the effect of fill ratio from Figure 2.43 to Figure 2.46, there were very small variations from FR =1.0 to FR = 0.25. The R_{HP} decreased from 2.0 to 0.25 $^oC/W$ across run A/3-A/6. There was no distinct FR that performed the best; all FR performed similarly when evaluated with the thermal resistance method.

2.4.5 Effect of inclination.

The effects of inclination at various FRs (1.00, 0.75, 0.5, and 0.25) for runs A/3-A/18 are shown in Figure 2.39 to Figure 2.42 and Figure 2.47 to Figure 2.50. The results of Figure 2.39 and Figure 2.40 show that with FR = 1.00 and 0.75, the vertical thermosyphon out-performed the others. The vertical heat pipe was shown to have the lowest value of RHP. This indicates that it has the best performance. The reason why the vertical thermosyphon performs better than the other is due to the operation of the thermosyphon. In the vertical orientation as vapour rises, condensate returns as liquid film at the inner pipe wall with gravity assistance this improves the rate of return of condensate. At an angle (i.e 23^{o} from the horizontal) the condensate travels back at only one side of the wall and gravity does not function as well as in the vertical orientation, due to the slower rate of return of the condensate, the performance of the heat pipe decreases rendering the vertical orientation to be the best performing orientation. Figure 2.41 and Figure 2.42 show that at FR = 0.50 and 0.25, the vertical thermosyphon did not perform as well as the others. Using the thermal resistance method to evaluate the effect of inclination from Figure 2.47 to Figure 2.50, similarly in section 2.4.4, the difference obtained in thermal resistance values were small and there was no distinct inclination that performed the best. The thermal resistance decreased from 2.0 to 0.25 ^{o}C/W as power increased from 5 W to 360 W.

Considering R_{HP}, the inclination and FR indicated that there was no real change in thermal resistance value as observed in Figure 2.51, in which the

thermal resistance of various FR and inclination was plotted against input power. Thermal resistance decreased from 1.5-0.25 ^{o}C/W as power increased from 5-360 W. An average $R_{HP} = 3.9P^{-0.5}$ with a regression value of $R^2 = 0.956$ was obtained when cross plotting for run A/3-A/18.

2.4.6 Evaporator and condenser heat transfer coefficients.

Evaporator and condenser heat transfer coefficients calculated from Equation 18 and Equation 19 were plotted against power in Figure 2.52 to Figure 2.65 and the overall heat transfer coefficients in Figure 2.68 and Figure 2.69 respectively, for runs A/3-A/18. The results show that evaporator and condenser heat transfer coefficients increased with input power.

The effects of FR at various inclinations (90^{o}, 67^{o}, 45^{o}, and 22.5^{o}) on heat transfer coefficients, h_e and h_c, for runs A/3-A/18 are shown in Figure 2.52 to Figure 2.57, respectively. The results show that input power (P), or heat transfer from the thermosyphon, has a quadratic relationship with h_e and h_c. At high power input, the h_e curve reached a maximum value of about 600 W/K m^2 with regression coefficients about 0.98 in Figure 2.52, Figure 2.54, Figure 2.56 and Figure 2.56. At high power input, the h_c curve was still increasing at around 8000 W/K m^2 with regression coefficients of about 0.99 in Figure 2.53, Figure 2.55, Figure 2.55 and Figure 2.57. At this high power, the results of Figure 2.52 showed that at 90^{o} inclination, the thermosyphon with FR = 1.00 had the highest value of h_e and h_c. Figure 2.54 to Figure 2.57 show that at low

inclinations, the lesser filled thermosyphons produced higher values of h_e and h_c.

The effect of inclination at various FRs (1.00, 0.75, 0.5 and 0.25) on h_e and h_c for run A/3-A/18 are shown in Figure 2.60 to Figure 2.65. Figure 2.60 to Figure 2.63 showed that at FR = 1.00 and 0.75, the vertical thermosyphon produced a higher h_e and h_c value. Figure 2.62 to Figure 2.65 showed that at FR = 0.50 and 0.25, the vertical thermosyphon produced lower h_e and h_c values.

When considering $h_{e,avg}$, the inclination and FR indicated that there was no real change in h_e value as shown in Figure 2.68, in which the h_e of various FR and inclination was plotted against input power. The h_e increased from 80-500 W/K m^2 as power increased from 5-360 W. The $h_{e,avg} = -0.004P^2 + 2.5P + 73$ with a regression value of $R^2 = 0.9986$ was obtained when cross plotted for run A/3-A/18. Large inclination angles (90° and 68°) produced slightly higher values of h_e and the smaller inclination angles (45° and 23°) produced a lower h_e value. This shows that the higher inclinations are preferred for better performance.

Considering the $h_{c,avg}$, the inclination and FR indicated that there was some variation in h_c value as shown in Figure 2.69 where the h_c of various FR and inclination was plotted against input power. The h_c increased from 200-7000 W/K m^2 (± 1000 W/K m^2 at high power) as power increased from 5-360 W.

The $h_{c,avg} = 0.0001P^2 + 17.3P + 645$ with a regression value of $R^2 = 0.9986$ was obtained when cross plotted for run A/3-A/18.

2.4.7 Effect of aspect ratio (AR).

Three different thermosyphons with different ARs were tested. The AR effect was shown in Figure 2.70 for run A/3, A/19 and A/20. The results showed that thermosyphon HP#1 with AR = 10 performed better with a 25% drop in R_{HP} than ARs equal to 6.7 and 5 based on Figure 2.70 at 100W. The dimensions of thermosyphons used by other researchers are summarized in Table 1. A comparison of literature results with the present experiment in Figure 2.70 showed that at a certain fixed power input, the thermal resistance decreased with increasing AR. The results obtained from runs A/3, A/19 and A/20 agree well with other researchers (Jouhara 2010 and Noie 2005), and indicated that the thermal resistance of a heat pipe reduced from 0.8 ^{o}C/W to 0.1 ^{o}C/W as power input increased from 10-815 W.

2.5 Chapter conclusion

The thermal performance of three water-filled thermosyphons subjected to evaporator wall temperatures between 30-150 ^{o}C were investigated. The effect of condenser cooling rates together with various fill ratios, pipe inclinations and aspect ratios were considered. The following conclusions were drawn:

- High power input results in higher thermosyphon wall temperatures.
- High condenser cooling rate results in lower thermosyphon wall temperatures.
- Axial temperature distribution was uniform at low power input (< 18 W) and non-uniform at high power input (> 18 W).
- Differences in evaporator wall temperatures based on bulk and mean definitions could be as much as 14 ^{o}C.
- There are two distinct operating regions observed at around 40 W.
- The best performing thermosyphon was found to be at a fill ratio of 1.0 and at a 90^{o} inclination.
- A high aspect ratio thermosyphon of 10 is preferred.

CHAPTER 3

PHASE B: METHOD FOR COMPARATIVE PERFORMANCE

In this chapter, a brief review on thermosyphons types and thermosyphon performance testing methods are presented. The procedure for phase B is described. A novel method to determine the performance of a heat pipe is proposed and presented. The results are compared to literature and existing experimental results as well as the theoretical model results. Part of this chapter has been published on frontiers of heat pipe, FHP, and has been included in the list of references. The abstract for the journal has been included in Appendix B.

The objective of phase B is to propose a method to obtain comparative performance test data of various HPs rapidly and economically.

3.1 Literature survey

3.1.1 Testing methods and performance evaluation methods

The performance of a HP could be evaluated by determining the amount of heat input at the evaporator section or by measuring the heat transferred at the condenser section to the coolant. At steady state, these two heat transfer rates should be equal if there is no heat loss from the pipe. In order to compare the performances of various heat pipes, the heat transfer rates

could be plotted against the temperature difference between the evaporator and condenser sections. This would give an indication of the thermal resistance of the pipe. A high thermal resistance would indicate a poor performing HP and vice versa.

Ong et al. (2014) investigated the performance of water and R410a filled thermosyphons at various power inputs (100 to 830 W), fill ratios (0.25 to 0.93) and inclinations (30^o to 90^o). The authors used a 38 mm OD x 807 mm long thermosyphon with a 71 mm OD cooling water jacket and electrical heating bands to supply heat to the evaporator section. By plotting input power against temperature difference between evaporator and condenser sections, the R410a filled thermosyphon was found to perform better in the vertical position at all FR's and the water filled thermosyphon performed better at low FR and when inclined. The evaporator wall temperature was shown to be non-uniform, especially at high power inputs, low fill ratios, and large inclinations.

Shanthi and Velraj (2014) experimented with a two-phase gravity-assisted thermosyphon. The authors used a 12.5 mm ID x 300 mm long thermosyphon with a 200 mm long cooling water jacket and a 1000 W nichrome heating wire wound around the 75 mm long evaporator section. They measured the performance of their thermosyphon by plotting efficiency defined as ratio of power output over power input, and versus power input, obtaining values as high as 0.9.

Anjakar and Yarasu (2012) determined the effect of condenser length on the performance of a thermosyphon by using a 32 mm OD x 1000 mm long thermosyphon with a 450 mm long water cooled jacket and a 300 mm long nichrome heating element at the evaporator section. The authors determined efficiency as the ratio of heat conducted by the coolant water at the condenser section to the power input at the evaporator section and found values of 0.5 to 0.95. In theory the ratio should be equal to 1.0.

Buschmann and Franzke (2013) compared the performance of thermosyphons filled with deionised water (DI) and titanium oxide-based DI water and gold nanofluid. They showed that nanofluids reduced thermal resistance up to 24 %. They also noted that nanoparticles depositing on the evaporator wall after prolonged heating operations resulted in an absence of nanoparticles being transported to the condenser section that eventually reduced the thermal transport capacity of the nanofluid and increased the overall thermal resistance.

Huminic et al. (2011) experimented with thermosyphons filled with iron oxide nanoparticles and found that a concentration level of 5.3 % improved the thermal performance of their HP. Solomon et al. (2012) determined the thermal performance of a heat pipe using a nanoparticle-coated wick. They found that thermal resistance reduced from 0.32 to 0.11 ^{o}C/W when subjected to power input ranging from 100 to 200 W.

Qu and Wang (2013) showed that a thermosyphon with an FR of 40 to 50 % resulted in faster response times and lowest overall thermal resistance. Shabgard et al. (2014) studied the thermal characteristics of HPs with different FRs. They showed that when the HP is under-filled, dry out occurs; and that overfilling causes the overall thermal resistance to increase. The authors suggested that HPs should be filled slightly more than the optimal FR to prevent the breakdown of liquid film.

Qu and Wang (2013) showed that high heat flux results in lower thermal resistance of the evaporator section. Wang (2009) investigated the transient thermal performance of a bent HP with internal grooved surface and showed that straight pipes responded faster to high heat flux compared to bent shape HPs. They also found that heat pipes have response times varying from 50 to 180 s depending on the pipe angle (0 to 140^{o}).

HPs behave differently when inclined at different angles. Wang (2009) noted that with the increase in inclination, the temperature difference between the evaporator and condenser section increased.

Huminic and Huminic (2011) investigated the heat transfer characteristics of two-phase closed thermosyphons using nanofluids. The authors plotted thermal resistance versus inclination angle to determine the performance of their HP. They found that water has the highest thermal resistance of 0.05 K/W compared to iron oxide nanoparticles.

In their investigation using heat pipes to enhance heat transfer during the charging and discharging rates of hydrogen in metal hydride tanks, Chung et al. (2013) found that the thermal resistance of their heat pipe ranged from 1.6 to 0.6 K/W at power inputs from 20 to 80 W.

Celata et al. (2010) investigated water filled stainless steel flat evaporators for space application. The authors plotted thermal resistance versus power input and found that the overall thermal resistance decreased from 50.7 to 3.3 ^{o}C/W when power input increased from 20 to 80 W.

Chang et al. (2012) investigated the thermal performance of two-phase water-filled closed-loop thermosyphons and plotted thermal resistance versus power input. They found that thermal resistance decreased from 0.30 to 0.05 K/W as the power input increased from 90 to 210 W.

Solomon et al. (2013) determined the thermal performance of anodized two-phase closed thermosyphon by using a 16.5 mm ID x 350 mm long thermosyphon with a 150 mm long water cooled jacket and a 100 mm long resistance heater (1000 W) at the evaporator section. The authors plotted the thermal resistance versus power input and found that resistance reduced from 0.4 to 0.2 ^{o}C/W as power input increased from 50 to 250 W.

3.2 Theoretical calculations

The following are the equations used in phase B for rapid evaluation of the performance of various heat pipes.

The total heat removed from the container, $\dot{q}_b$, can be calculated from the transient bath temperature versus time results, viz.,

$$\dot{q}_b = W_b c_{pw} \left| \frac{dT_b}{d\theta} \right| \qquad \text{[W]} \qquad \textbf{Equation 23}$$

In the case of a thermosyphon provided with a concentric pipe water cooling jacket, heat transfer from the condenser section, $\dot{q}_w$, of the thermosyphon to the cooling water is given by

$$\dot{q}_w = \dot{m}_w c_{pw} (T_{wo} - T_{wi}) \qquad \text{[W]} \qquad \textbf{Equation 24}$$

The natural convection heat loss, $\dot{q}_{ins}$, from the container to the ambient can be estimated from

$$\dot{q}_{ins} = h_a A_{ins} (T_{ins} - T_a) \qquad \text{[W]} \qquad \textbf{Equation 25}$$

The total heat removed from the container was the sum of the heat transfer to the coolant plus the natural convection heat loss, viz.,

$$\dot{q}_b = \dot{q}_w + \dot{q}_{ins} \quad [\text{W}] \qquad \textbf{Equation 26}$$

A cooling index, γ, is introduced here, defined as the ratio of heat transfer to the coolant/total heat removed from the container, viz.,

$$\gamma = \frac{\dot{q}_w}{\dot{q}_b} \qquad \textbf{Equation 27}$$

or

$$\gamma = \frac{\dot{q}_w}{\dot{q}_w + \dot{q}_{ins}} \qquad \textbf{Equation 28}$$

In the absence of heat loss to the ambient, γ = 1.00.

The mean operating temperature difference between bath and coolant water is defined as

$$\Delta T_w = (T_b - T_w) \qquad [^{\circ}\text{C}] \qquad \textbf{Equation 29}$$

where, T_b is the mean bath temperature and T_w was the mean coolant water temperature defined by.

$$T_W = \frac{T_{wo} + T_{wi}}{2} \qquad [^{\circ}C] \qquad \textbf{Equation 30}$$

3.3 Experimental investigation

3.3.1 Experimental apparatus

The experimental set up is shown in Figure 3.1. The equipment consisted of a 3.2 litre capacity hot water container (± 0.001 litre). All temperatures were measured using type T copper-constantan thermocouples (± 0.5 ^{o}C) connected to a data logger and were logged every minute. Water temperature in the container was measured using two thermocouples immersed in the upper (280 mm from the base) and lower portions (90 mm from the base) of the container. Temperature differences of less than 3 ^{o}C were obtained. Mean container water temperature was taken as the arithmetic mean of the two positions. Two more thermocouples were attached to the outside of the insulated container to determine the external surface temperature of the container in order to calculate the natural convection heat loss from the external surface of the free-standing container. These thermocouples were insulated from the atmosphere using duct tape. Ambient temperature was measured with another thermocouple located nearby. Cross-pieces were attached to the top of each thermosyphon, holding a pressure gauge to measure the saturation pressure, a thermocouple to measure the saturation temperature, and a filling valve. Inlet and outlet water temperatures were measured with thermocouples inserted inside the connecting plastic hoses of the cooling jacket.

Experiments were conducted at two water flow rates, viz.: at 0.9 and 50.0 ml/s (± 1 ml/s).

In order to demonstrate the effectiveness of the method, five copper thermosyphons were fabricated. The thermosyphon dimensions are shown in Table 3 together with the summary of experiments conducted. Details of the thermosyphon are shown in Figure 3.1 and Figure 3.3. The first unit (HP # 1) was a water cooled type. The condenser section consisted of a 38 mm diameter x 127 mm long copper water cooled jacket. The second unit (HP # 2) was an air cooled type with a stainless steel spiral fin measuring 30 mm diameter x 0.5 mm thick stainless steel fins spaced 5 mm apart. The air cooled units (HP# 3, 4, 5) were provided with parallel aluminum fins each 0.5 mm thick x 22.5 mm square x 2 mm pitch at the condenser section respectively. Thermocouples were mechanically attached to the adiabatic and condenser sections of the thermosyphons are shown in Figure 3.3. Forced air circulation rate was provided with an electric fan. Air flow was measured with a hot wire anemometer (± 0.1 m/s). For natural convection, the fan was switched off.

Table 3 Dimensions and experimental runs conducted for comparative method, Phase B

Run	HP #	Pipe shape	Coolant	Flow rate (ml/s), (m/s)	D_e (cm)	L_e (cm)	L_c (cm)	L_{ad} (cm)	A_e (cm^2)	L_e/D_e	L_c/D_e	L_e/L_c
B/1	-	-	-	-	-	-	-	-	-	-	-	-
B/2	1	straight	water	0.9	2.54	12.7	12.7	5	101	5	5	1
B/3	1	straight	water	50	2.54	12.7	12.7	5	101	5	5	1
B/4	2	straight	air	0	1.2	12.7	12.7	5	48	11	11	1
B/5	2	straight	air	2	1.2	12.7	12.7	5	48	11	11	1
B/6	3	straight	air	2	0.9	12.7	25.4	5	36	14	28	0.5
B/7	4	J shape	air	2	0.9	12.7	25.4	75	36	14	28	0.5
B/8	5	L shape	air	2	0.9	12.7	25.4	75	36	14	28	0.5

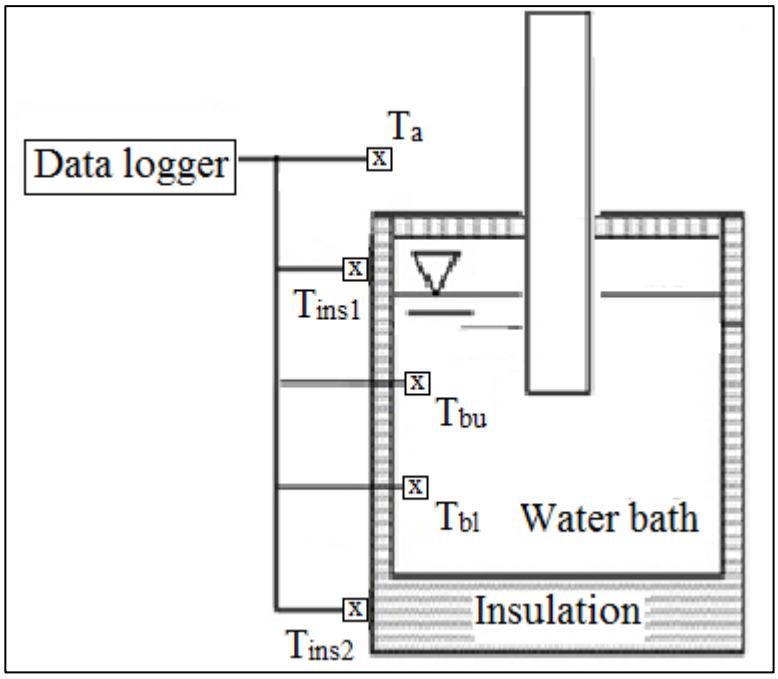

Figure 3.1 Schematic of experimental set up

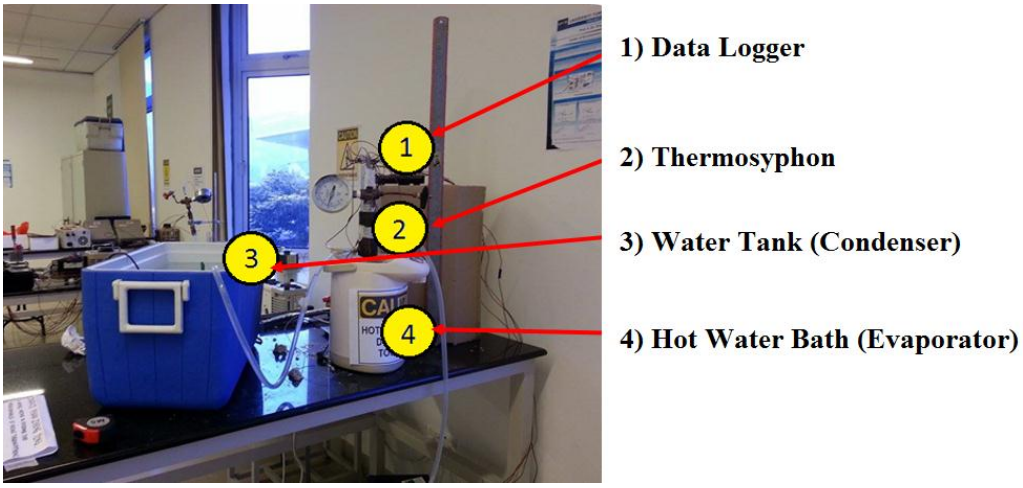

Figure 3.2 Photograph of experimental set up

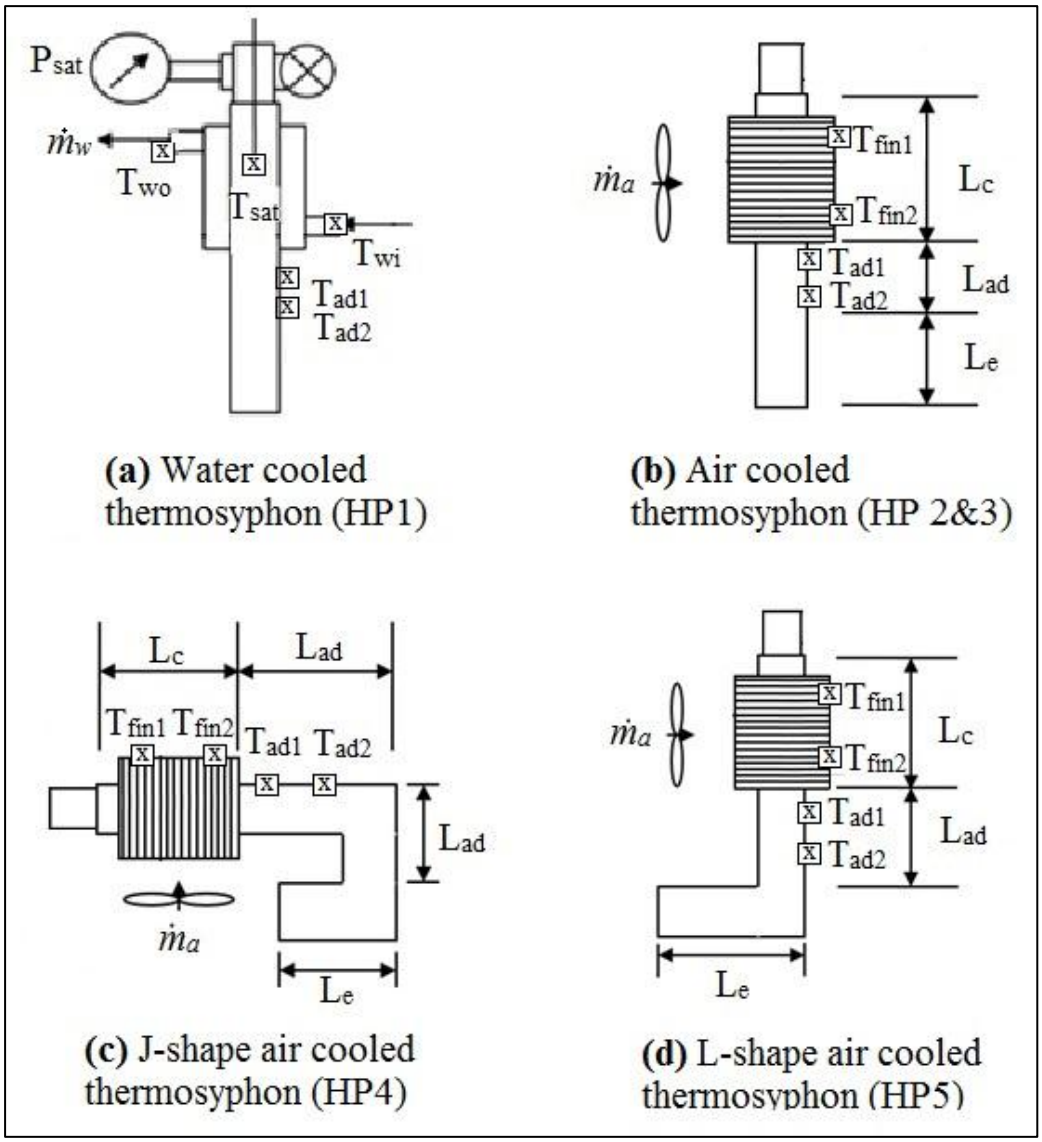

Figure 3.3 Details of thermosyphon

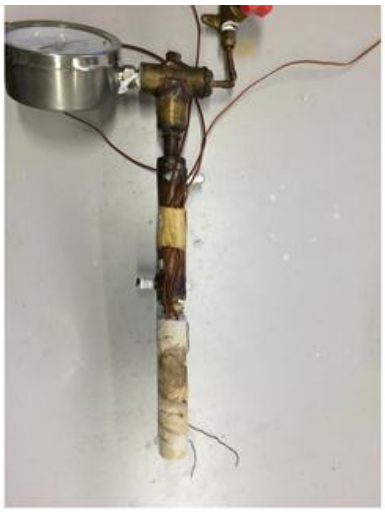

(a) Water cooled thermosyphon (HP1)

(b) Air cooled thermosyphon (HP 2&3)

(c) J-shape air cooled thermosyphon (HP4)

(d) L-shape air cooled thermosyphon (HP5)

Figure 3.4 Photograph of thermosyphon

3.3.2 Experimental procedure

Altogether, eight experimental runs were conducted. The experimental procedure involved heating up the insulated container of water to a temperature of 100 ^{o}C and then allowing it to cool down. The water temperature was measured throughout the cooling process. Experiments were repeated by inserting and immersing the various thermosyphons into the container and measuring the temperature of the hot water as it cooled to 50 ^{o}C before each test. Tests were conducted with varying water flow rates, under natural or forced-air circulation. Each experimental run was repeated three times and the average results were calculated and plotted. Details of the test conditions under which the experiments were carried out are tabulated in Table 3.

The proposed method involves, firstly, determining the transient temperature of an insulated container containing pre-heated hot water. Next, the thermosyphon under investigation was inserted into the container and the temperature recorded. Heat was removed from the container by the thermosyphon throughout the cooling process and also through natural convection heat loss from the side walls of the container.

3.3.3 Experimental results

Figure 3.5 to Figure 3.12 shows the transient temperature response for run B/1 to B/8.

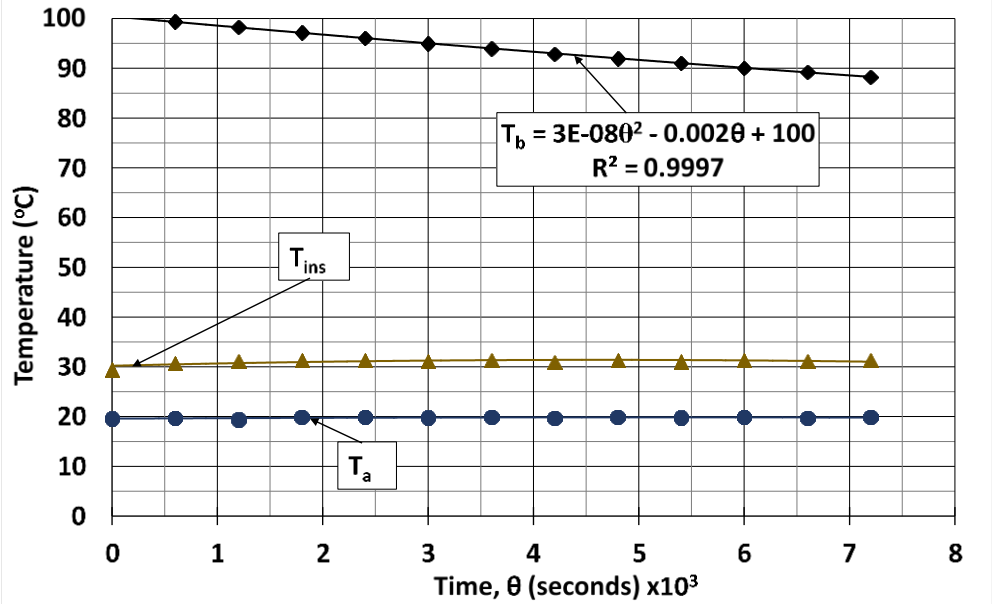

Figure 3.5 Transient temperatures for Run B/1 (no thermosyphon)

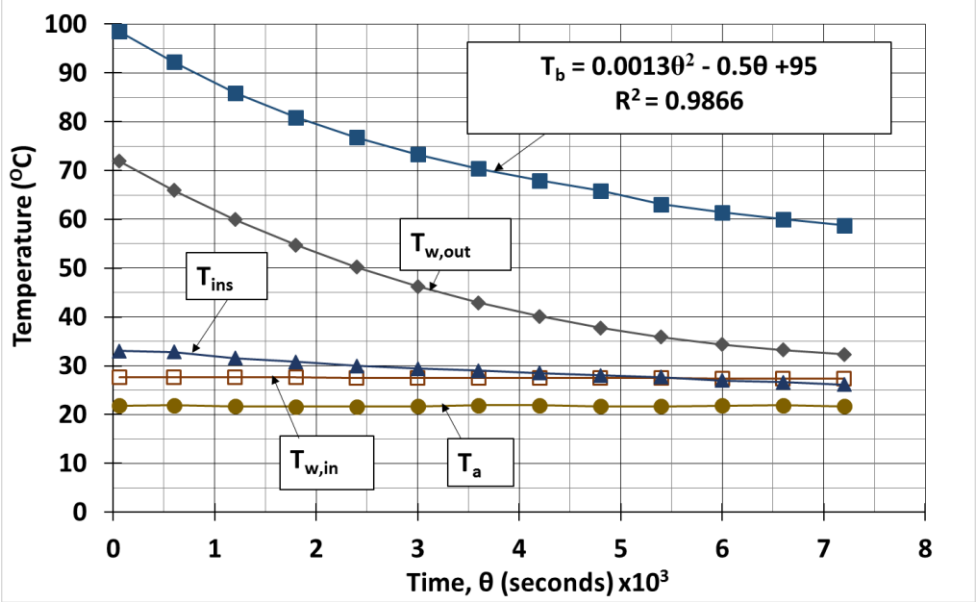

Figure 3.6 Transient temperatures for Run B/2 (water cooled at 0.9ml/s)

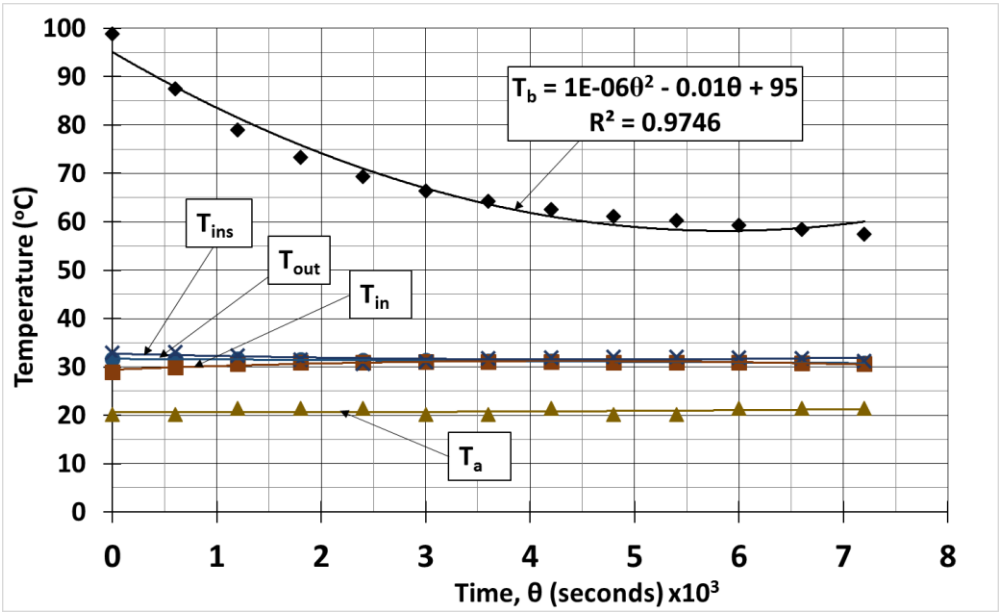

Figure 3.7 Transient temperatures for Run B/3 (water cooled at 50ml/s)

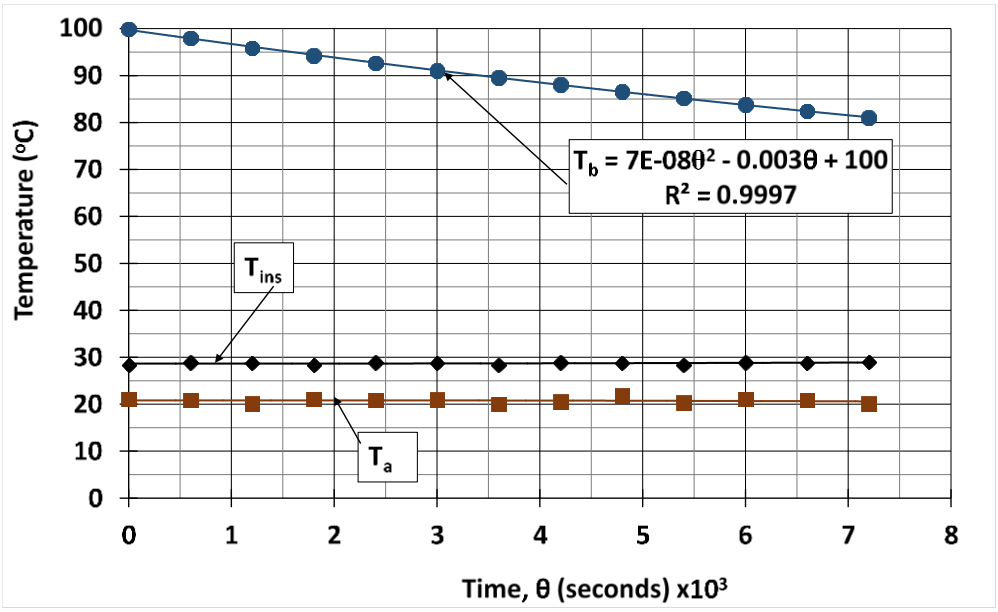

Figure 3.8 Transient temperatures for Run B/4 (air cooled at 0m/s)

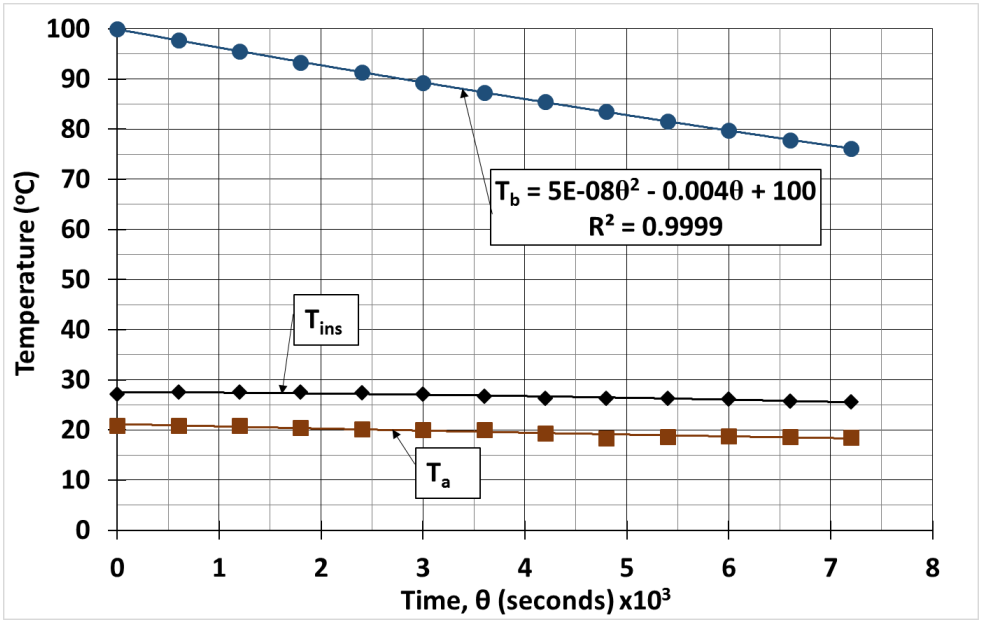

Figure 3.9 Transient temperatures for Run B/5 (air cooled at 2m/s)

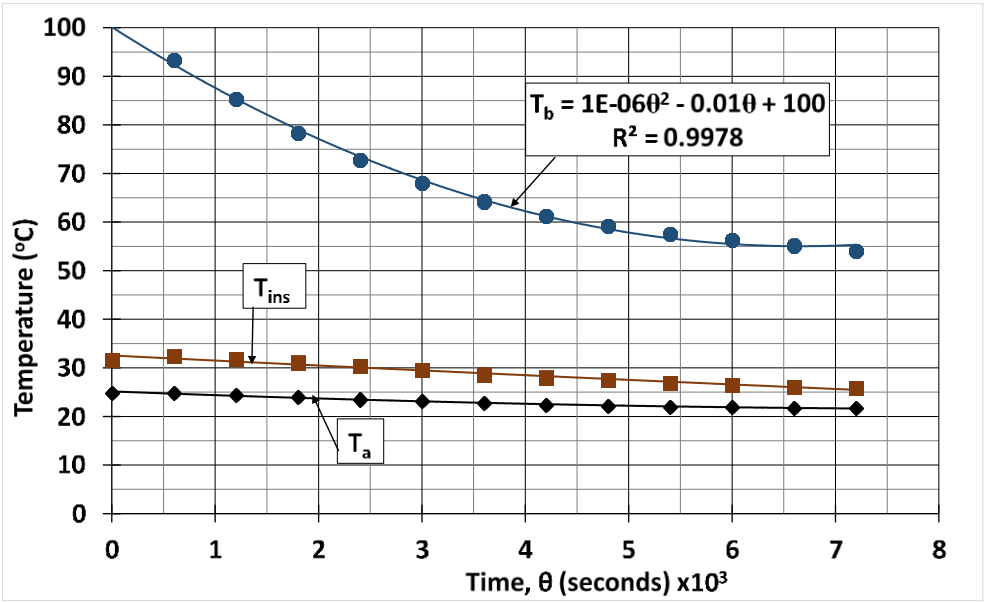

Figure 3.10 Transient temperatures for Run B/6 (air cooled at 2m/s)

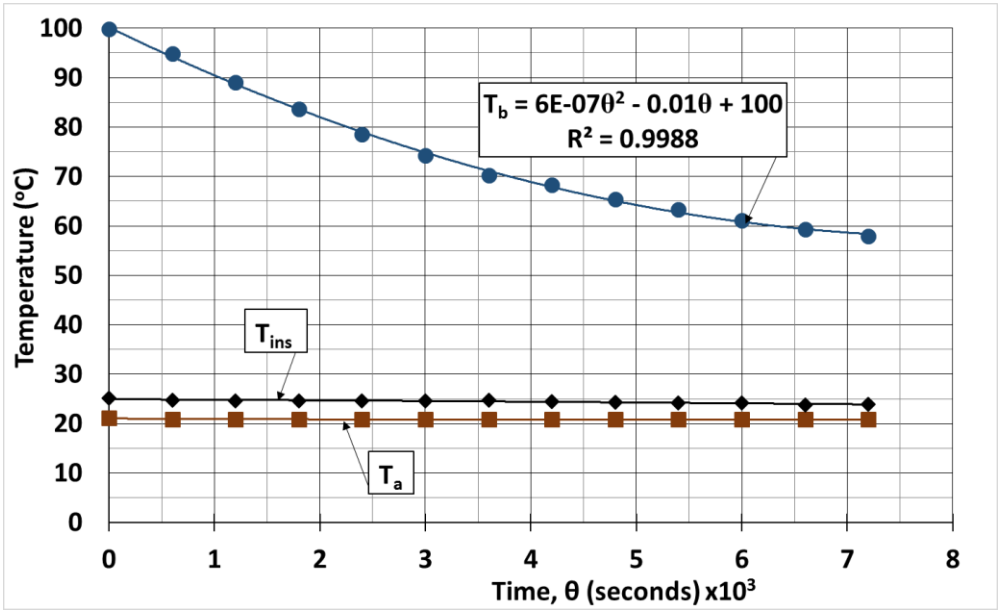

Figure 3.11 Transient temperatures for Run B/7 (air cooled at 2m/s)

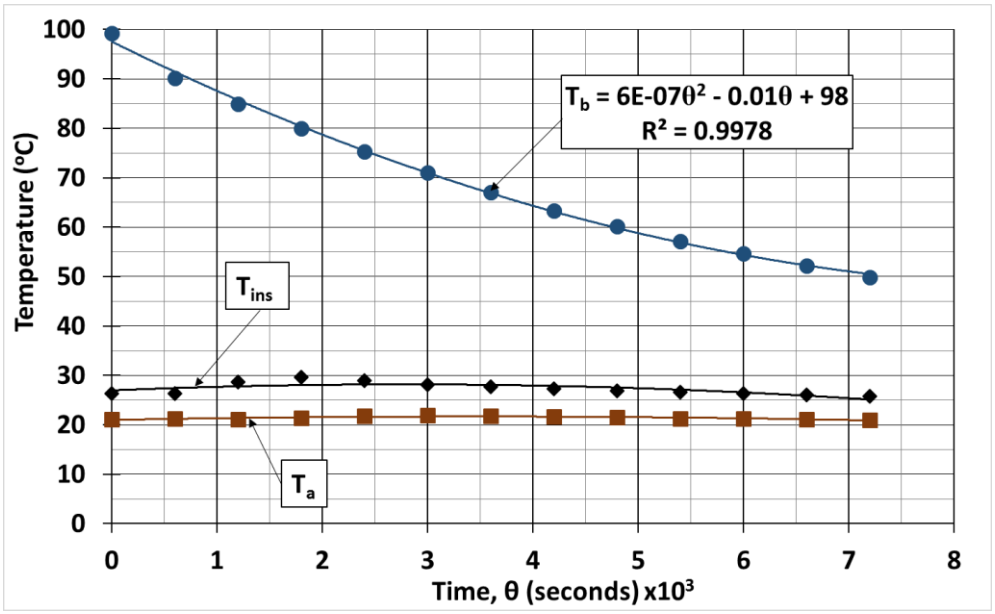

Figure 3.12 Transient temperatures for Run B/8 (air cooled at 2m/s)

Figure 3.13 shows the typical cooling heat rates for run B/2 and its corresponding γ values.

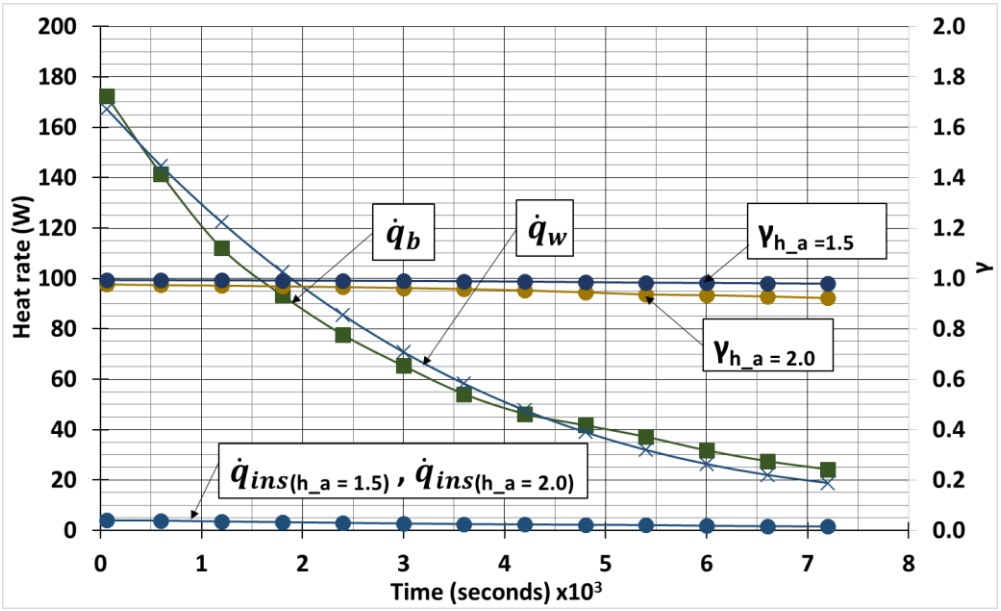

Figure 3.13 Typical cooling heat rates for run B/2

Figure 3.14 to Figure 3.15 compares the performance of various heat pipes using the transient method and the cooling heat rate method.

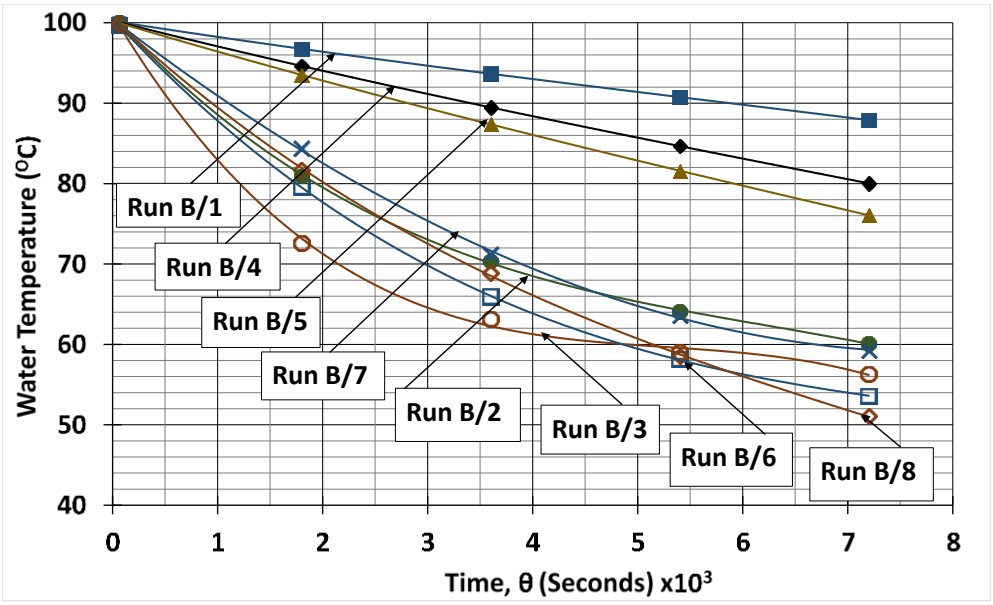

Figure 3.14 Comparison of transient water temperatures for all runs

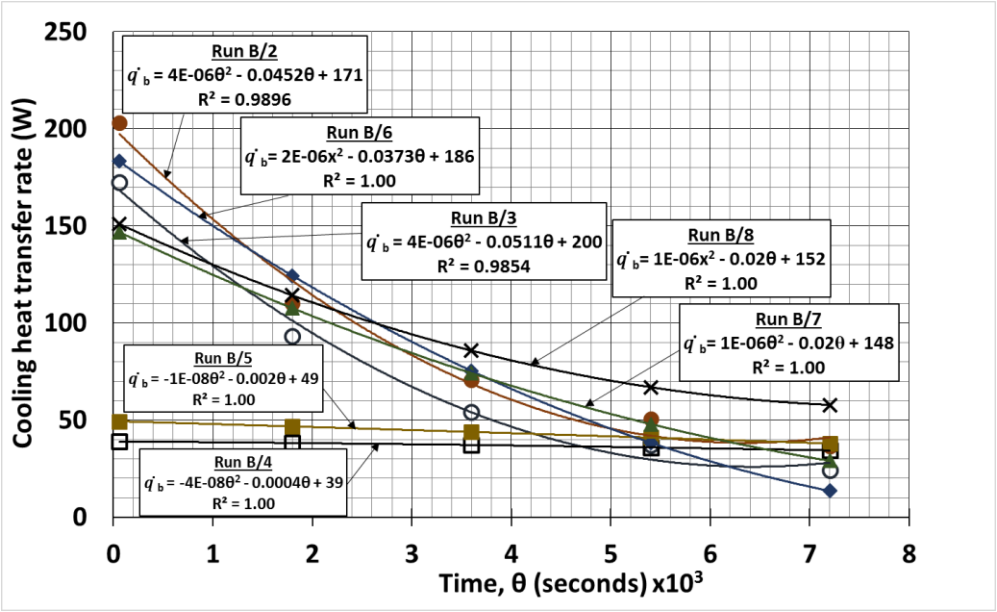

Figure 3.15 Comparison of cooling heat transfer rates with various thermosyphons (Runs B/2-B/8)

Figure 3.16 shows the heat removed from the bath (run B/3) compared to run A/20 and a simulated run based on the same parameters as run B/3 and A/20.

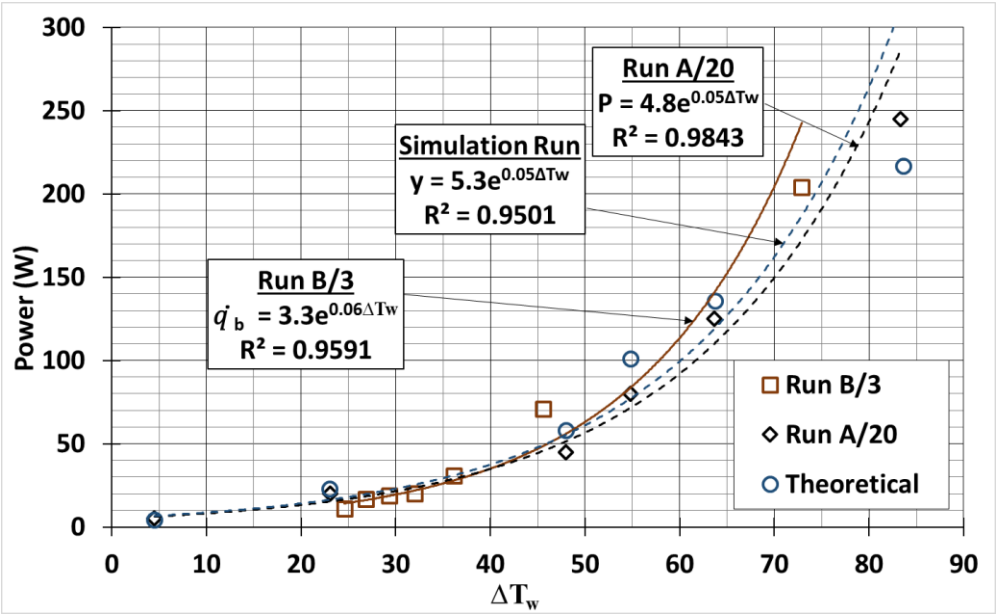

Figure 3.16 Heat removed from bath and input power to thermosyphon vs operating temperature difference (Run A/20 and Run B/3)

3.4 Discussion of experimental results

3.4.1 Transient temperature

A typical set of transient temperature results obtained in Run B/2 with a minimum coolant flow rate of 0.9 ml/s is shown in Figure 3.6. Mean water container (T_b), coolant water inlet (T_{wi}), coolant water outlet (T_{wo}), mean insulation (T_{ins}), and ambient temperatures were plotted. The results show that it took more than 3 hours for the water to be cooled down from 100 ^oC to 50 ^oC with the HP1 type thermosyphon. The experiment was stopped after 3.33 hours. A quadratic temperature-time relationship ($T_b = 0.0013\ \theta^2 - 0.47\ \theta + 95$) was calculated for the mean container temperature with a regression coefficient of 0.9866. The coolant water outlet temperature dropped from 72 ^oC initially to 30 ^oC after 3.33 hours. The temperature difference between inlet and outlet of the coolant water was about 44 ^oC initially and about 5 ^oC after 2 hours of cooling indicating that not much cooling could be performed when the container temperature dropped to about 50 ^oC and below.

3.4.2 Heat transfer cooling rates

Typical heat transfer cooling rates in Run B/2 are plotted up to 2 hours of operation in Figure 3.13. The heat removed from the container ($\dot{q}_b$), heat transfer rate to the coolant water ($\dot{q}_w$), and the natural convection heat loss ($\dot{q}_{ins}$) are plotted together with the cooling index (γ). The results show that the

cooling rate of the thermosyphon decreased with time or as the container cools, which is to be expected. The heat loss from the container ($\dot{q}_{ins}$) was small. At the start of the experiment, $\dot{q}_{ins}$ was 3 W and h_a = 1.5 W/m^{2}K. Towards the end of the experiment, $\dot{q}_{ins}$ = 2 W and h_a = 1.5 W/m^{2}K. γ varied between 1.00 and 0.98. When h_a = 2.0 W/m^{2}K, γ varied between 0.98 and 0.93. The variation in the γ factor was attributed to the value of h_a assumed to calculate ambient heat loss.

3.4.3 Comparative performance of thermosyphons

The performance of the thermosyphons could be compared using the transient container temperature results plotted in Figure 3.14. The rate at which container temperature decreases is a measure of the cooling efficiency of the thermosyphon. The result of natural cooling without immersion of the thermosyphon in the container (Run B/1) is shown as a base for comparison, showing the slowest cooling rate. All the results show that systems with the thermosyphons increased the cooling rate (Run B/2 to B/9). For natural cooling (Run B/1), it took nearly 2 hours to cool the water from 100 ^{o}C to 88 ^{o}C. With the HP1 type water-cooled thermosyphon (Run B/2), and a low coolant flow rate of 0.9 ml/s, 100 ^{o}C water was cooled to 60 ^{o}C in 2 hours. The same thermosyphon performed better at high coolant flow rate (Run B/3) than at low flow rate (Run B/2), as was expected. The results also show that forced convection air cooling (Run B/5) was better than natural convection air cooling (Run B/4) for the HP2 type thermosyphon, as predicted. From the results, it

would seem that the L-shaped type HP5 thermosyphon (Run B/8) performed better than the straight pipe of type HP3 (Run B/6) followed by the J-shape type HP4 (Run B/7) unit. For the air cooled HP2 & HP3 type pipes, Run 6 with the longer condenser length performed better than the shorter one in Run B/5. It should be pointed out here that the thermosyphons are of different sizes and the length of the evaporator sections that were immersed in the hot water varied from pipe to pipe as indicated in Table 3. Hence, in order to determine which geometrical pipe performs better, it would be necessary to build and compare pipes with equivalent sizes.

3.4.4 Effect of coolant water flow rate and natural and forced convection air cooling

The effect of coolant water flow rate, and natural and forced convection air cooling in Runs B/2 to B/5 are demonstrated in Figure 3.15. Better performance resulted in lower container temperature as seen in Figure 3.14 or greater heat removal rate from the container. The heat transfer rate results in Figure 3.15 show that thermosyphons with higher coolant flow rate (Run B/3) performed better than at low flow rates (Run B/2). In the case of air cooling, thermosyphons with forced convection air flow (Run B/6 > Run B/7 > Run B/8 > Run B/5) performed better than natural convection (Run B/4).

3.4.5 Comparison between performance testing methods and simulation

The comparison between the novel method and a traditional method (experimental methods carried out in phase A) as well as a simulated run are demonstrated in Figure 3.16. The simulation results shows a similar trend to Run A/20. Run A/20 and Run B/3 are in agreement which shows that the novel method and traditional method are comparable.

The simulation run was modeled after the same parameters as Run A/20 and Run B/3 where the dimension of the heat pipe used in Run A/20 and Run B/3 was fed into the thermal network model described in Section 2.2. The heat transfer coefficients were derived from the experiments in phase A. From the simulation the interface temperatures were simulated and the temperature difference and the power was obtained from this model and plotted in Figure 3.16. The results can be seen in Appendix B.

3.5 Chapter conclusion

In phase B, a method to compare the performance of various thermosyphons rapidly and economically was proposed. The ease and simplicity of the procedure was demonstrated by cooling a container of hot water using various thermosyphons. From the results obtained it was found that forced air convection cooling was better than natural convection, and that high water flow rate was better than low flow rate.

CHAPTER 4

PHASE C: DEVELOPMENT AND TESTING OF THERMOSYPHON HEAT PIPE HEAT EXCHANGER (THPHE) COOLER TO REPLACE A COOLING TOWER

In chapter 4, a brief review on heat exchangers designs, thermosyphon heat pipe heat exchangers and work done on heat exchanger systems are introduced. The procedure and fabrication of the THPHE cooler details are described in chapter 4. The performance of the thermosyphon heat pipe heat exchanger, THPHE, cooler using water and R410a are presented and discussed. The results obtained from phase C experimentally are compared against the results from the theoretical model are presented and discussed as well.

The objective of phase C, to fabricate and test a modular THPHE cooler to replace a conventional cooling tower for the cooling of molds and dies in the foundry industry.

4.1 Literature survey

4.2 Heat Pipe Heat Exchangers (HPHE)

Jouhara et al. (2015) conducted an experimental and numerical investigation of an air-to-water heat pipe-based heat exchanger. The authors used a water-filled HPHE system. The system comprised two rows of heat pipes with three heat pipes in each row. The heat pipes measured 28 mm OD x

2000 mm long, all six of the heat pipes were identical. A 30 kW heater and a centrifugal fan supplied hot air (0.05-0.14 kg/s) to the evaporator section between 100-250 ^{o}C and a cold water circuit was used to cool down the condenser. The pressure and temperature was controlled by a constant water head on the water tank and a small cooler inside the tank; water was supplied at 0.08 kg/s and temperature was kept at about 14 ^{o}C. This HPHE system has a high heat transfer rate of 6000 W (highest) at 250 ^{o}C and 1000 W at 100 ^{o}C at the evaporator respectively. The author mentions that the effectiveness of this HPHE was 13-28 % over a varying air mass flow rate and power setting.

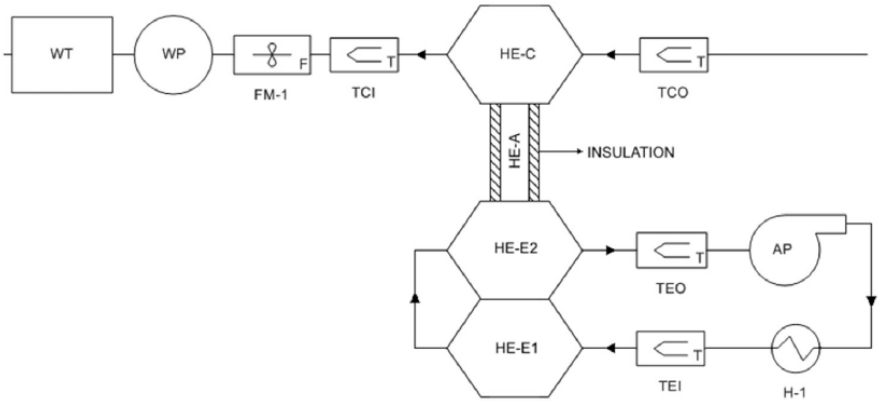

Figure 4.1 Schematic drawing of the heat exchanger: WT - water tank, WP - water pump, FM - flow meter, TCI - thermocouple condenser inlet, TCO - thermocouple condenser (Jouhara et al. 2015)

Longo et al. (2014) conducted an experimental and theoretical analysis of a heat pipe heat exchanger operating with a refrigerant with low global warming potential. Longo designed an air-to-air HPHE system for a heating, ventilating, and air conditioning (HVAC) system using HFC134a and HFO1234ZE(E) as fill liquid. The authors' HPHE system consist of 54 horizontal copper heat pipes measuring 12.7 mm, micro-fin copper tubes 700

mm in length, and aluminium continuous fins 0.115 mm in thickness with 3 mm of fin spacing. Its evaporator, condenser, and adiabatic length are 270 mm, 270 mm, and 160 mm, respectively. The evaporator temperature was kept at 25 ^{o}C for summer and 20 ^{o}C for winter, whereas the condenser was kept between 35-40 ^{o}C during summer and 7-10 ^{o}C during winter. The authors mention that the effectiveness of this system was 30-55 % and was able to transfer up to 1500 W. This HPHE system agrees with the findings of Ong and Haider (2003), that heat pipes are able to function at low temperature difference between the condenser and evaporator section, at about 5 ^{o}C.

Yang et al. (2003) studied waste heat recovery using heat pipe heat exchangers for heating automobiles using exhaust gas. The author used steel heat pipes with water as the fill liquid. This system consisted of 50 tubes measuring 20 mm OD x 310 mm. The length of the evaporator, condenser, and adiabatic were 150 mm, 150 mm, and 5 mm, respectively. The heat source used was from a bus exhaust and the condenser section was the ambient air within the bus carriage. The authors mention that this system was able to transfer 1000-7000 W over a temperature range of 50-350 ^{o}C.

Geld et al. (2007) experimented on air heat exchangers with long heat pipes. This system consists of 54 heat pipes distributed into 4 rows with a 14-13-14-13 formation. The author used R134a as the fill liquid at FRs of 0.19 and 0.59. The heat pipes measured 16 mm OD x 1500 mm. The condenser section was effected by a variable speed fan between 0.4-2.0 kg/s. The evaporator and condenser temperature range was between 40-70 ^{o}C and 20-50 ^{o}C respectively.

The system was able to extract up to 20kW and the effectiveness was rated at 90 %.

Noie (2006) investigated the thermal performance of an air-to-air thermosyphon heat exchanger using the ε-NTU method. Noie used water as the fill liquid at FR = 0.6. This system consisted of 90 copper tubes measuring 15 mm OD x 1300 mm. There are 6 rows in this system; 15 tubes in each row. The aluminium fins attached to the evaporator and condenser sections were 0.4 mm thick with 300 fins per meter. The evaporator, condenser, and adiabatic length were 600 mm, 600 mm, and 100 mm respectively. The evaporator was supplied with hot air (110-260 ^{o}C) by means of a variable speed centrifugal fan and a 72 kW heating element. The condenser section was cooled down with ambient air by means of a centrifugal fan at speeds between 2.5-5.34 m/s. The author mentions the effectiveness of this system was 60 %.

4.3 Theoretical calculations

The following are the equations used in phase C for evaluating the thermal performance of a modular THPHE cooler as a cooling tower replacement. Equation 22 to Equation 27 are common equations in phase B and C, as both phases share the same method of determining the performance of their respective systems. The difference between phase B and C are the equations used to determine the performance at the condenser.

The mean operating temperature difference between bath and the condenser section was defined as

$$\Delta T_{b-air,mean} = (T_b - T_{air,mean}) \ [^{\circ}C] \qquad \textbf{Equation 31}$$

where, T_b is the mean bath temperature and $T_{air,mean}$ is the mean condenser temperature defined by:

$$T_{air,mean} = \frac{T_{air,in} + T_{air,out}}{2} \ [^{\circ}C] \qquad \textbf{Equation 32}$$

4.4 Experimental investigation

4.4.1 Experimental apparatus

The experimental set up is shown in Figure 4.2. The equipment consisted of a 26 litre capacity hot water container (± 0.001 litre). All temperatures were measured using type T copper-constantan thermocouples (± 0.5 ^{o}C) connected to a data logger and were logged every minute. Water temperature in the container was measured using three thermocouples immersed in the upper, middle, and lower portions of the container. Temperature differences of less than 3 ^{o}C were obtained. Mean container water temperature was taken as the arithmetic mean of the three positions. Four more thermocouples were attached to the outside of the insulated container to determine the external surface temperature of the container in order to calculate

the natural convection heat loss from the external surface of the free-standing container. These thermocouples were insulated from the atmosphere using duct tape. Ambient temperature was measured with another thermocouple located nearby. Cross-pieces were attached to the middle of each thermosyphon, holding a pressure gauge to measure the saturation pressure and a filling valve. Inlet and outlet air temperatures were measured with thermocouples inserted inside the inlet and outlet of the duct of the condenser section. Experiments were conducted at one air flow rate, viz., at 0.6 m/s (± 0.1 m/s).

Dimensions of the thermosyphon are shown in Figure 4.5 and Figure 4.6. The condenser section consisted of a 10 mm OD x 352 mm long copper air cooled parallel fins (500 fins per meter). The evaporator section consisted of a 10 mm OD x 152 mm long copper with parallel aluminium fins (500 fins per meter) submerged in a hot water bath. The location of thermocouples are shown in Figure 4.4. Forced air circulation rate was provided with an electric fan. Air flow was measured with a hot wire anemometer (± 0.1 m/s).

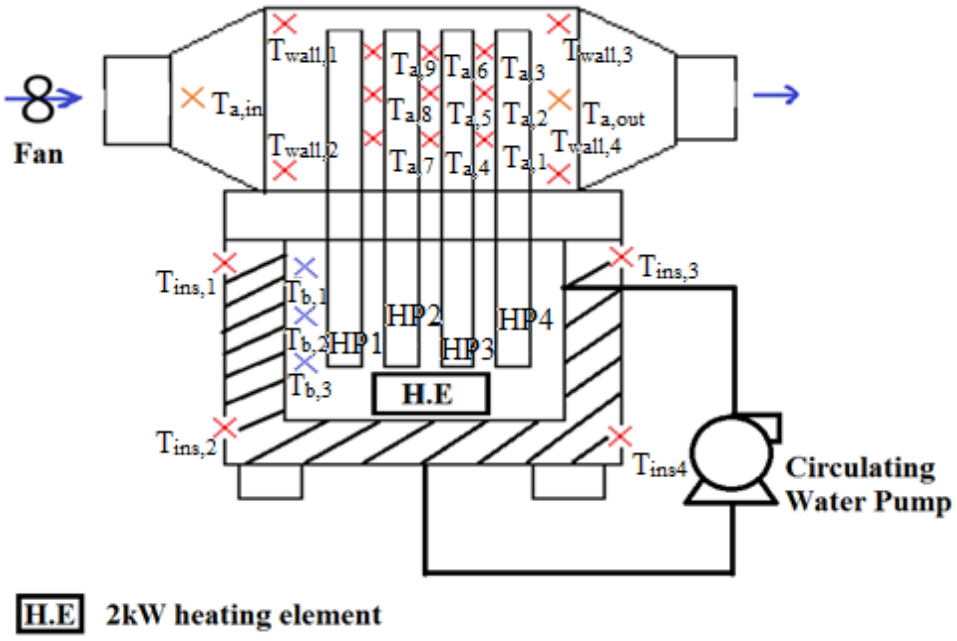

Figure 4.2 Experimental set up for THPHE

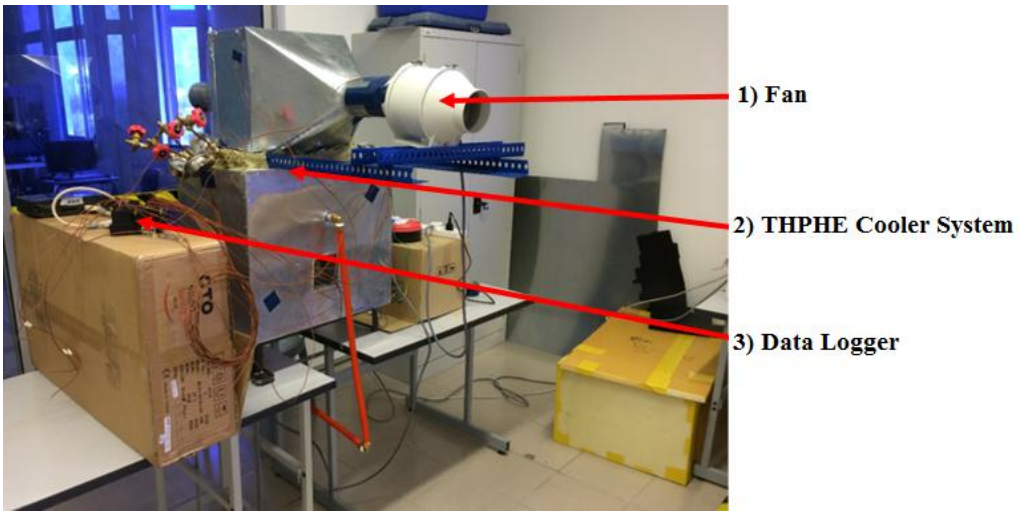

Figure 4.3 Photograph of set up for THPHE

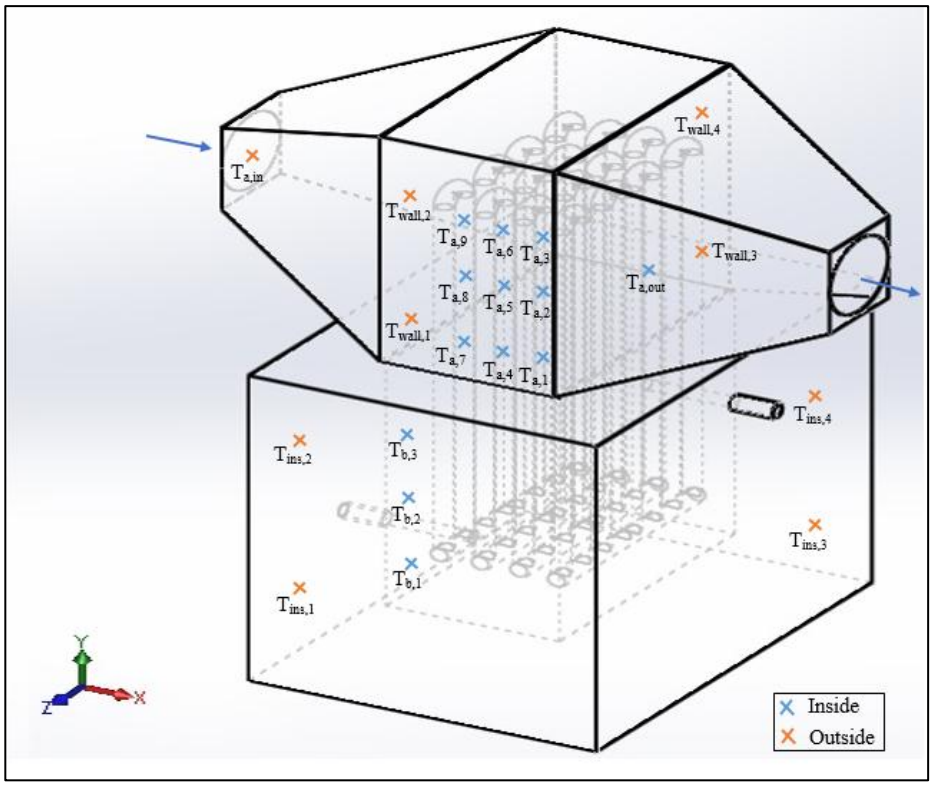

Figure 4.4 Isometric sketch with thermocouple locations

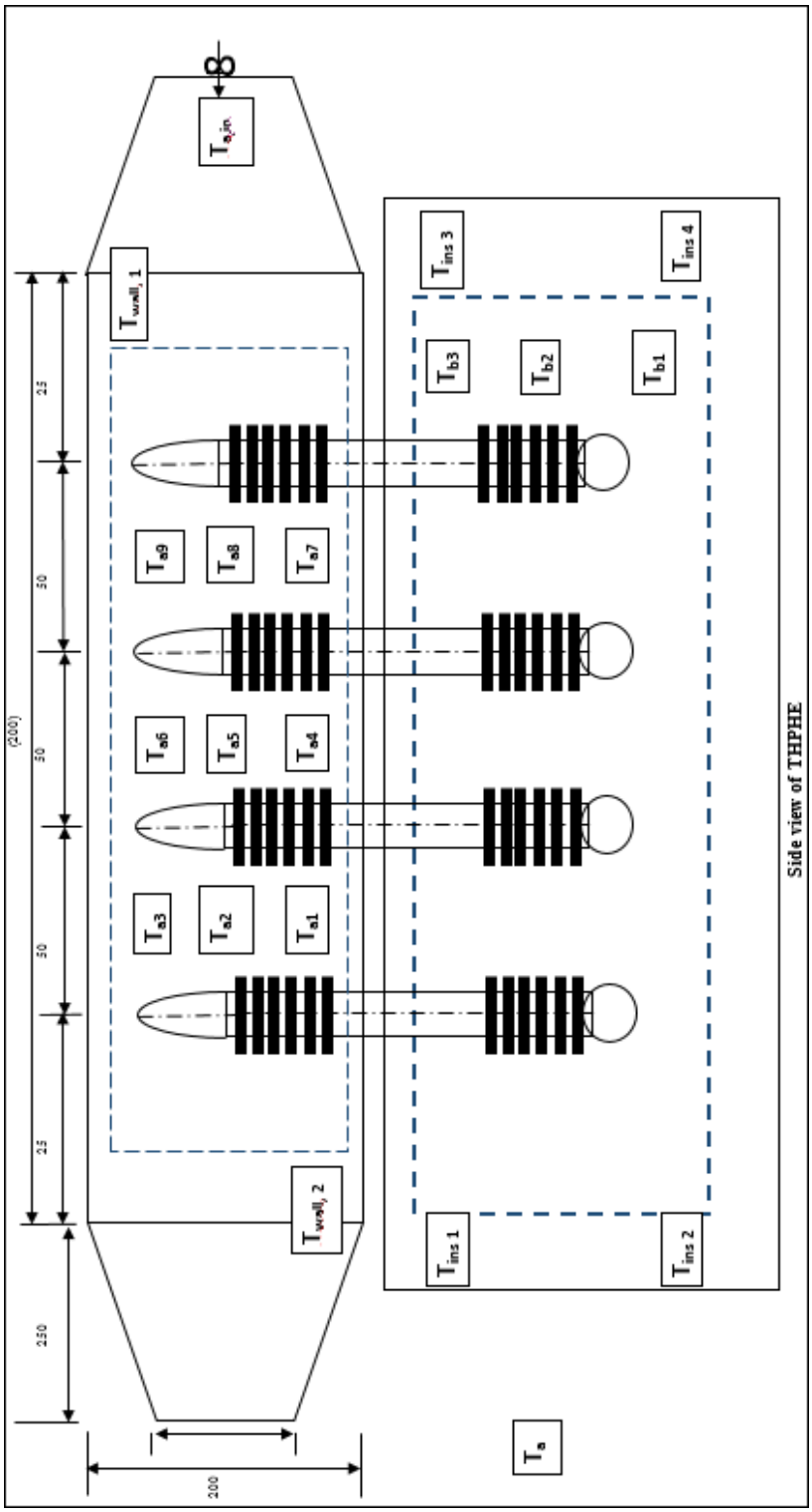

Figure 4.5 Side view of the experimental set-up and probe positioning

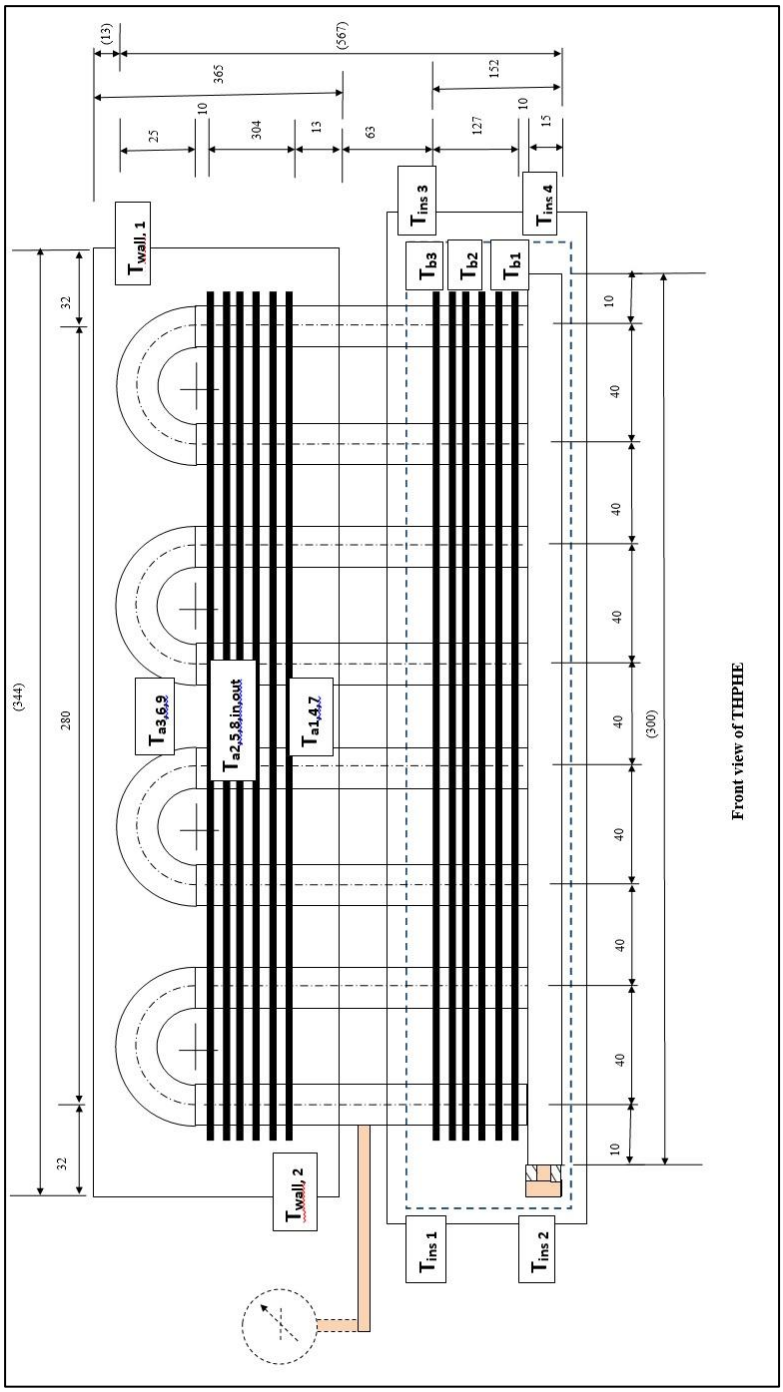

Figure 4.6 Sectional XX view of the experimental set-up

4.4.2 Experimental procedure

Altogether, nine experimental runs were conducted. The experimental procedure involved heating up the insulated container of water to a temperature of 80 ^{o}C and then allowing it to cool down. The water temperature was measured throughout the cooling process. Experiments were repeated by varying the amount of FR and type of FR in the thermosyphons to be tested into the container and measuring the temperature of the hot water as it cooled for two hours. Each experimental run was repeated three times and the average results were obtained and plotted; each individual repeated run is defined as, viz.. C/1a, C/1b, C/1c respectively. Details of the test conditions under which the experiments were carried out are tabulated in Table 4.

Table 4 Experimental runs conducted for THPHE cooler, Phase C

Run	Fill Liquid	FR	$\dot{u}_a$ (m/s)
C/1	-	-	-
C/2	R410a	1.0	0.6
C/3	R410a	0.75	0.6
C/4	R410a	0.5	0.6
C/5	R410a	0.25	0.6
C/6	Distilled Water	1.0	0.6
C/7	Distilled Water	0.75	0.6
C/8	Distilled Water	0.5	0.6
C/9	Distilled Water	0.25	0.6

4.4.3 Experimental results

Figure 4.7 shows the repeatability of the experiment for Run C/2a, C/2b and C/2c. The three runs have the same parameters as run C/2.

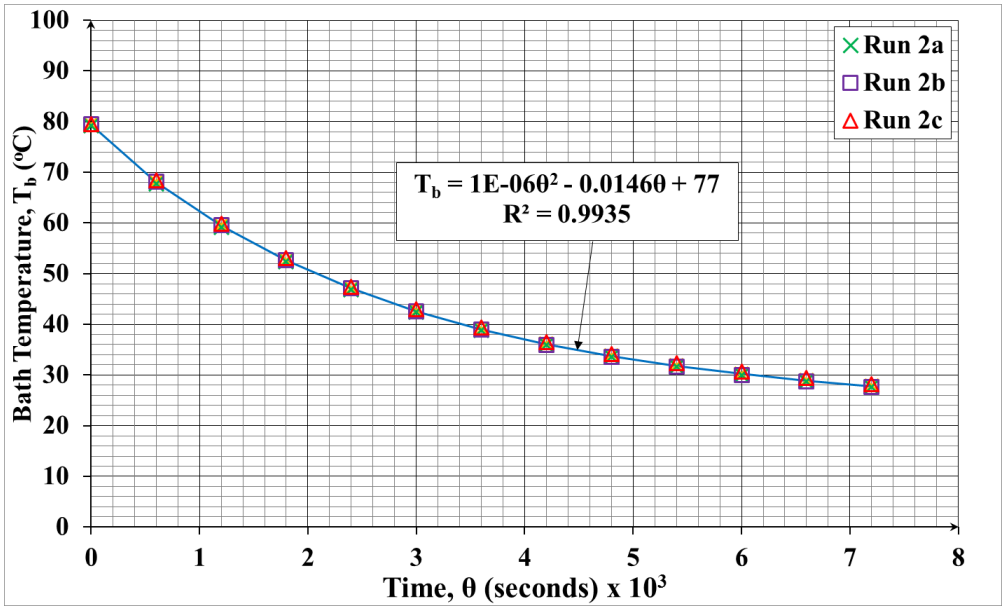

Figure 4.7 Repeatability test for runs C/2a, C/2b and C/2c

Figure 4.8 to Figure 4.16 show the transient bath temperature for run C/1 to C/9

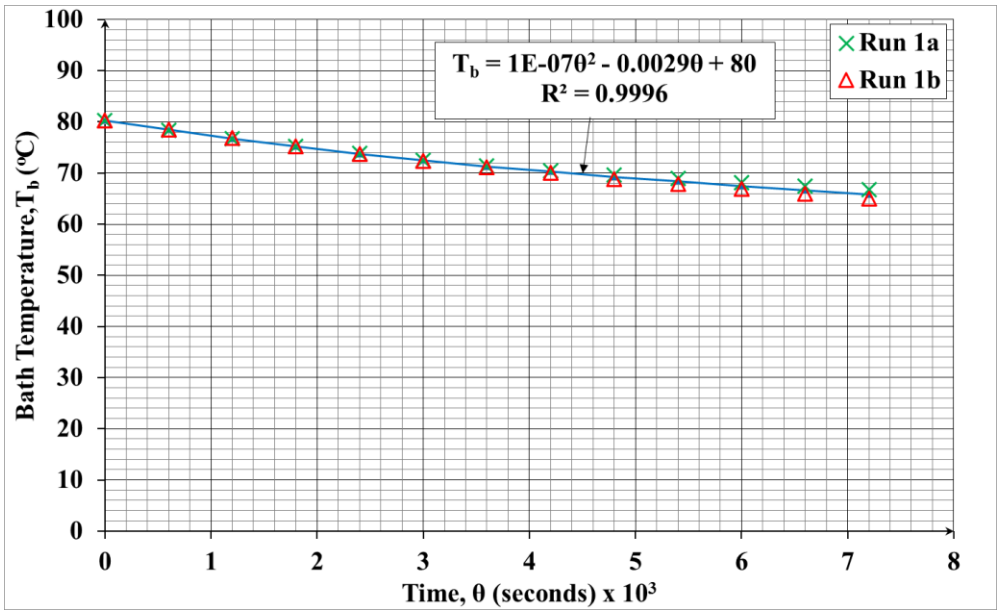

Figure 4.8 Transient bath temperatures for Run C/1

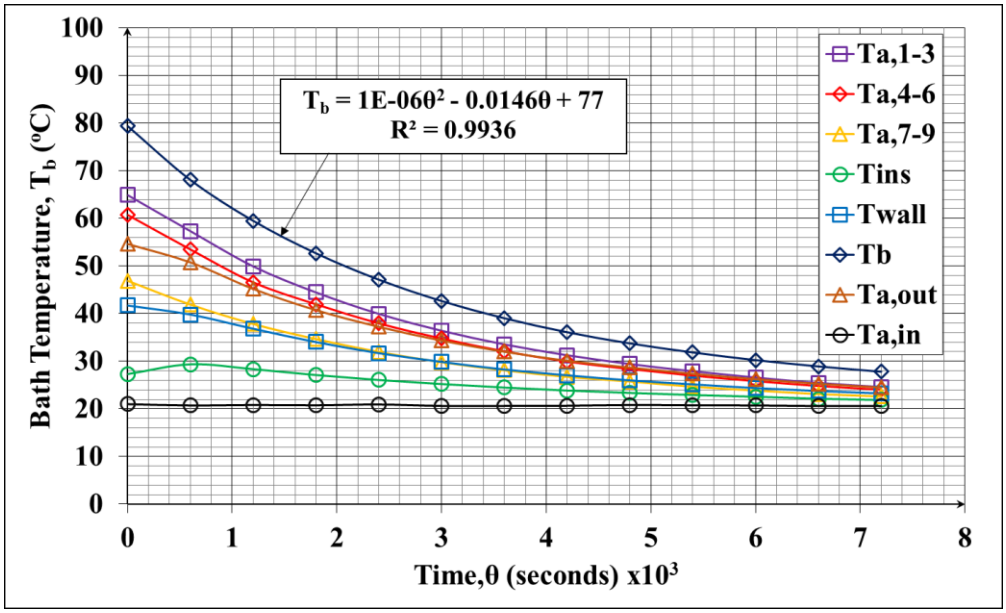

Figure 4.9 Transient bath temperatures for Run C/2

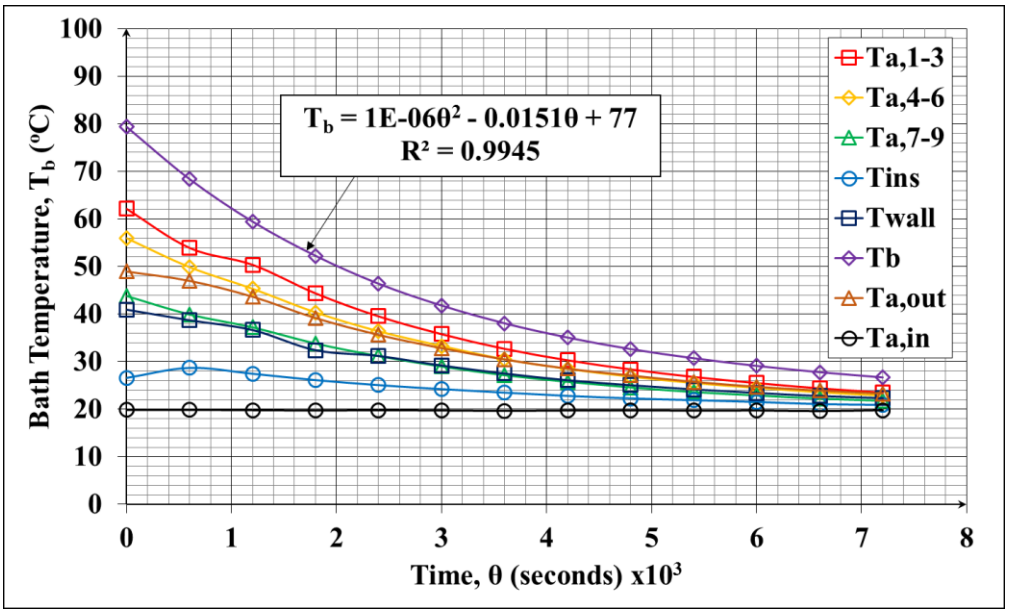

Figure 4.10 Transient bath temperatures for Run C/3

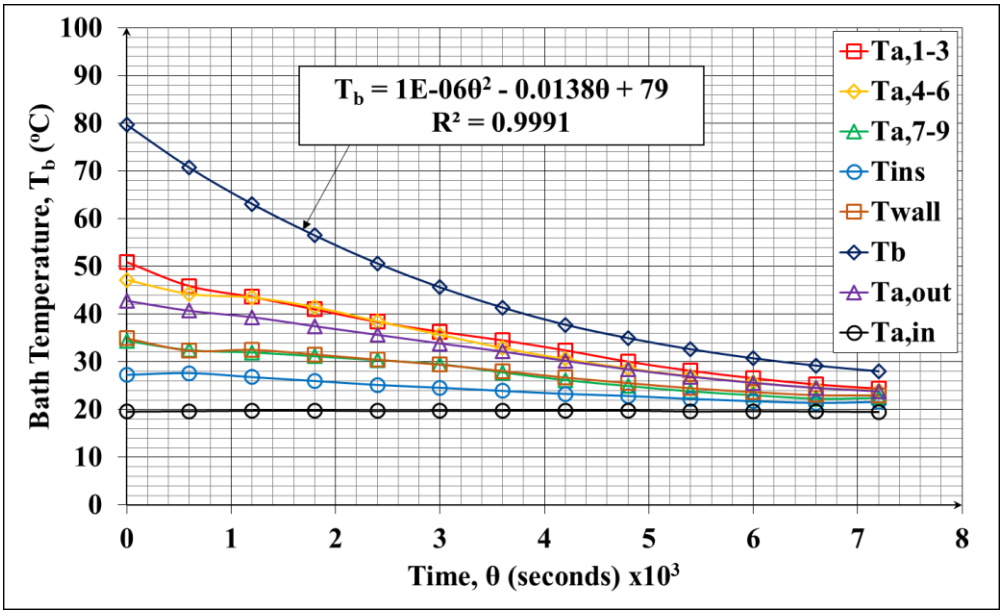

Figure 4.11 Transient bath temperatures for Run C/4

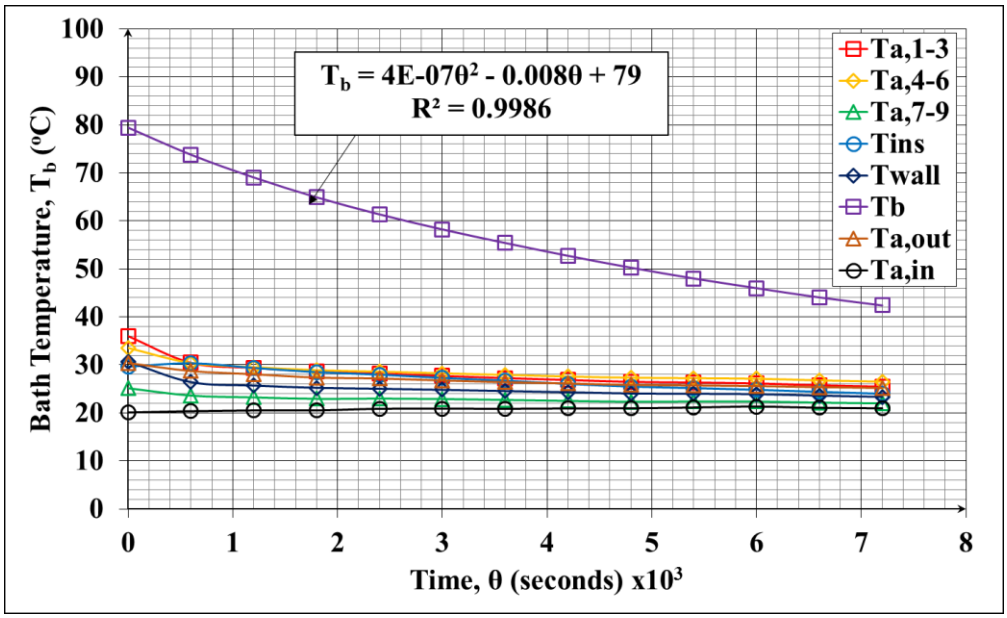

Figure 4.12 Transient bath temperatures for Run C/5

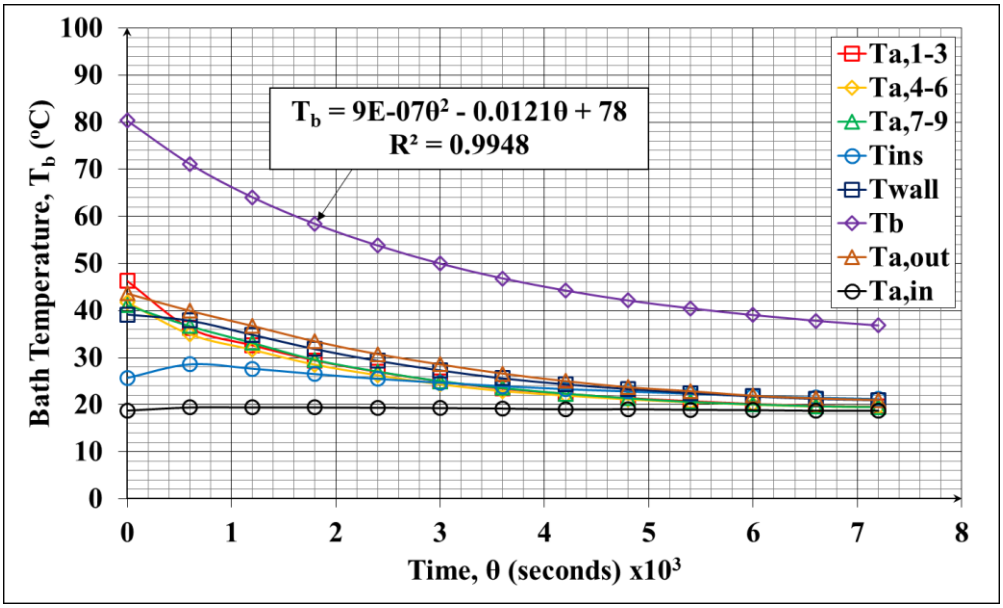

Figure 4.13 Transient bath temperatures for Run C/6

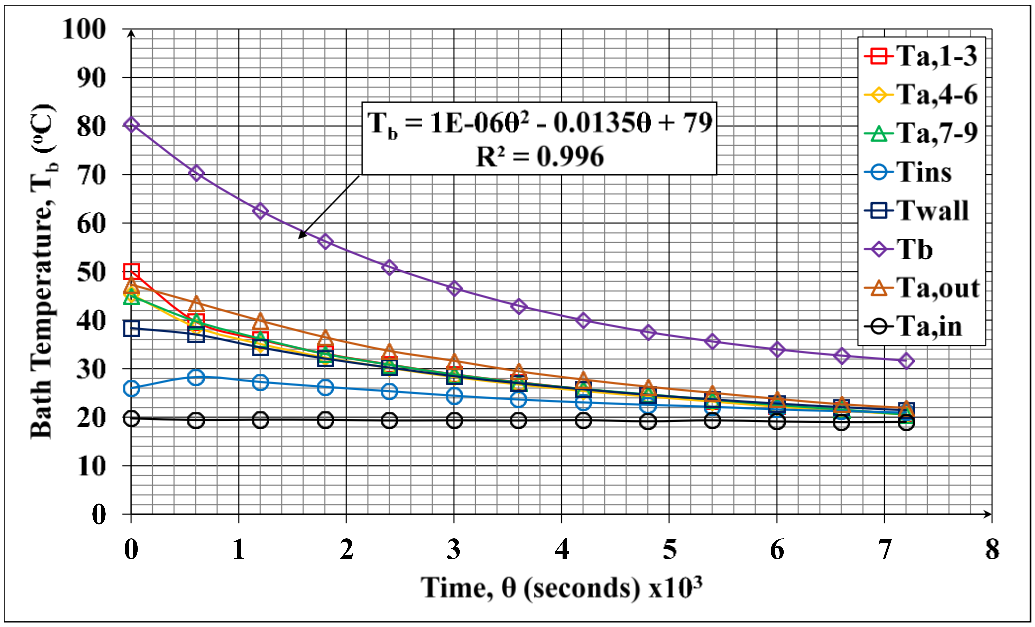

Figure 4.14 Transient bath temperatures for run C/7

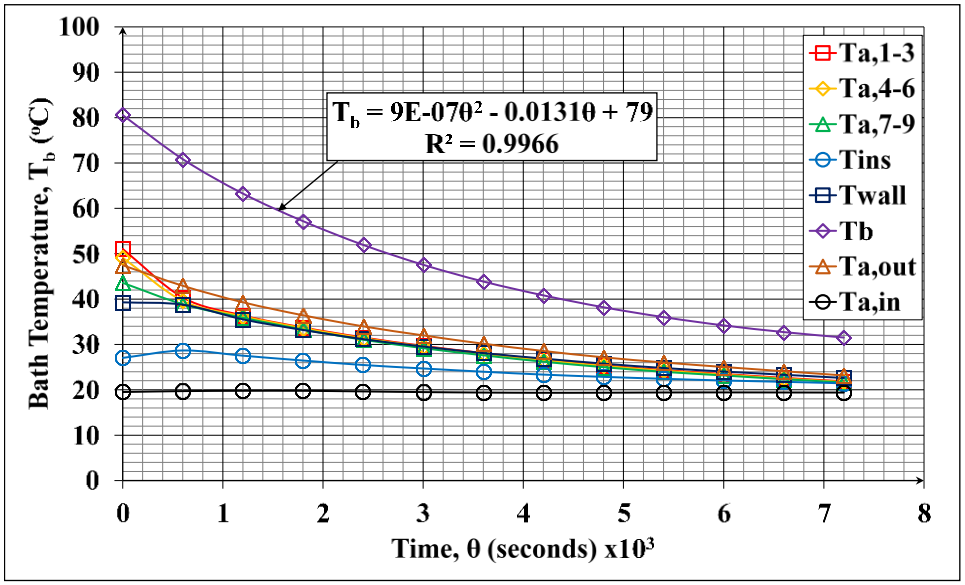

Figure 4.15 Transient bath temperatures for run C/8

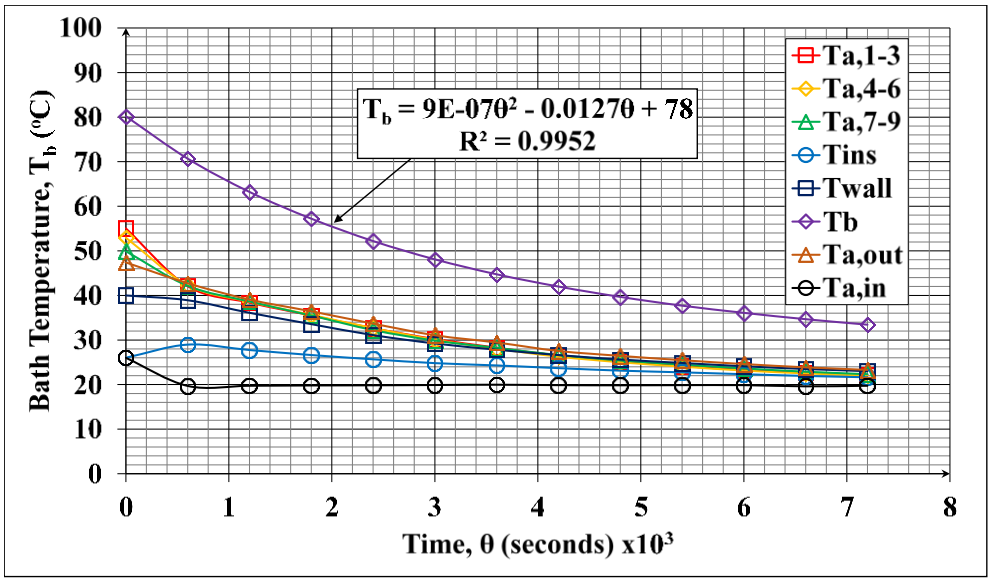

Figure 4.16 Transient bath temperatures for run C/9

Figure 4.17 and Figure 4.18 shows the effect of FR on the performance of the THPHE cooler with R410a and water as fill liquid.

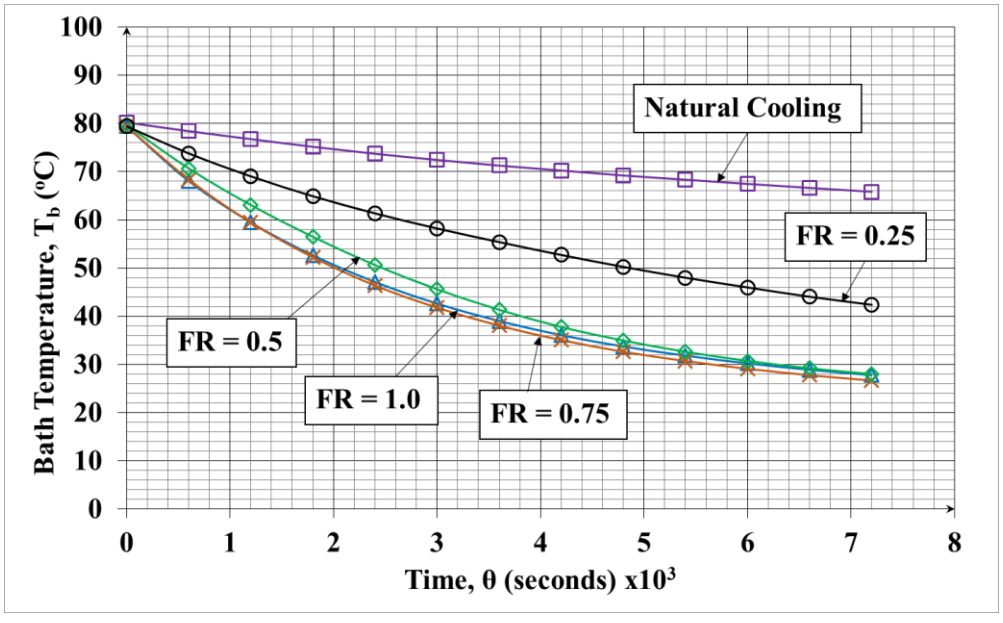

Figure 4.17 Effect of fill ratio on R410a filled THPHE cooler (Run C/1-C/-5)

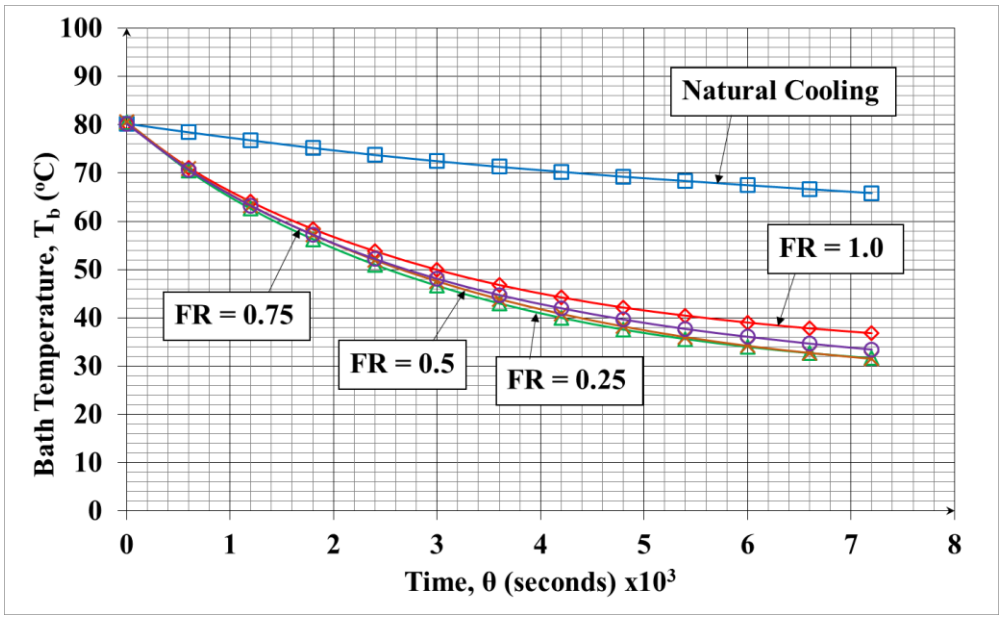

Figure 4.18 Effect of fill ratio on water filled THPHE cooler (Run C/1, C/6-C/9)

Figure 4.19 shows the effect of fill liquid type on the performance of the THPHE cooler.

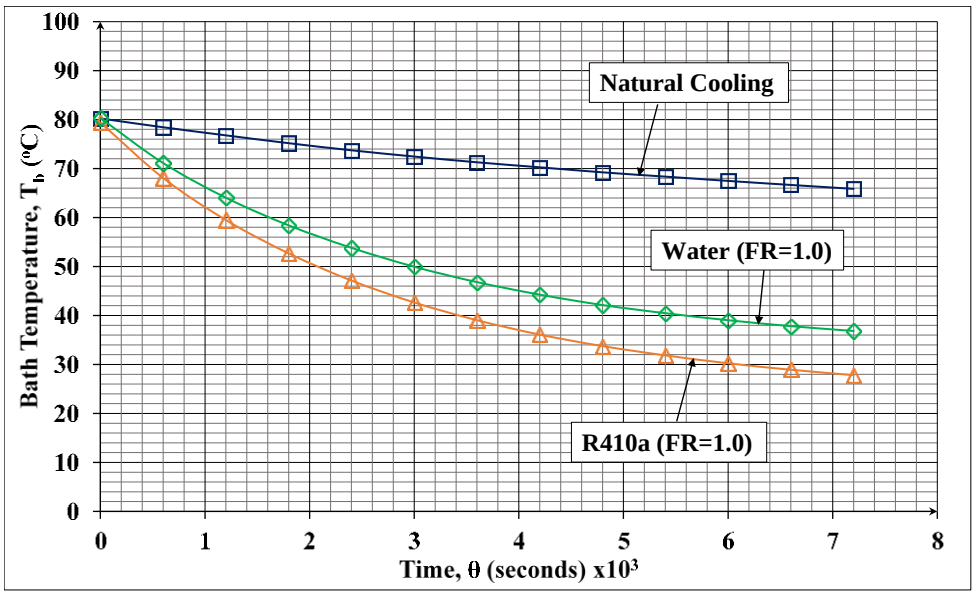

Figure 4.19 Effect on fill liquid type on THPHE cooler (Run C/3 and Run C/8)

Figure 4.20 to Figure 4.23 shows the effect of number of rows on the THPHE cooler at different instance of time at 600s and 3600s respectively.

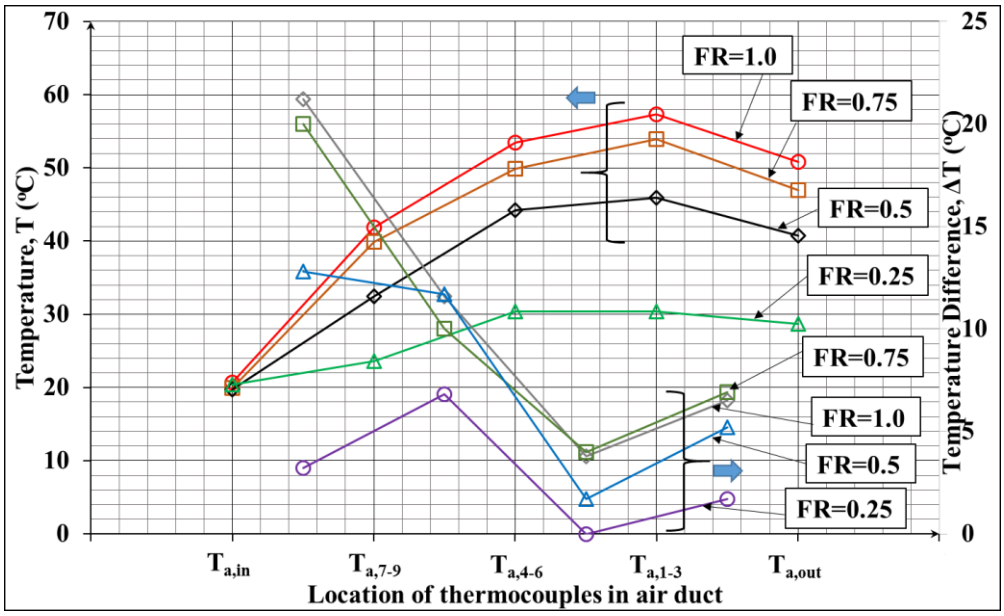

Figure 4.20 Effect of number of rows in THPHE cooler at time, 600s for run C/2-C/5

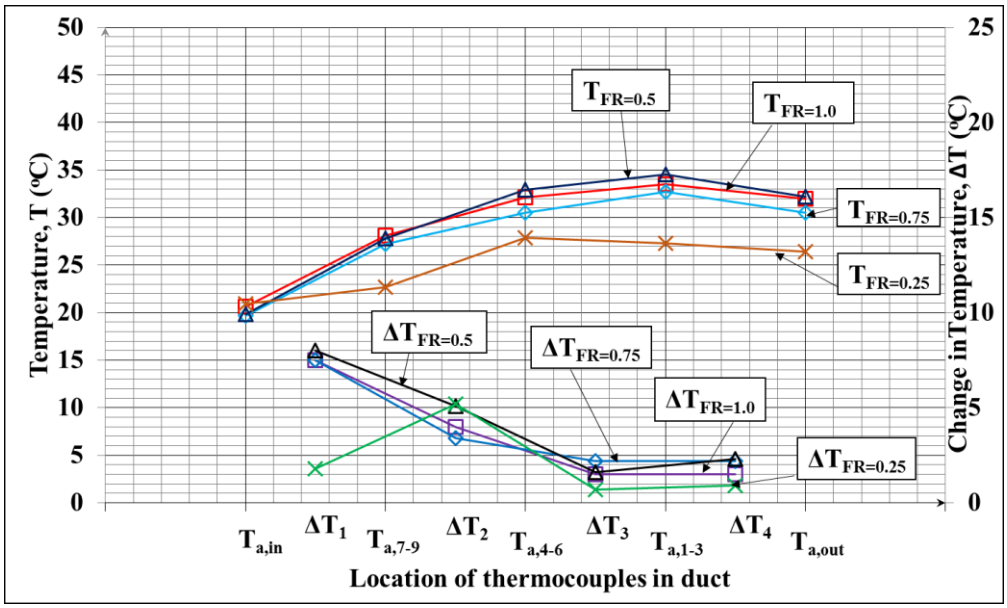

Figure 4.21 Effect of number of rows in THPHE cooler at time, 3600s for run C/2-C/5

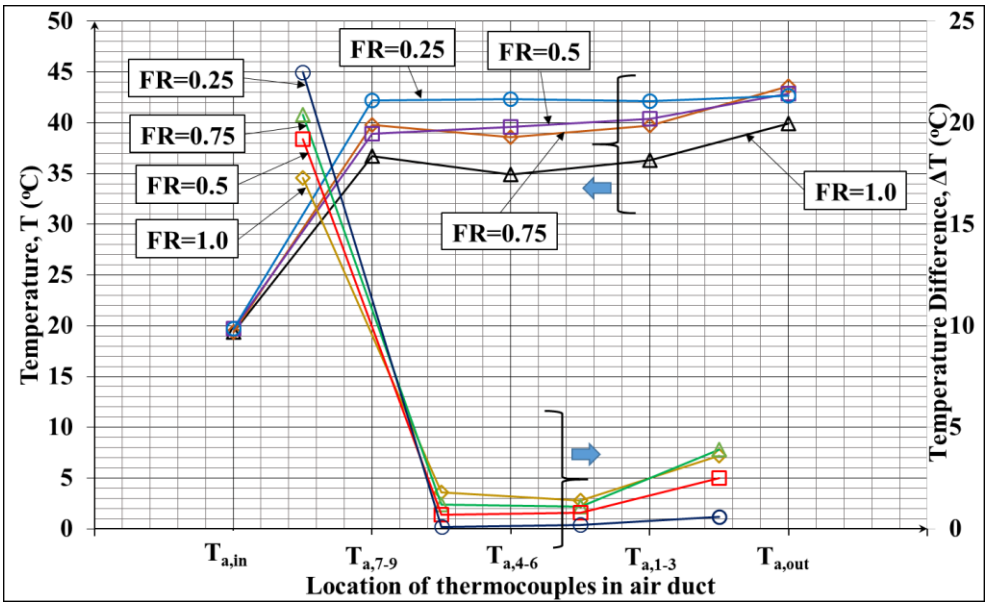

Figure 4.22 Effect of number of rows in THPHE cooler at time, 600s for run C/6-C/9

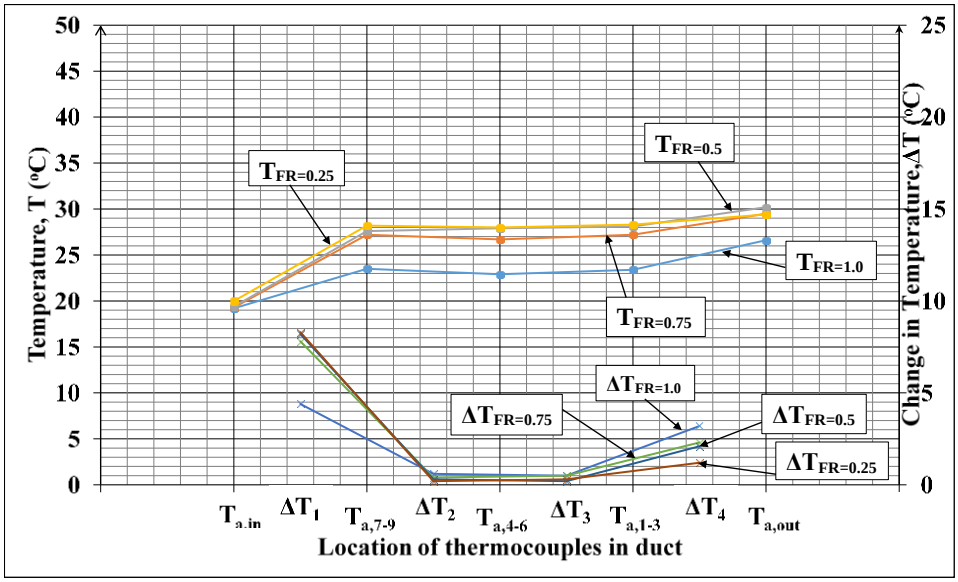

Figure 4.23 Effect of number of rows in THPHE cooler at time, 3600s for run C/6-C/9

Figure 4.24 shows the performance of the THPHE cooler at various FR and various fill liquids. In addition the simulation results for the water filled THPHE cooler was included at FR = 0.25 to 1.0.

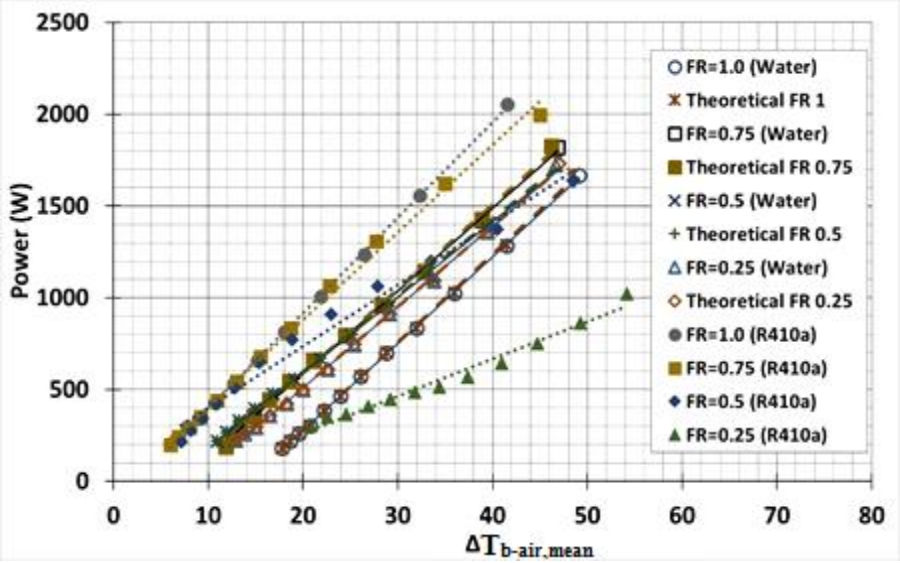

Figure 4.24 Comparison between water filled, R410a filled thermosyphons and simulation results (Runs C/2-C/9)

Table 5 Trend line equation and regression values for run C/2-C/9 and the simulation results for run C/6-C/9

Run	$P=m\Delta T_{b\text{-}air,mean} + c$	R^2
Run C/2	$P = 51.9\Delta T_{b\text{-}a,m} - 122$	$R^2 = 0.9997$
Run C/3	$P = 47.6\Delta T_{b\text{-}a,m} - 72$	$R^2 = 0.9963$
Run C/4	$P = 33.5\Delta T_{b\text{-}a,m} + 66$	$R^2 = 0.9834$
Run C/5	$P = 20.3\Delta T_{b\text{-}a,m} - 144$	$R^2 = 0.9766$
Run C/6	$P = 47.2\Delta T_{b\text{-}a,m} - 667$	$R^2 = 0.9997$
Run C/6 Theoretical	$P = 47.9\Delta T_{b\text{-}a,m} - 682$	$R^2 = 0.9992$
Run C/7	$P = 45.2\Delta T_{b\text{-}a,m} - 318$	$R^2 = 0.9987$
Run C/7 Theoretical	$P = 45.9\Delta T_{b\text{-}a,m} - 329$	$R^2 = 0.9982$
Run C/8	$P = 41.1\Delta T_{b\text{-}a,m} - 231$	$R^2 = 0.997$
Run C/8 Theoretical	$P = 41.6\Delta T_{b\text{-}a,m} - 237$	$R^2 = 0.996$
Run C/9	$P = 44.1\Delta T_{b\text{-}a,m} - 373$	$R^2 = 0.9983$
Run C/9 Theoretical	$P = 44.0\Delta T_{b\text{-}a,m} - 369$	$R^2 = 0.9987$

4.5 Discussion of experimental results

4.5.1 Repeatability of results

A typical set of transient results obtained for run C/2a, C/2b and C/2c with fill liquid, R410a and FR = 1.0 is shown in Figure 4.7. Mean water container (T_b) was plotted for C/2a, C/2b and C/2c respectively. The results show that it cooled the hot water container from 80 ^oC to 28 ^oC in 2 hours. An average quadratic temperature-time relationship ($T_b = 1x10^{-6}\ \theta^2 - 0.0146\ \theta + 77$) was obtained for the mean container temperature for run C/2a, C/2b and C/2c with a regression of 0.9935.

4.5.2 Transient temperature

A typical set of transient results for run C/1, natural cooling is shown in Figure 4.8. The mean water temperatures (T_b) are plotted for run C/1a and C/1b. The water container cooled down from 80 ^oC to 66 ^oC without the THPHE cooler and to the ambient. A quadratic temperature-time relationship ($T_b = 1x10^{-7}\ \theta^2 - 0.0029\ \theta + 80$) was obtained for the mean container temperature for run C/1 with regression of 0.9996. This indicates that the experiment was repeatable, as well as noting the natural heat loss rate of the hot water container.

A typical set of transient results for run C/2 with fill liquid, R410a and FR = 1.0 is shown in Figure 4.9. Mean water container (T_b), air inlet ($T_{a,in}$), air

out ($T_{a,out}$), evaporator insulation wall temperature (T_{wall}), condenser insulation wall temperature (T_{ins}) and condenser air probes ($T_{a,1-3}$, $T_{a,4-6}$, $T_{a,7-9}$) are plotted. The results show that it took 2 hours to cool down from 80 ^{o}C to 28 ^{o}C with the THPHE cooler. The experiment was stopped after 2 hours. A quadratic temperature-time relationship ($T_b = 1x10^{-6}\ \theta^2 - 0.0146\ \theta + 77$) was obtained for the mean container temperature for run C/2 with a regression of 0.9935. The air outlet dropped from 55 ^{o}C to 24 ^{o}C after 2 hours. The temperature difference between inlet and outlet of air was about 34 ^{o}C initially and about 3 ^{o}C after 2 hours.

4.5.3 Effect of fill ratio on R410a filled THPHE cooler

The effect of fill ratio and natural cooling for run C/1 to C/5 are demonstrated in Figure 4.17. Better performance results in lower container temperature or greater heat removal from the container. Bath temperature results in Figure 4.17 show that the THPHE cooler with a FR = 0.75 performed better than FR = 0.5, FR = 1.0 and FR = 0.25 in a descending order. FR = 0.75 and FR = 1.0 performed similarly throughout the experiment and the difference was only ± 2 ^{o}C which could be due to experimental accuracy. FR = 0.5 performed similarly to FR =0.75 and FR = 1.0 however at initial stages FR = 0.5 was shown to have lower performance from bath temperatures 70 ^{o}C to 40 ^{o}C. FR = 0.25 show to be the least performing FR. Overall bath temperature reduced from 80^{o}C to 28 ^{o}C in 2 hours as compared to the natural cooling rate that reduced from 80 ^{o}C to 66 ^{o}C, which indicates that the THPHE cooled the water container 2.3 times faster than natural cooling. Figure 4.17 indicates that

a higher FR was preferred for better performance when using an R410a filled THPHE cooler.

4.5.4 Effect of fill ratio on the water filled THPHE cooler

The effect of fill ratio and natural cooling for run C/1, C/6 to C/9 are demonstrated in Figure 4.18. Better performance results in lower container temperature or greater heat removal from the container. Bath temperature results in Figure 4.18 show that the THPHE cooler with a FR = 0. 5 performed better than FR = 0.25, FR = 0.75 and FR = 1.0 in a descending order. FR = 0. 5 and FR = 0.25 performed similarly throughout the experiment and the difference was only ± 2 ^{o}C which could be due to experimental accuracy. FR = 0.75 performed similarly to FR =0.5 and FR = 0.25 however at end stages FR = 0.75 was shown to have lower performance from bath temperatures 45 ^{o}C to 34 ^{o}C. FR = 1.0 show to be the least performing FR. Bath temperature reduced from 80 ^{o}C to 33 ^{o}C in 2 hours as compared to the natural cooling rate that reduced from 80 ^{o}C to 66 ^{o}C only, this indicates that the THPHE cooled the water container 2 times faster than natural cooling. Figure 4.18 indicates that a lower FR was preferred for better performance when using a water filled THPHE cooler.

4.5.5 Effect of fill liquid type

The effect of fill liquid type and natural cooling for run C/1, C/3 and C/8 are demonstrated in Figure 4.19. Both R410a- and water-filled THPHE cooler had higher cooling rates than natural cooling. R410a performed better than water-filled THPHE. R410a-THPHE cooled the hot water container from 80 ^{o}C to 28 ^{o}C whereas water-THPHE cooled down the hot water container from 80 ^{o}C to 33 ^{o}C. There was a 5 ^{o}C difference at the end of the 2 hour experiment and throughout the experiment R410a-THPHE performed better than water-THPHE in cooling rate.

4.5.6 Effect of number of rows in THPHE cooler

The effect of number of rows in THPHE cooler in run C/2 to C/5 and C/6 to C/9 are demonstrated in Figure 4.20 to Figure 4.21 and Figure 4.22 to Figure 4.23, respectively. The working state of a heat pipe results in large temperature differences between each temperature probe at each end of a row of heat pipes. If there was no difference in temperature, it was an indication that heat pipe was not working. In Figure 4.20 and Figure 4.22 there are one set of arrows (one pointing to the left and one pointing to the right) this shows which Y-axis the series of data belongs to.

In Figure 4.20 and Figure 4.21 the difference between $T_{a,in}$ and $T_{a,7\text{-}9}$ was 20 ^{o}C and 8 ^{o}C respectively and reduced to 10 ^{o}C and 5 ^{o}C respectively

from $T_{a,7\text{-}9}$ to $T_{a,4\text{-}6}$ and reduces even further 2-3 ^{o}C and maintained from $T_{a,4\text{-}6}$ through $T_{a,1\text{-}3}$ to $T_{a,out}$ respectively. This trend was observed across the different FRs for R410a-THPHE, indicating that after the second row of heat pipes the function of the third and fourth row was minimal or was not functioning.

In Figure 4.22 and Figure 4.23 the difference between $T_{a,in}$ and $T_{a,7\text{-}9}$ was 20 ^{o}C and 8 ^{o}C respectively and reduced to 2 ^{o}C from $T_{a,7\text{-}9}$ and maintained from $T_{a,4\text{-}6}$ through $T_{a,1\text{-}3}$ to $T_{a,out}$, This trend is seen across the different FR for water-THPHE, and indicates that after the first row of heat pipes, the function of the second, third and fourth row was minimal and wasn't functioning.

4.5.7 Performance of various fill liquids, FR and comparison to simulation results.

The graph of power versus temperature difference, $\Delta T_{b\text{-}air,mean}$ is plotted in Figure 4.24. The performance of the THPHE cooler can be gauged from Figure 4.24; the steeper the gradient the lower the overall thermal resistance. The R410a-THPHE with FR = 1.0 and FR = 0.75 performed the better than water-THPHE with FR=1.0, FR = 0.75, FR = 0.5 and FR = 0.25. R410a-THPHE with FR 0.5 performed similarly with the average performance of water-THPHE at the temperature difference, $\Delta T_{b\text{-}air,mean}$, 30-48 ^{o}C. At a lower temperature difference it performed similarly to R410a-THPHE with FR = 1.0 and FR = 0.75. R410a-THPHE with FR = 0.25 had the lowest performance rate among all the fill ratios for both R410a- and water-THPHE. Water-THPHE

with FR = 0.25, FR = 0.5 and FR = 0.75 performed similarly within ± 3^{o}C of each other and better than with FR = 1.0.

The simulation run was modeled after the thermal network model described in Section 2.2 the dimensions of the THPHE cooler was inserted into the model. The heat transfer coefficients were derived from the experiments in phase A. From the simulation the interface temperatures were simulated and the temperature difference and the power was obtained from this model and plotted in Figure 4.24. The results can be seen in Appendix C.

The simulation results coincided with about 95 % of the experimental results for all FRs for water as shown in Figure 4.24. The simulation model used h_e and h_c values obtained from phase A. To further improve the accuracy of the simulation results, the h_e and h_c values used were divided into temperature ranges in steps of 10 ^{o}C and was also based on FR results from Figure 2.52 to Figure 2.69. Through trial and error, it was found that there was no single h_e or h_c value that can be used to determine the performance of a thermosyphon accurately. Selection of h_e and h_c value had to be specific to the temperature range, FR and inclination.

4.6 Chapter conclusion

In phase C, a THPHE cooler was developed and tested as a cooling tower replacement. The following conclusions were drawn:

- R410a-THPHE cooler performed better than water-THPHE cooler.
- High fill ratio was preferred when using R410a-THPHE cooler. The best performing fill ratio was FR =0.75 for R410a-THPHE cooler.
- Low fill ratio was preferred when using water-THPHE cooler. The best performing fill ratio was FR = 0.5 for water-THPHE cooler.
- The maximum number of heat pipe rows should not be more than 2.
- The simulation model showed 95 % similarity when compared to experimental results.

CHAPTER 5

SUGGESTIONS FOR FUTURE WORK

This research was performed in three phases. The following are suggestions for future work in each phase.

For phase A, the thermal performance testing of thermosyphons:-

- The temperature range could be further increased to 200-300 ^{o}C.

- Further experiments should be conducted at lower temperatures (<60 ^{o}C) as this research shows that there are two linear operating regions at around 40 ^{o}C.

- The temperature of the water source could be lowered (<20 ^{o}C).

- A wider variety of aspect ratios could be experimented on for further verification on the effects of aspect ratio on performance.

- The effects of mass flow rate could be studied further with more flow rates between 3 and 50 ml/s.

For phase B, a novel method to compare performance of thermosyphons, the following are suggestions for future work:-

- A stirrer could be added to the hot water container to reduce stratification effect.

- Further experiments with a wider range of HP with different dimensions should be conducted.

For phase C, development and testing of a THPHE cooling tower replacement, the following are suggestions for future work:-

- The THPHE cooler could be optimised to only two rows of heat pipes in series. More heat pipes could also be added to each row if needed to increase the cooling potential.

- The fan speed could be controlled to study the effect of different air flowrates.

- A separate water heating tank should be constructed as a source of water leading into the THPHE system to control the inlet water temperature.

CHAPTER 6

CONCLUSIONS

This chapter concludes and highlights all the key findings in the thesis. The following are the conclusions drawn for phase A. High power input results in higher thermosyphon wall temperatures. High condenser coolant flow rates result in lower thermosyphon wall temperatures. Axial temperature distribution was quite uniform at low power input (< 18 W) and non-uniform at high power input (> 18 W). Differences in evaporator wall temperatures based on bulk and mean definitions could be as much as 14 ^{o}C. There are two distinct operating regions observed at around 40 W. The best performing thermosyphon was found to have a fill ratio of 1.0 and inclination at 90 ^{o}. A high aspect ratio thermosyphon of 10 was preferred.

In phase B, a method to compare the performance of various thermosyphons rapidly and economically was proposed. The ease and simplicity of the procedure was demonstrated by cooling a container of hot water using various thermosyphons. From the results obtained it was found that forced air convection cooling was better than natural convection and that high coolant water flow rate was preferred to low flow rate.

In phase C, the following conclusions can be drawn. R410a-THPHE cooler performed better than water-THPHE cooler. High fill ratio was preferred when using R410a-THPHE cooler as it cools down the hot water bath to the lowest temperature for a fixed amount of time. The best performing fill

ratio was FR = 0.75 for R410a-THPHE cooler. Low fill ratio was preferred when using water-THPHE cooler. The best performing fill ratio was FR = 0.5 for water-THPHE cooler. The maximum number of heat pipe rows should not be more than 2. The simulation model shows around 95 % similarity when compared to experimental results.

REFERENCES

Alizadehdakhel, A., Alsairafi, A.A. and Rahimi, M., 2010, “CFD modelling of flow and heat transfer in a thermosyphon,” *International Communications in Heat and Mass Transfer*, 37, 312-318.

Anjakar, P.G. and Yarasu, D.R.B., 2012, "Experimental analysis of condenser length effect on the performance of thermosyphon," *International Journal of Emerging Technology and Advanced Engineering*, 2, 494-499.

Buschmann, M. H. and Franzke, U., 2013, "Improvement of thermosyphon performance by employing nanofluid," *International Journal of Refrigeration*, 40, 416-428.

Celata, G.P., Cumo, M. and Furrer, M., 2010, "Experimental tests of a stainless steel loop heat pipe with flat evaporator," *Experimental Thermal and Fluid Science*, 34, 866-878.

Chang, S. W., Lo, D. C., Chiang, K. F. and Lin, C. Y., 2012, "Sub-atmospheric boiling heat transfer and thermal performance of two-phase loop thermosyphon," *Experimental Thermal and Fluid Science*, 39, 134-147.

Dry cooling tower operation, n.d. photograph, viewed 19 March 2015, <http://www.cts-cooling.com/_img/trockenluftkuehlung_en.jpg>.

Fadhl, B., Jouhara, H. and Wrobel, L.C., 2013, “Numerical modelling of the temperature distribution in a two-phase closed thermosyphon,” *Applied Thermal Engineering*, 60, 122-131.

Fadhl, B., Jouhara, H. and Wrobel, L.C., 2015, “CFD modelling of a two-phase closed thermosyphon charged with R134a and R404a,” *Applied Thermal Engineering*, 78, 482-490.

Fluid cooling tower cut away section, n.d. photograph, viewed 19 March 2015, <http://www.baltimoreaircoil.com/english/wp-content/uploads/2009/08/CCCT_CombinedFlow1.jpg>.

Fluid cooling tower operation, n.d. photograph, viewed 19 March 2015, <http://www.baltimoreaircoil.com/english/wp-content/uploads/2009/10/CCCT_CombinedFlowParallel-300x240.jpg>.

Guo, W. and Nutter, D.W., 2009, “An experimental study of axial conduction through a thermosyphon pipe wall,” *Applied Thermal Energy*, 29, 3536-3541.

Gurses, A.C. and Cannistraro, C., 1991, “The inclination effect on the performance off water-filled heat pipes,” *Renewable Energy*, 1, 667- 674.

Hagens, H., Ganzevles, F.L.A., Grooten, M.H.M. and Geld, C.W.M.V.D., 2007, "Air heat exchangers with long heat pipes: Experiments and predictions," *Applied Thermal Engineering*, 27, 2426-2434.

Huminic G., Huminic, A., Morjan, I. and Dunitrache, F., 2011, "Experimental study of the thermal performance of thermosyphon heat pipe using iron oxide nanoparticles," *International Journal of Heat and Mass Transfer*, 54, 656-661.

Huminic, G. and Huminic, A., 2011, "Heat transfer characteristics of a two-phase closed thermosyphons using nanofluids," *Experimental Thermal and Fluid Science*, 35, 550-557.

Imura, H., Kusada, K., Oyata, J. and Sakamoto, N., 1977, "Heat transfer in two-phase closed-type thermosyphons," *Trans. Japan Society of Mechanical Engineers*, 22, 485-493.

Jouhara, H. and Robinson, A.J., 2010, "Experimental investigation of small diameter two-phase closed thermosyphons charged with water, FC-84, FC-77, and FC-3283," *Applied Thermal Engineering*, 30, 201- 211.

Khandekar, S., Dollinger, N. and Groll, M., 2003, "Understading operational regimes of closed loop pulasating heat pipes: an experimental study," *Applied Thermal Engineering*, 23, 707-719.

Mroue, H., Ramos, J.B., Wrobel, L.C and Jouhara, H., 2015, "Experimental and numerical investigation of an air-to-water heat pipe-based heat exchanger," *Applied Thermal Engineering*, 78, 339-350

Nguyen-Chi, H. and Groll, M., 1981, "Entrainment or flooding limit in a closed two-phase thermosyphon," *Heat Recovery Systems*, 1, 275.

Noie, S., 2005, "Heat transfer characteristics of a two-phase closed thermosyphon," *Applied Thermal Engineering*, 25, 495-506.

Noie, S.H., 2006, "Investigation of thermal performance of an air-to-air thermosyphon heat exchanger using ε-NTU method," *Applied Thermal Engineering*, 26, 559-567.

Ong K.S. and Christopher Lim, 2015, "An experimental procedure to compare thermal performance of thermosyphons rapidly," *Frontiers of Heat Pipe*, 6, 2. (Chapter 3)

Ong, K.S. and Haider-E-Alahi, M., 2003, "Performance of a R-134a filled thermosyphon," *Applied Thermal Energy*, 22, 2373-2381.

Ong, K.S., Tong, W.L., Gan, J.S. and Hisham, N., 2014, "Axial temperature distribution and performance of R410a and water filled thermosyphon at various fill ratios and inclinations," *Frontiers of Heat Pipes*, 5, 1-7.

Open air type cooling tower, n.d. photograph, viewed 19 March 2015, <http://www.terlyntech.com/promovideo.html>.

Payaruk, T., Terdtoon, P. and Ritthidech, S., 2000, "Correlations to predict heat transfer characteristics of an inclined closed two-phase thermosyphon at normal operating conditions," *Applied Thermal Engineering*, 20, 781-90.

Peterson, G., 1994, An Introduction to Heat Pipes Modeling, Testing, and Applications, *New York: Wiley Interscience*.

Qu, J. and Wang, Q., 2013, "Experimental study on the thermal performance of vertical closed-loop oscillating heat pipes and correlatiion modeling," *Applied Energy*, 112, 1154-1160.

Righetti, G., Zilio, C., Bertolo, F. and Longo, G.A., 2014, "Experimental and theoretical analysis of a heat pipe heat exchanger operating with a low global warming potential refrigerant," *Applied Thermal Engineering*, 65, 261-368.

Rohsenow, W.M., 1962, "A method of correlating heat transfer data for surface boiling curves," *International Journal of Heat Transfer*, ASME, 84, 969.

Shabgard, H., Xiao, B., Faghri, A., Gupta, R. and Weissman, W., 2014, "Thermal characteristics of a closed thermosyphon under various filling conditions," *International Journal of Heat and Mass Transfer*, 70, 91-102.

Solomon, A. B., Mathew, A., Ramachandran, K., Pillai, B. C. and Karthikeyan, V. K., 2013, "Thermal performance of anodized two phase closed thermosyphon (TPCT)," *Experimental Thermal and Fluid Science*, 48, 49-57.

Solomon, A. B., Ramachandran, K. and Pillai B.C., 2012, "Thermal performance of a heat pipe with nanoparticles coated wick," *Applied Thermal Energy*, 36, 106-112.

Terdtoon, P., Ritthidej, S. and Shiraishi, M., 1996, "Effect of aspect ratio and bond number on heat transfer characteristics of an inclined two-phase closed thermosyphon at normal operating conditions," *5th International Symposium on Heat Pipes*, Melbourne.

Turan, A. and Kafeel, K., 2014, "Simulation of the response of a thermosyphon under pulsed heat input conditions," *International Journal of Thermal Sciences*, 80, 33-40.

Wang J., 2009, "Experimental investigation of the transient thermal performance of a bent heat pipe with grooved surface," *Applied Energy*, 86, 2030-2037.

Yuan, X., Lin, G. and Yang, F., 2003, "Waste heat recovery using heat pipe heat exchanger for heating automobile using exhaust gas," *Applied Thermal Engineering*, 23, 367-372.

Zhang, M., Ma, G., Cheng, S. and Liu, Z., 2009, "Numerical simulation and experimental verification of a flat two-phase thermosyphon," *Energy Conversion and Management*, 50, 1095-1100.

APPENDIX A

Table 6 Experimental results obtained for phase A

Series	HP #	FR	m_w	Θ (°)	P	T_{wi}	T_{wo}	ΔT_w	$T_{e,b}$	$T_{e,m}$	$T_{c,m}$	ΔT_b	ΔT_m	T_{sat}	T_{ad1}	T_{ad2}	T_a	h_e	h_c	R_{hp}
						(°C)	(°C)	(°C)	(°C)	(°C)	(°C)	(°C)	(°C)	(°C)	(°C)	(°C)	(°C)			
A/1	2	1	3	90	5	24.8	25.2	0.5	34.0	33.7	25.3	8.7	8.5	27.5	26.8	26.8	19.0	82.3	554.2	1.59
					18	24.8	25.8	1.1	57.0	55.9	29.0	28.0	26.9	29.0	33.5	33.6	18.2	91.5	677.6	1.41
					38	24.8	27.3	2.5	65.1	63.5	33.0	32.1	30.5	30.4	40.7	40.3	20.0	187.7	878.7	0.74
					70	25.2	29.6	4.4	79.3	76.0	37.3	42.0	38.8	33.3	47.5	46.9	18.5	276.5	1225.2	0.50
					113	25.8	33.7	7.9	87.6	82.8	40.1	47.5	42.7	38.1	49.8	49.3	21.0	387.0	2090.3	0.35
					210	27.4	42.0	14.6	114.4	105.9	46.9	67.5	59.0	56.8	56.1	55.8	20.1	478.8	4065.9	0.27
					360	30.1	57.6	27.4	160.5	146.4	64.2	96.3	82.1	76.8	67.6	67.9	19.5	521.7	18439.0	0.23
A/2	2	1	19	90	5	25.9	26.1	0.2	33.3	33.0	25.9	7.4	7.1	28.9	27.3	27.1	18.6	97.9	666.1	1.33
					18	26.1	26.3	0.2	57.5	56.3	29.2	28.3	27.1	29.4	33.0	33.1	20.7	88.1	786.1	1.43
					38	25.8	26.3	0.5	66.8	65.0	32.2	34.6	32.8	29.4	40.1	39.5	19.6	171.5	875.7	0.79
					70	26.5	26.9	0.4	77.9	74.6	34.3	43.6	40.3	30.8	43.5	43.1	18.6	254.8	1346.1	0.53
					113	26.7	28.0	1.3	88.7	83.4	36.5	52.2	46.9	31.6	47.1	46.6	21.3	351.6	1912.2	0.38
					210	29.4	31.8	2.3	116.1	106.6	40.6	75.5	66.0	38.2	51.7	51.7	19.5	435.9	3266.6	0.30
					360	33.6	37.7	4.1	156.8	141.9	48.8	108.0	93.0	58.4	59.0	60.0	19.8	498.0	5742.3	0.25
A/3	2	1	50	90	5	27.6	27.8	0.1	36.9	36.6	28.0	8.9	8.6	31.5	29.4	29.4	21.6	79.1	599.7	1.63
					18	24.2	24.5	0.3	55.6	54.5	27.9	27.7	26.6	27.5	31.8	31.9	22.9	90.5	776.2	1.40
					38	27.6	27.8	0.3	64.9	63.3	33.3	31.6	30.0	31.9	39.7	39.8	22.2	183.9	1002.2	0.73
					70	25.1	26.0	0.9	77.2	74.0	34.4	42.8	39.6	30.2	44.1	43.7	21.0	264.5	1274.3	0.52

					113	29.9	30.5	0.7	83.7	79.2	37.2	46.5	41.9	34.6	45.4	45.5	22.4	381.9	2351.9	0.35
					210	31.1	32.1	1.0	106.5	98.5	39.3	67.3	59.2	36.3	48.2	48.4	21.8	476.7	3992.2	0.27
					360	34.1	35.8	1.7	138.9	126.0	43.5	95.4	82.5	49.5	53.0	53.1	21.0	562.4	6608.0	0.22
A/4	2	0.75	50	90	5	28.6	28.4	0.2	-	33.5	27.8	-	5.7	30.2	28.5	28.8	20.0	117.8	885.1	1.09
					18	28.2	28.1	0.1	-	48.5	28.7	-	19.9	30.0	31.6	31.0	19.7	118.8	1242.3	1.05
					38	28.0	28.0	0.0	-	60.6	30.3	-	30.3	30.2	35.2	34.2	19.9	167.0	1562.2	0.75
					70	28.3	28.4	0.1	-	68.6	31.6	-	37.0	31.0	37.5	36.4	20.0	251.5	2375.9	0.50
					113	29.5	29.8	0.3	-	80.1	33.6	-	46.5	32.9	40.4	39.2	20.1	319.3	3303.1	0.39
					210	32.2	33.1	0.9	-	108.6	38.1	-	70.5	42.0	47.0	45.5	20.4	383.6	4664.1	0.32
					360	36.2	37.6	1.4	-	140.3	45.4	-	94.9	54.1	54.8	52.4	20.5	473.2	8307.8	0.25
A/5	2	0.5	50	90	5	28.0	27.9	0.1	-	35.7	27.4	-	8.3	31.4	28.4	28.5	20.2	78.2	783.4	1.60
					18	27.7	27.6	0.1	-	53.0	28.6	-	24.5	31.6	31.5	31.2	20.5	94.6	1128.1	1.30
					38	27.6	27.6	0.0	-	59.1	29.7	-	29.4	31.9	33.7	33.4	20.0	169.2	1717.5	0.74
					70	28.0	28.2	0.2	-	66.8	31.2	-	35.5	33.3	36.6	36.0	20.2	261.6	2449.0	0.48
					113	29.2	29.5	0.3	-	76.9	33.3	-	43.6	34.3	40.0	39.2	20.2	344.5	3211.3	0.37
					210	32.4	33.2	0.8	-	104.1	38.0	-	66.0	44.8	45.4	44.3	20.5	403.8	5578.8	0.30
					360	36.5	38.1	1.6	-	145.2	48.0	-	97.2	57.1	54.4	52.7	21.8	447.3	12601.4	0.26
A/6	2	0.25	50	90	5	28.0	27.8	0.1	-	37.9	27.2	-	10.8	30.4	28.5	28.5	19.6	60.4	625.3	2.06
					18	27.5	27.5	0.1	-	51.1	28.6	-	22.5	31.0	32.0	31.6	18.9	106.0	991.4	1.19
					38	27.4	27.4	0.1	-	57.9	30.3	-	27.7	31.7	35.5	34.9	18.9	190.2	1359.9	0.68
					70	27.5	27.6	0.1	-	65.3	31.5	-	33.8	32.3	37.3	36.5	19.6	280.8	2292.2	0.46
					113	29.1	29.2	0.1	-	78.2	34.0	-	44.2	36.9	40.4	39.6	19.6	336.7	3351.0	0.37
					210	31.8	32.2	0.3	-	106.7	37.9	-	68.8	42.9	46.4	45.0	20.0	392.0	4887.0	0.31
					360	36.0	37.7	1.7	-	143.9	43.5	-	100.4	60.7	56.4	50.7	20.9	453.6	7401.7	0.27

A/7	2	1.0	50	68	5	27.3	27.5	0.2	-	33.6	27.2	-	6.4	30.8	28.1	28.3	19.3	105.8	808.2	1.22
					18	26.8	27.1	0.2	-	53.9	29.3	-	24.6	31.1	32.7	32.7	19.8	96.8	897.2	1.30
					38	26.8	27.1	0.4	-	71.5	33.7	-	37.8	31.4	41.5	41.5	20.1	143.9	830.8	0.93
					70	27.4	27.9	0.4	-	80.1	36.6	-	43.5	32.2	47.2	46.7	19.9	240.5	1171.1	0.57
					113	28.5	29.1	0.6	-	90.9	38.6	-	52.3	33.5	49.9	49.7	20.2	312.9	1746.1	0.43
					210	30.9	31.9	1.0	-	114.4	41.7	-	72.7	36.5	53.2	53.7	20.1	392.0	3063.9	0.33
					360	35.9	37.6	1.7	-	150.6	47.7	-	102.9	49.0	59.3	60.8	20.0	452.8	4924.4	0.28
A/8	2	0.75	50	68	5	26.9	27.1	0.2	-	33.2	26.6	-	6.6	23.3	27.7	27.6	20.4	102.0	834.6	1.25
					18	26.9	27.2	0.3	-	55.7	29.5	-	26.3	25.4	32.0	33.2	19.7	88.5	892.8	1.41
					38	27.0	27.3	0.3	-	64.6	32.4	-	32.3	25.7	37.3	39.1	19.2	163.5	1032.8	0.81
					70	27.5	27.9	0.4	-	73.0	34.0	-	39.0	30.6	39.8	41.9	19.2	248.1	1618.5	0.53
					113	28.4	29.0	0.6	-	86.2	36.3	-	49.9	28.9	43.1	45.6	19.0	307.2	2242.4	0.42
					210	30.4	31.3	0.9	-	111.1	39.5	-	71.6	28.7	46.4	50.1	19.3	380.3	3761.5	0.33
					360	32.2	33.7	1.5	-	148.9	43.9	-	105.0	29.5	50.8	56.1	19.5	429.6	5760.3	0.29
A/9	2	0.5	50	68	5	27.4	27.6	0.2	-	34.5	26.8	-	7.7	30.1	28.0	27.9	19.2	87.1	760.1	1.46
					18	27.0	27.2	0.2	-	46.6	28.2	-	18.5	30.7	29.9	30.9	19.1	126.1	1234.0	0.99
					38	27.0	27.4	0.4	-	53.3	29.9	-	23.4	32.0	33.3	34.1	19.2	220.5	1631.0	0.59
					70	27.5	28.0	0.5	-	61.9	31.1	-	30.8	32.2	34.8	36.2	19.2	302.0	2540.3	0.42
					113	28.1	28.7	0.6	-	71.9	32.5	-	39.5	33.6	36.3	38.3	19.0	371.5	3658.7	0.34
					210	30.2	31.3	1.1	-	99.5	37.2	-	62.3	42.7	40.9	44.3	19.7	420.5	5876.5	0.29
					360	36.4	38.4	2.0	-	144.6	48.5	-	96.1	57.5	51.2	57.0	20.1	453.1	9053.5	0.26
A/10	2	0.25	50	68	5	27.8	27.9	0.1	-	36.4	27.0	-	9.4	30.5	28.5	28.2	19.8	71.0	645.1	1.78
					18	27.5	27.7	0.2	-	51.1	29.2	-	21.9	30.4	31.3	32.9	19.4	107.8	919.6	1.18
					38	27.3	27.6	0.3	-	57.8	30.8	-	27.0	31.1	34.1	36.3	18.9	191.7	1302.9	0.68

					70	27.6	28.0	0.4	-	66.2	32.3	-	33.9	33.7	35.9	38.7	19.0	275.8	2112.9	0.47
					113	28.8	29.4	0.6	-	77.7	34.4	-	43.3	35.8	37.9	41.3	19.3	337.5	3229.3	0.37
					210	31.4	32.4	1.0	-	102.8	39.8	-	63.0	42.0	45.0	49.0	20.2	428.9	4423.9	0.29
					360	35.6	37.3	1.7	-	142.5	46.7	-	95.8	54.9	52.6	59.7	20.0	475.0	5602.5	0.26
A/11	2	1.0	50	45	5	28.3	28.5	0.2	-	34.8	28.0	-	6.8	31.4	29.0	29.2	19.2	99.7	743.5	1.29
					18	27.7	28.0	0.3	-	54.7	30.0	-	24.7	31.8	33.6	33.5	19.3	97.0	869.7	1.30
					38	27.5	27.8	0.3	-	71.6	33.3	-	38.2	32.0	40.2	40.3	19.2	138.2	932.5	0.95
					70	27.9	28.4	0.5	-	79.8	35.7	-	44.1	32.8	45.0	44.5	19.2	227.5	1338.6	0.59
					113	29.1	29.7	0.6	-	89.7	38.4	-	51.4	34.2	49.0	48.8	18.9	315.1	1849.5	0.42
					210	31.7	32.9	1.2	-	113.2	41.9	-	71.3	38.0	52.8	53.3	19.1	397.8	3220.1	0.32
					360	36.8	38.6	1.8	-	148.7	48.7	-	99.9	54.5	58.8	60.1	19.2	459.7	5680.3	0.27
A/12	2	0.75	50	45	5	27.6	27.7	0.1	-	34.3	26.9	-	7.5	29.5	28.3	28.2	17.5	93.6	621.5	1.40
					18	27.3	27.5	0.2	-	57.5	30.1	-	27.4	29.9	32.7	34.2	20.4	85.3	826.7	1.47
					38	27.4	27.7	0.3	-	64.8	33.0	-	31.8	31.3	38.0	39.9	19.5	167.3	1004.8	0.79
					70	27.9	28.3	0.4	-	74.1	34.8	-	39.3	31.7	41.0	43.2	19.7	249.2	1530.3	0.53
					113	28.9	29.4	0.5	-	86.2	36.9	-	49.3	33.2	43.6	46.3	19.4	311.9	2216.6	0.42
					210	30.8	31.8	1.0	-	113.2	40.1	-	73.1	37.3	47.0	50.8	19.8	371.9	3712.7	0.34
					360	33.3	34.9	1.6	-	150.4	46.2	-	104.2	50.0	52.1	57.6	19.5	429.0	6291.8	0.28
A/13	2	0.5	50	45	5	23.2	23.4	0.2	-	31.5	23.1	-	8.4	24.7	24.1	24.0	18.2	76.5	925.2	1.61
					18	23.2	23.5	0.3	-	62.8	26.3	-	36.5	26.3	28.6	30.2	18.9	61.3	880.0	1.98
					38	23.5	23.8	0.3	-	72.5	31.4	-	41.1	27.3	36.9	40.1	19.2	127.1	822.9	1.03
					70	24.1	24.5	0.4	-	81.2	34.8	-	46.5	28.4	42.5	46.0	19.8	215.3	1155.9	0.63
					113	25.1	25.8	0.7	-	93.2	37.1	-	56.1	29.9	46.0	49.9	19.6	284.0	1640.7	0.47
					210	27.9	28.9	1.0	-	122.2	41.5	-	80.8	34.6	51.2	56.0	19.4	348.3	2713.6	0.37

					360	31.1	32.7	1.6	-	158.4	46.4	-	112.1	45.6	55.7	62.4	19.1	412.5	4351.1	0.30
A/14	2	0.25	50	45	5	29.2	29.4	0.2	-	39.0	28.2	-	10.8	32.0	29.9	29.6	20.0	61.6	560.3	2.05
					18	28.8	28.9	0.1	-	52.3	30.5	-	21.8	31.9	32.5	33.9	23.6	107.3	1010.5	1.17
					38	29.1	29.3	0.2	-	58.0	32.4	-	25.6	33.9	35.4	37.8	19.1	202.4	1343.5	0.65
					70	29.2	29.7	0.5	-	66.4	33.2	-	33.2	35.0	36.9	39.6	19.2	282.7	2103.6	0.46
					113	30.7	31.2	0.5	-	78.8	37.2	-	41.7	38.7	40.0	43.5	18.5	346.9	3573.8	0.36
					210	33.0	34.0	1.0	-	105.2	41.5	-	63.7	43.9	45.1	50.3	18.4	416.1	4842.9	0.30
					360	37.4	39.0	1.6	-	143.1	46.8	-	96.4	55.6	51.7	59.6	18.5	468.8	5787.4	0.26
A/15	2	1.0	50	23	5	24.8	25.0	0.2	-	33.7	25.1	-	8.6	28.7	25.9	26.1	19.3	74.3	848.4	1.66
					18	22.7	23.0	0.3	-	48.4	25.5	-	22.9	28.2	28.7	28.8	19.2	103.9	948.0	1.21
					38	22.9	23.2	0.3	-	66.9	28.0	-	38.8	28.9	33.7	33.7	18.4	130.2	1150.6	0.97
					70	23.4	23.9	0.5	-	75.6	30.3	-	45.3	29.4	37.6	37.7	18.6	209.8	1620.3	0.61
					113	25.1	25.7	0.6	-	84.8	32.7	-	52.1	30.9	41.0	40.8	18.6	293.0	2368.8	0.44
					210	28.0	29.1	1.1	-	109.3	37.0	-	72.3	37.8	46.0	46.4	18.5	378.7	3905.1	0.33
					360	33.5	35.1	1.7	-	145.6	47.9	-	97.8	52.8	54.0	55.0	23.1	449.8	9293.4	0.27
A/16	2	0.75	50	23	5	24.7	24.9	0.2	-	31.7	24.5	-	7.2	27.0	25.7	25.5	18.0	94.0	777.5	1.36
					18	24.6	24.8	0.2	-	54.5	27.8	-	26.7	28.0	30.3	31.7	20.4	87.0	867.6	1.44
					38	24.7	25.0	0.3	-	64.3	30.3	-	34.0	28.6	34.4	36.6	20.3	150.3	1132.1	0.86
					70	25.4	25.9	0.5	-	74.4	32.6	-	41.8	30.0	38.1	40.7	19.7	227.8	1602.2	0.57
					113	26.7	27.4	0.7	-	85.5	34.7	-	50.9	31.6	40.8	43.6	19.6	296.9	2359.1	0.43
					210	28.8	29.8	1.0	-	111.2	38.1	-	73.1	38.5	44.1	48.3	19.1	368.0	3959.1	0.34
					360	33.0	34.5	1.5	-	150.0	47.2	-	102.8	50.8	51.3	57.3	19.4	428.5	7368.4	0.28
A/17	2	0.5	50	23	5	25.0	25.1	0.1	-	33.6	24.6	-	9.0	27.2	25.7	25.6	18.2	71.9	795.6	1.72
					18	24.8	25.0	0.2	-	60.8	27.3	-	33.5	28.3	29.6	31.0	18.0	67.1	906.0	1.82

					38	24.9	25.2	0.3	-	71.8	31.2	-	40.6	28.7	36.3	38.8	17.9	126.1	932.5	1.02
					70	25.5	25.9	0.4	-	79.2	33.3	-	45.9	29.7	39.2	42.4	17.9	207.6	1446.8	0.63
					113	26.6	27.2	0.6	-	91.8	36.5	-	55.3	31.2	44.2	47.8	17.7	281.0	1867.4	0.47
					210	28.5	29.6	1.1	-	118.1	40.7	-	77.4	37.0	48.9	54.1	17.8	358.9	2997.6	0.36
					360	31.9	33.7	1.8	-	163.6	49.5	-	114.1	52.4	55.7	63.2	18.3	393.6	5311.5	0.31
A/18	2	0.25	50	23	5	26.6	26.7	0.1	-	34.8	25.9	-	9.0	28.4	27.1	26.9	18.5	72.6	777.5	1.71
					18	26.4	26.6	0.2	-	50.8	28.4	-	22.4	30.3	30.1	31.8	18.8	103.1	1036.1	1.21
					38	26.3	26.6	0.3	-	56.2	30.4	-	25.8	31.6	32.7	34.9	19.4	193.4	1651.8	0.66
					70	27.0	27.5	0.5	-	66.3	33.5	-	32.9	34.0	35.4	38.4	19.7	270.9	2877.1	0.46
					113	28.3	28.8	0.5	-	76.2	36.4	-	39.8	37.7	37.5	41.2	19.8	348.8	5082.7	0.35
					210	30.0	31.0	1.0	-	101.9	40.0	-	61.9	41.2	42.8	48.1	19.9	423.3	5410.2	0.29
					360	35.7	37.4	1.7	-	143.2	47.0	-	96.2	53.8	51.0	59.3	20.1	465.7	6165.4	0.26
A/19	1	1.0	50	90	50	26.2	26.4	0.2	-	61.1	32.6	-	28.5	27.7	36.9	37.7	22.2	239.5	1735.0	0.54
					100	29.9	30.3	0.4	-	70.9	36.9	-	34.0	30.1	42.7	43.2	21.0	406.9	2794.6	0.32
					150	29.0	29.6	0.6	-	83.5	37.6	-	45.9	32.6	45.5	45.5	22.4	449.2	3283.6	0.29
A/20	3	1.0	50	90	50	24.5	24.7	0.2	-	72.6	34.7	-	37.9	27.6	45.0	45.4	18.8	207.9	806.9	0.69
					90	25.3	25.7	0.4	-	80.3	41.9	-	38.4	28.8	58.0	58.9	18.6	468.5	918.2	0.37
					130	26.9	27.5	0.6	-	90.9	47.5	-	43.4	29.9	67.0	68.6	18.4	642.7	1075.6	0.28
					250	29.6	30.8	1.2	-	113.6	57.5	-	56.1	32.7	85.0	85.5	19.0	1008.3	1536.4	0.19

Performance of water filled thermosyphons between 30-150°C (Front Page)

Frontiers in Heat Pipes (FHP), 6, 3 (2015)
DOI: 10.5098/fhp.6.3

Global Digital Central
ISSN: 2155-658X

Frontiers in Heat Pipes

Available at www.ThermalFluidsCentral.org

PERFORMANCE OF WATER FILLED THERMOSYPHONS BETWEEN 30-150°C

K. S. Ong* and Christopher Lim

Department of Industrial Engineering, Universiti Tunku Abdul Rahman, 31900 Kampar, Perak, Malaysia.

ABSTRACT

The thermal performances of three water-filled thermosyphons subjected to evaporator wall temperatures between 30-150°C were investigated. The effect of condenser cooling rates together with various fill ratios from 0.25-1.00, thermosyphon inclination angles from 23°-90° and aspect ratios from 5.0-10.0 were investigated. Power inputs from 5-405 W resulted in evaporator wall temperatures up to 185°C. Water coolant flow rates from 0.003-0.05 kg/s were employed. Axial temperature distribution was found to be uniform at power input < 18 W and non-uniform at high power input. Evaporator wall temperatures based on bulk and mean values show differences of at least 14°C at the high power values. The performance of the thermosyphons based on heat transferred varied linearly with mean or bulk temperature difference and was dependent upon fill ratio and inclination. The best performing thermosyphon was found to be at a fill ratio of 1.00 in the vertical position. Also, a high length/diameter aspect ratio thermosyphon performed better than one with a low aspect ratio.

Keywords: *Thermosyphon, condenser cooling rates, high power input, inclination, fill ratio, aspect ratio.*

1. INTRODUCTION.

Heat pipes (HPs) are very effective heat transfer devices capable of transferring large amounts of heat effectively and efficiently. Peterson (1994) mentions that a HP typically consists of a sealed container lined with a wicking material. The container is evacuated and filled with just enough liquid to fully saturate the wick. A wickless HP, known as a thermosyphon is shown in Fig. 1. Heat applied at the evaporator section causes the liquid to boil and vaporize, picking up latent heat of vaporization. Vapor rises to the condenser section where it condenses and gives up its latent heat of condensation. The condensate then travels back to the evaporator section by gravity. The performance of a thermosyphon is dependent on the fill ratio (FR), types of fill liquid, power input at the evaporator (P), heat removed from the condenser, inclination (θ) and length/diameter aspect ratio (AR). An optimal FR is important as too much fill liquid can cause flooding and too little will cause dry out. Both these phenomena are undesirable as they reduce the performance of the heat pipe. Flooding occurs when liquid collecting in the condenser and adiabatic regions are unable to return to the evaporator section. Dry out occurs when the rate of return of the condensate from the condenser section is insufficient to meet the evaporation rate due to high heat flux in the evaporator section. The operating heat flux applied to the evaporator section is important as well. A high heat flux can induce violent boiling in the evaporator section causing blockage of condensate. Prolong exposure to high heat flux can also induce dry out. There is an optimum pipe diameter related to a vapour flow such that any increase in the pipe diameter may contribute to the flooding phenomenon. An increased pipe diameter is desirable to avoid flooding. Axial heat conduction occurs along the pipe wall. The magnitude of this heat transfer compared to the heat transfer by evaporation and condensation in a thermosyphon would be comparable if the heat input is small. Generally, a temperature difference between evaporator and condenser section of about 5°C is required to initiate operation of the thermosyphon. This would depend upon the type of fill liquid and the physical dimensions of the pipe.

Nguyen-Chi and Groll (1981) investigated the entrainment or flooding limit in a closed two-phase thermosyphon with a water filled 20 mm OD x 17 mm I/D x 2.5 m long copper thermosyphon with inner circumferential grooves. Evaporator and condenser sections were each 1.0 m long. The evaporator section was heated with electrical resistance wires and the condenser cooled via a water cooling jacket. FR was between 0.38-0.88, inclination angle from 1-80°, evaporator wall temperature from 20-80°C and power input between 100-420W. They derived an empirical correlation to predict the maximum performance for the inclined thermosyphon and recommended further work to be performed to determine the influence of parameters like FR, aspect ratio, internal surface roughness of pipe and type of working fluid.

Gurses and Cannistraro (1991) studied the inclination effect on water filled heat pipes for solar energy applications with an 18 mm OD x 15 mm I/D x 1.93 m long copper pipe. The air-cooled condenser was 420 mm long fitted with external 400 mm diameter fins. Power input of up to 1200 W resulted in a evaporator wall temperature range of up to 70°C. They concluded that the best inclination angles are between 45-90° due to entrainment limit and capillary limit, and is dependent on the power input range. Terdtoon et. al. (1996) investigated the effect of aspect ratio and Bond number on the heat transfer characteristics of a two-phased closed loop thermosyphon. They used copper pipes with 7.5, 11.1 and 25.9 mm diameter with corresponding AR values of 5, 10, 20, 30 and 40. Evaporator temperatures were kept around 10°C and FR at 0.8. Fill liquids were R22, ethanol and distilled water. They concluded that the best inclination angles were between 40-70° depending on aspect ratio. The authors mentioned that the aspect ratio had more effect on the performance of a thermosyphon compared to type of fill liquid and inclination. Payaruk et. al. (2000) correlated the heat transfer characteristics of an inclined closed two-phase thermosyphon at normal operating conditions. They used pipes of 7.5,

* *Corresponding author. Email: skong@utar.edu.my*

APPENDIX B

Table 7 Experimental results obtained for phase B

Run	HP #	Pipe Shape	Coolant	Flowrate (ml/s)	Time (s)	T_b (°C)	T_{ins} (°C)	T_a (°C)	T_{in} (°C)	T_{out} (°C)
B/1	-	-	-	-	0	100.3	29.5	19.6	-	-
					600	99.5	30.8	19.7	-	-
					1200	98.2	31.2	19.4	-	-
					1800	97.2	31.3	19.9	-	-
					2400	96.1	31.3	19.9	-	-
					3000	95.1	31.2	19.8	-	-
					3600	94.1	31.3	19.9	-	-
					4200	93.1	31	19.7	-	-
					4800	92.1	31.3	19.9	-	-
					5400	91.2	31.1	19.8	-	-
					6000	90.2	31.3	19.9	-	-
					6600	89.3	31.2	19.7	-	-
					7200	88.4	31.3	19.9	-	-
B/2	1	straight	water	0.9	0	99.2	34.4	20.1	29.1	77.5
					600	93.8	33	20.1	28.5	63.1
					1200	86	30.8	21.5	28.2	56.8
					1800	81	30.7	21.5	28.5	52.4
					2400	78.9	30.5	21.4	28.9	48.5
					3000	74.3	29.9	20.1	29.1	45
					3600	71.3	29.4	20.6	28.5	41.8
					4200	68.7	29.1	20	28.2	39.3
					4800	66.6	28.8	20.6	28.2	37.2
					5400	64.3	28.6	21.2	28.5	35.3
					6000	61.1	28.3	21.1	28.9	33.7
					6600	60	27.8	20.6	29.1	32.2
					7200	58.5	27.5	20.3	28.5	30.9
B/3	1	straight	water	50	0	98.9	32.9	20.1	29	31.6
					600	87.5	33	20.1	30	31.6
					1200	79	32.4	21.5	30.6	31.6
					1800	73.3	31.5	21.5	30.9	31.5
					2400	69.3	30.6	21.4	31	31.4
					3000	66.4	31.1	20.1	31.1	31.3
					3600	64.2	31.8	20.1	31.1	31.2
					4200	62.5	32	21.5	31.1	31.2

					4800	61.2	32.1	20.1	31	31
					5400	60.3	32.1	20.1	31	31
					6000	59.3	32	21.5	30.9	30.9
					6600	58.4	31.8	21.5	30.8	30.9
					7200	57.5	31.2	21.4	30.7	30.8
B/4	2	straight	air	0	0	100	27.2	20.9	-	-
					600	97.7	27.6	20.9	-	-
					1200	95.5	27.6	20.8	-	-
					1800	93.3	27.5	20.4	-	-
					2400	91.3	27.4	20.2	-	-
					3000	89.3	27.1	20	-	-
					3600	87.3	26.7	20	-	-
					4200	85.4	26.3	19.4	-	-
					4800	83.5	26.3	18.4	-	-
					5400	81.6	26.3	18.6	-	-
					6000	79.7	26.1	18.8	-	-
					6600	77.8	25.8	18.6	-	-
					7200	76.1	25.6	18.5	-	-
B/5	2	straight	air	2	0	99.9	28.4	21.1	-	-
					600	98	28.9	20.9	-	-
					1200	95.9	28.8	20.1	-	-
					1800	94.3	28.4	21.1	-	-
					2400	92.7	28.9	20.9	-	-
					3000	91.1	28.8	21	-	-
					3600	89.6	28.4	20	-	-
					4200	88.1	28.9	20.5	-	-
					4800	86.6	28.8	21.8	-	-
					5400	85.2	28.4	20.3	-	-
					6000	83.8	28.9	21.1	-	-
					6600	82.4	28.8	20.9	-	-
					7200	81	29	20.1	-	-
B/6	3	straight	air	2	0	100.2	31.6	24.8	-	-
					600	93.4	32.4	24.9	-	-
					1200	85.3	31.8	24.4	-	-
					1800	78.4	31.1	24	-	-
					2400	72.7	30.3	23.5	-	-
					3000	68.1	29.5	23.1	-	-
					3600	64.2	28.6	22.7	-	-
					4200	61.3	28	22.4	-	-
					4800	59.2	27.5	22.2	-	-
					5400	57.6	26.9	22	-	-
					6000	56.3	26.5	21.9	-	-
					6600	55.2	26.1	21.8	-	-
					7200	54.1	25.8	21.7	-	-

B/7	4	J shape	air	2	0	99.8	25.2	21.1	-	-
					600	94.9	24.7	20.9	-	-
					1200	89	24.6	20.9	-	-
					1800	83.6	24.6	20.8	-	-
					2400	78.6	24.6	20.8	-	-
					3000	74.3	24.6	20.8	-	-
					3600	70.3	24.7	20.8	-	-
					4200	68.3	24.4	20.8	-	-
					4800	65.4	24.3	20.8	-	-
					5400	63.3	24.2	20.8	-	-
					6000	61.1	24.2	20.8	-	-
					6600	59.3	23.8	20.8	-	-
					7200	57.9	23.9	20.8	-	-
B/8	5	L shape	air	2	0	99.3	26.4	21.1	-	-
					600	90.2	26.3	21.2	-	-
					1200	84.9	28.7	21.1	-	-
					1800	80	29.6	21.4	-	-
					2400	75.3	28.9	21.8	-	-
					3000	71.1	28.1	21.9	-	-
					3600	67.1	27.7	21.8	-	-
					4200	63.4	27.3	21.6	-	-
					4800	60.2	26.9	21.5	-	-
					5400	57.2	26.6	21.3	-	-
					6000	54.7	26.4	21.3	-	-
					6600	52.2	26	21.1	-	-
					7200	49.9	25.8	21	-	-

Table 8 Simulation results for Phase B

Power (P), W	Temperature difference (ΔT_w), ^oC
4.4	4.5
22.8	23
58	48
101	54.8
136	63.7
217	83.6

An experimental procedure to obtain and compare thermal performance of thermosyphons rapidly (Front Page)

Frontiers in Heat Pipes (FHP), 6, 2 (2015)
DOI: 10.5098/fhp.6.2

Global Digital Central
ISSN: 2155-658X

Frontiers in Heat Pipes

Available at www.ThermalFluidsCentral.org

AN EXPERIMENTAL PROCEDURE TO COMPARE THERMAL PERFORMANCE OF THERMOSYPHONS RAPIDLY

K. S. Ong* and Christopher Lim

Universiti Tunku Abdul Rahman, 31900 Kampar, Perak, Malaysia

ABSTRACT

There are various methods employed to determine the performance of heat pipes and two-phase closed thermosyphons. Perhaps the most common method involves measuring the rate of heat transfer from the evaporator to the condenser section with a water cooled jacket surrounding the latter. This entails higher costs and requires extended testing times. A method is proposed here to obtain comparative performance test data on various heat pipes rapidly and economically. The method does not require fabricating a water jacket. It merely involves measuring and comparing the transient temperature of a pre-heated container of hot water obtained first without the heat pipe and then with the heat pipe immersed into the container. The more efficient system will result in faster cooling of the container. The method is demonstrated using a number of different thermosyphons employing both water jackets and air cooled finned condensers. Their performances are compared in the paper.

Keywords: *Thermosyphon, comparative performance, rapid experimental procedure, air cooled condenser, water cooled condenser.*

1. INTRODUCTION

Heat pipes (HPs) are devices capable of transferring large quantities of heat effectively and efficiently. A HP typically consists of a sealed container lined with a wicking material. The container is evacuated and filled with just enough liquid to fully saturate the wick. A wickless HP is also known as a thermosyphon, shown in Fig.1. Heat applied to the evaporator section causes it to boil and vaporize, picking up latent heat of vaporization. The vapor then rises to the condenser section where it condenses. Here vapor gives up its latent heat of condensation. The condensate then travels back to the evaporator section of the heat pipe by gravity or capillary action. The performance of HPs depend on various factors such as type of fill liquid, fill ratio (FR), heat input at the evaporator section, inclination and physical dimensions of the pipe.

The performance of a HP could be evaluated by determining the amount of heat input at the evaporator section or by measuring the heat transferred at the condenser section to the coolant. At steady state, these two heat transfer rates should be equal if there is no heat loss from the pipe. In order to compare the performances of various heat pipes the heat transfer rates could be plotted against the temperature difference between the evaporator and condenser sections. This would give an indication of the thermal resistance of the pipe. A high thermal resistance would indicate a poor performing HP and vice versa.

Ong et al. (2014) investigated the performance of water and R410a filled thermosyphon at various power inputs (100 to 830 W), fill ratios (0.25 to 0.93) and inclinations (30º to 90º). The authors used a 38 mm OD x 807 mm long thermosyphon with a 71 mm OD cooling water jacket and electrical heating bands to supply heat to the evaporator section. By plotting input power against temperature difference between evaporator and condenser sections, found that the R410a filled thermosyphon performed better in the vertical position at all FR's and that the water filled thermosyphon performed better at low FR and when inclined. They showed that the evaporator wall temperature was not uniform especially at high power inputs, low fill ratios and large inclinations.

Shanthi and Velraj (2014) experimented with a two phase gravity assisted thermosyphon. The authors used a 12.5 mm ID x 300 mm long thermosyphon with a 200 mm long cooling water jacket and a 1000 W nichrome heating wire wound around the 75 mm long evaporator section. They measured the performance of their thermosyphon by plotting efficiency defined as ratio of power output over power input, versus power input and obtained values as high as 0.9. Anjakar and Yarasu (2012) determined the effect of condenser length on the performance of thermosyphon by using a 32 mm OD x 1000 mm long thermosyphon with a 450 mm long water cooled jacket and a 300 mm long nichrome heating element at the evaporator section. The authors determined the efficiency using the ratio of heat conducted away by the coolant water at the condenser section to the power input at the evaporator section and found values of 0.5 to 0.95. In theory the ratio should be equal to 1.0.

Buschmann and Franzke (2013) compared the performance of thermosyphons filled with deionised water (DI) and titanium oxide-based DI water and gold nanofluid. They showed that the nanofluids reduced thermal resistances up to 24 %. They also noted that nanoparticles depositing on the evaporator wall after prolonged heating operations resulted in an absence of nanoparticles being transported to the condenser section that eventually reduced the thermal transport capacity of the nanofluid and increased the overall thermal resistance. Huminic et al. (2011) experimented with thermosyphons filled with iron oxide nano particles and found that a concentration level of 5.3 % improved the thermal performance of their HP. Solomon et al. (2012) determined the thermal performance of a heat pipe with a nano particles-coated wick. They found that the thermal resistance reduced from 0.32 to 0.11 ºC/W when subjected to power input ranging from 100 to 200 W, respectively.

Qu and Wang (2013) showed that the thermosyphon with a FR of 40 to 50 % resulted in faster response time and lowest overall thermal resistance. Shabgard et al. (2014) studied the thermal characteristics of

* *Corresponding author. Email: skong@utar.edu.my*

APPENDIX C

Table 9 Experimental results obtained for phase C

Run	Time (seconds)	$T_{a,1-3}$ (°C)	$T_{a,4-6}$ (°C)	$T_{a,7-9}$ (°C)	$T_{ins,m}$ (°C)	$T_{wall,m}$ (°C)	$T_{b,m}$ (°C)	$T_{a,out}$ (°C)	Ta,in (°C)
1	0	-	-	-	-	-	80.2	-	-
	600	-	-	-	-	-	78.4	-	-
	1200	-	-	-	-	-	76.8	-	-
	1800	-	-	-	-	-	75.2	-	-
	2400	-	-	-	-	-	73.7	-	-
	3000	-	-	-	-	-	72.5	-	-
	3600	-	-	-	-	-	71.3	-	-
	4200	-	-	-	-	-	70.3	-	-
	4800	-	-	-	-	-	69.2	-	-
	5400	-	-	-	-	-	68.4	-	-
	6000	-	-	-	-	-	67.5	-	-
	6600	-	-	-	-	-	66.7	-	-
	7200	-	-	-	-	-	65.9	-	-
2	0	64.9	60.7	46.9	27.3	41.7	79.4	54.6	21.0
	600	57.3	53.5	41.9	29.4	39.8	68.1	50.8	20.7
	1200	49.9	46.6	37.8	28.4	36.8	59.5	45.2	20.8
	1800	44.5	42.0	34.7	27.1	34.0	52.7	40.7	20.8
	2400	40.0	38.0	32.0	26.1	31.7	47.1	37.2	20.9
	3000	36.4	34.8	29.8	25.2	29.9	42.7	34.3	20.6
	3600	33.5	32.1	28.1	24.5	28.3	39.0	32.0	20.6
	4200	31.3	29.9	26.7	23.9	27.1	36.1	30.1	20.7
	4800	29.4	28.4	25.8	23.4	26.0	33.7	28.7	20.8
	5400	27.9	27.0	24.7	22.9	25.2	31.9	27.4	20.8
	6000	26.6	25.8	23.9	22.6	24.4	30.2	26.2	20.7
	6600	25.5	24.8	23.1	22.1	23.8	28.9	25.3	20.6
	7200	24.6	24.0	22.6	21.9	23.3	27.8	24.5	20.6
3	0	62.1	56.0	43.8	26.6	40.9	79.4	49.0	19.8
	600	53.9	49.9	39.9	28.7	38.7	68.4	47.0	19.9
	1200	50.4	45.3	37.2	27.5	36.7	59.5	43.7	19.8
	1800	44.4	40.4	33.8	26.1	32.4	52.3	39.2	19.7
	2400	39.5	36.4	31.2	25.1	31.2	46.4	35.6	19.8
	3000	35.8	33.3	29.0	24.2	29.2	41.8	32.8	19.7
	3600	32.7	30.5	27.2	23.5	27.5	38.1	30.5	19.7
	4200	30.3	28.5	25.8	22.8	26.1	35.1	28.5	19.7
	4800	28.4	26.9	24.6	22.3	25.1	32.7	27.1	19.8

	5400	26.8	25.5	23.6	21.9	24.2	30.7	25.8	19.7
	6000	25.5	24.5	22.9	21.5	23.4	29.1	24.7	19.7
	6600	24.4	23.6	22.2	21.1	22.8	27.8	23.9	19.6
	7200	23.5	22.9	21.8	20.9	22.3	26.7	23.3	19.8
4	0	50.9	47.2	34.4	27.3	34.9	79.7	42.8	19.6
	600	45.9	44.2	32.5	27.6	32.3	70.7	40.7	19.7
	1200	43.6	43.5	32.0	26.8	32.5	63.1	39.4	19.8
	1800	41.0	41.5	31.2	26.0	31.6	56.5	37.5	19.8
	2400	38.4	38.5	30.3	25.2	30.4	50.6	35.7	19.7
	3000	36.3	35.7	29.5	24.6	29.4	45.6	33.9	19.7
	3600	34.5	32.9	27.8	23.9	28.1	41.4	32.2	19.8
	4200	32.4	30.6	26.2	23.3	26.7	37.8	30.2	19.8
	4800	30.1	28.6	24.9	22.9	25.6	35.0	28.4	19.8
	5400	28.1	27.0	23.8	22.2	24.5	32.7	26.9	19.6
	6000	26.6	25.7	23.0	21.8	23.7	30.8	25.6	19.7
	6600	25.3	24.6	22.3	21.4	23.0	29.2	24.5	19.6
	7200	24.4	24.0	22.4	21.6	23.0	28.0	23.8	19.5
5	0	36.0	33.5	25.2	29.6	30.7	79.4	30.4	20.1
	600	30.4	30.4	23.6	30.3	26.4	73.8	28.7	20.4
	1200	29.4	29.5	23.2	29.4	25.7	69.1	28.1	20.5
	1800	28.6	28.9	22.9	28.5	25.2	64.9	27.4	20.5
	2400	28.2	28.6	23.0	28.0	25.0	61.4	27.2	20.9
	3000	27.7	28.3	22.9	27.3	24.8	58.2	26.8	20.9
	3600	27.3	27.9	22.7	26.7	24.6	55.4	26.4	20.9
	4200	26.9	27.6	22.5	26.0	24.3	52.7	26.1	20.9
	4800	26.5	27.3	22.3	25.5	24.1	50.3	25.8	21.0
	5400	26.3	27.2	22.4	25.2	24.0	48.0	25.7	21.1
	6000	26.1	27.1	22.4	24.8	23.9	46.0	25.6	21.3
	6600	25.8	26.8	22.1	24.4	23.6	44.1	25.4	21.1
	7200	25.5	26.5	22.0	24.0	23.3	42.4	25.2	21.0
6	0	46.3	41.7	41.1	25.7	39.1	80.3	43.6	18.7
	600	36.3	34.9	36.7	28.6	37.8	71.1	39.9	19.4
	1200	32.6	31.7	33.1	27.6	34.8	64.0	36.7	19.4
	1800	29.4	28.5	29.5	26.5	31.8	58.4	33.4	19.4
	2400	27.0	26.3	27.0	25.5	29.3	53.8	30.7	19.3
	3000	25.0	24.3	25.0	24.7	27.3	50.0	28.5	19.3
	3600	23.4	22.9	23.5	23.9	25.6	46.8	26.6	19.2
	4200	22.3	21.9	22.3	23.3	24.3	44.3	25.0	19.0
	4800	21.4	21.1	21.4	22.8	23.3	42.1	23.7	19.0
	5400	20.7	20.5	20.6	22.3	22.4	40.5	22.9	18.9
	6000	20.1	20.0	20.1	21.9	21.8	39.0	21.9	18.8
	6600	19.8	19.6	19.7	21.5	21.2	37.8	21.3	18.7
	7200	19.5	19.5	19.5	21.2	21.0	36.8	21.0	18.7
7	0	50.1	45.4	45.0	26.0	38.4	80.4	47.3	19.8

	600	39.7	38.6	39.8	28.3	37.1	70.4	43.6	19.4
	1200	36.0	35.1	36.2	27.3	34.4	62.6	39.9	19.5
	1800	33.1	32.3	33.1	26.3	32.1	56.3	36.5	19.5
	2400	30.9	30.2	30.8	25.4	30.2	51.0	33.7	19.3
	3000	28.8	28.3	28.8	24.4	28.5	46.6	31.6	19.4
	3600	27.2	26.7	27.2	23.7	27.0	43.0	29.5	19.3
	4200	25.8	25.4	25.8	23.1	25.8	40.0	27.8	19.4
	4800	24.5	24.3	24.7	22.6	24.6	37.6	26.3	19.2
	5400	23.4	23.2	23.6	22.2	23.7	35.6	25.0	19.4
	6000	22.3	22.2	22.5	21.6	22.8	34.0	23.8	19.1
	6600	21.4	21.4	21.6	21.3	22.1	32.7	22.7	19.0
	7200	20.7	20.6	20.5	21.0	21.5	31.7	21.9	19.0
8	0	51.1	49.1	43.6	27.0	39.3	80.6	47.5	19.5
	600	40.4	39.6	38.9	28.7	38.8	70.8	42.9	19.7
	1200	36.4	36.2	35.9	27.5	35.5	63.3	39.3	19.8
	1800	33.7	33.6	33.3	26.5	33.2	57.2	36.4	19.8
	2400	31.5	31.4	31.0	25.5	31.2	52.0	34.0	19.7
	3000	29.7	29.6	29.2	24.7	29.5	47.6	32.0	19.5
	3600	28.1	27.9	27.6	24.0	28.1	43.9	30.2	19.4
	4200	26.7	26.5	26.2	23.4	26.9	40.8	28.6	19.4
	4800	25.4	25.3	25.0	22.9	25.8	38.2	27.2	19.4
	5400	24.4	24.2	24.0	22.4	24.8	36.0	26.0	19.4
	6000	23.5	23.4	23.2	22.1	24.0	34.2	25.0	19.4
	6600	22.6	22.5	22.3	21.8	23.3	32.7	24.1	19.4
	7200	21.9	21.8	21.6	21.4	22.6	31.5	23.2	19.4
9	0	55.0	53.0	49.9	26.0	40.0	80.2	47.4	19.7
	600	42.1	42.3	42.2	29.0	38.9	70.7	42.7	19.7
	1200	38.4	38.6	38.6	27.8	36.1	63.2	39.1	19.7
	1800	35.5	35.6	35.5	26.6	33.6	57.2	36.4	19.8
	2400	32.6	32.7	32.2	25.7	31.1	52.2	33.7	19.8
	3000	30.2	30.1	29.9	24.8	29.2	48.1	31.1	19.9
	3600	28.3	28.0	28.2	24.3	27.8	44.7	29.4	20.0
	4200	26.5	26.3	26.6	23.7	26.6	42.0	27.5	19.9
	4800	25.2	25.0	25.4	23.1	25.6	39.7	26.4	19.8
	5400	24.2	24.0	24.5	22.7	24.8	37.7	25.5	19.9
	6000	23.3	23.1	23.6	22.3	24.1	36.1	24.6	19.9
	6600	22.7	22.5	22.9	21.9	23.5	34.7	23.9	19.6
	7200	22.2	22.0	22.3	21.6	23.0	33.4	23.3	19.7

Table 10 Simulation results for Phase C

Theoretical FR 1.0		**Theoretical FR 0.75**		**Theoretical FR 0.5**		**Theoretical FR 0.25**	
Power (P), W	Temperature Difference ($\Delta T_{b\text{-}air,mean}$), ^{o}C	Power (P), W	Temperature Difference ($\Delta T_{b\text{-}air,mean}$), ^{o}C	Power (P), W	Temperature Difference ($\Delta T_{b\text{-}air,mean}$), ^{o}C	Power (P), W	Temperature Difference ($\Delta T_{b\text{-}air,mean}$), ^{o}C
180.0	17.8	188.1	11.9	220.4	11.0	224.5	12.9
220.4	18.7	234.6	12.5	266.9	12.0	258.8	13.9
260.9	19.6	297.3	13.4	331.6	13.3	293.2	15.0
303.3	20.8	353.9	14.8	396.4	14.9	357.9	16.5
386.2	22.3	444.9	16.4	477.2	16.9	422.6	18.3
465.1	23.9	544.0	18.6	556.1	19.1	499.5	20.0
572.3	26.1	661.3	21.1	671.4	21.8	610.7	22.6
701.7	28.8	796.8	24.5	798.8	25.1	748.2	25.5
835.2	32.0	960.6	28.3	952.5	29.1	914.0	29.1
1027.3	36.0	1144.6	32.9	1106.2	33.7	1092.0	33.8
1288.2	41.5	1427.7	38.9	1379.2	39.5	1358.9	39.5
1672.4	48.5	1824.0	46.2	1769.4	46.6	1729.0	47.0